DESIGN, PRODUCTION AND TESTS OF AN INHERENTLY BALANCED MECHANISM TO BE USED AS AN ENDOSCOPE HOLDER FOR ENDONASAL SKULL BASE SURGERY

A Thesis Submitted to the
Graduate School of Engineering and Sciences of
İzmir Institute of Technology
in Partial Fulfillment of the Requirements for the Degree of

MASTER OF SCIENCE

in Mechanical Engineering

by
Tuğrul YILMAZ

July 2023
İZMİR

We approve the thesis of **Tuğrul YILMAZ**

Examining Committee Members:

Prof. Dr. Gökhan KİPER
Department of Mechanical Engineering, İzmir Institute of Technology

Prof. Dr. Mehmet İsmet Can DEDE
Department of Mechanical Engineering, İzmir Institute of Technology

Assoc. Prof. Dr. Erkin GEZGİN
Department of Mechatronics Engineering, İzmir Katip Çelebi University

20 July 2023

Prof. Dr. Gökhan KİPER
Supervisor
Department of Mechanical Engineering
İzmir Institute of Technology

Dr. Volkert van der WIJK
Co-Supervisor
Department of Mechanical, Maritime and Materials Engineering
Delft University of Technology

Prof. Dr. Mehmet İsmet Can DEDE
Head of the Department of
Mechanical Engineering

Prof. Dr. Mehtap EANES
Head of the Graduate School of
Engineering and Sciences

ACKNOWLEDGMENTS

I wish to begin by expressing my profound and heartfelt gratitude to my supervisor, Prof. Dr. Gökhan Kiper. His inspirational perspective, constant guidance, and unwavering support have played a fundamental role in my academic journey. Similarly, I extend my sincerest appreciation to my co-advisor, Dr. Volkert Van Der Wijk, whose insightful counsel and encouragement have been invaluable throughout the course of this research project.

I am deeply thankful to my jury members, Prof. Dr. Mehmet İsmet Can Dede and Assoc. Prof. Dr. Erkin Gezgin. Their presence at my thesis defense seminar and their constructive suggestions greatly contributed to the improvement of my research.

My heartfelt thanks also go out to my beloved family, who have consistently stood by my side. Their unending faith and support have been the pillars of strength that enabled me to complete this study.

I am grateful for the camaraderie and shared curiosity of my fellow lab and project mates. I am particularly thankful to Tarık Kadak and İbrahimcan Görgülü whose companionship made this project more enjoyable.

Lastly, I wish to acknowledge the 1001 - The Scientific and Technological Research Projects Funding Program of The Scientific and Technological Research Council of Turkey (TÜBİTAK). This study was conducted with their financial support under the project named “BalanScope - Design of an Inherently Balanced Robotic Manipulator with Remote Center of Motion to be used as an Endoscope Holder for Endonasal Skull Base Surgery” with grant number 219M483. The funding was crucial in making this research possible.

ABSTRACT

DESIGN, PRODUCTION AND TESTS OF AN INHERENTLY BALANCED MECHANISM TO BE USED AS AN ENDOSCOPE HOLDER FOR ENDONASAL SKULL BASE SURGERY

Robotic surgery is popular in minimally invasive operations. Given the requirement for the manipulator to operate around the body-entrance point, it must have a remote center of motion. The main aim of the thesis is to design and prototype a surgical robotic arm with 3 degrees of freedom (2 rotation + 1 translation motion pattern) and a remote center of motion to be used as an endoscope holder in minimally invasive surgery.

First, a literature review is conducted on robotic surgery, robots used in minimally invasive surgery and mechanisms with remote center of motion. Then, possible kinematic structures are examined and the most suitable one was selected considering the requirements such as balancing compatibility and workspace. While circular tracking arc mechanism is known in the literature, manipulator based on the modified circular tracking arc is novel. Also, gravity compensation of the circular tracking arc is performed. After the gravity-compensation solution for the manipulator is developed and parametrized by considering the workspace, link lengths and geometries were determined and a solid model was developed for detailed construction. Finally, a prototype of the mechanism is manufactured.

ÖZET

ENDONAZAL KAFA TABANI AMELİYATI İÇİN ENDOSKOP TUTUCU OLARAK KULLANILACAK, KENDİNDEN DENGELİ BİR MEKANİZMA TASARIMI, ÜRETİMİ VE TESTLERİ

Robotik cerrahi, minimal invaziv cerrahi operasyonlarda popüler hale gelmiştir. Manipülatörün vücuda giriş noktası etrafında çalışması gerektiğinden bir uzaktan hareket merkezi olması gerekir. Tezin ana hedefi, minimal invaziv cerrahide endoskop tutucu olarak kullanılacak olan bir 3 serbestlik dereceli (2 dönüş ve bir öteleme) ve uzaktan hareket merkezli bir cerrahi robotik kol tasarlamak ve prototiplemektir.

Öncelikle, robotik cerrahi, minimal invaziv cerrahide kullanılan robotlar ve uzaktan hareket merkezli mekanizmalar üzerine bir literatür incelemesi yapıldı. Ardından, olası kinematik yapılar incelendi ve dengeleme ve çalışma alanı gibi gereklilikler göz önünde bulundurarak en uygun olanı seçildi. Literatürde çember yaylı mekanizma bilinmesine rağmen, bu mekanizmanın yeni bir hali sunulmuştur. Ayrıca, mekanizmanın yerçekimine karşı dengelemesi çalışılmıştır. Manipülatör için yerçekimi dengeleme çözümü geliştirildikten ve parametrize edildikten sonra, çalışma alanı dikkate alınarak uzuv uzunlukları ve geometrileri belirlendi ve detaylı bir konstrüksiyon için katı modeli geliştirildi. Son olarak mekanizmanın bir prototipi üretildi.

TABLE OF CONTENTS

LIST OF FIGURES

Figure **Page**

Figure **Page**

Figure **Page**

Figure **Page**

LIST OF TABLES

Table **Page**

CHAPTER 1

INTRODUCTION

Surgical operations are medical procedures that have evolved, with a history dating back to the third millennium BC, as documented in medical literature (Van Hee, 2014). These operations involve making incisions using various tools to repair damage in a living body or halt disease progression. Surgical operations supported by robotic equipment date back about 40 years ago; the first robot-assisted surgical operation in literature was performed in 1985 (Kwoh et al., 1988). In the last decades, it has been seen that the number of various surgical interventions operated using robotic technology has dramatically increased, and the literature has been expanding by increasing research in this field (Schreuder & Verheijen, 2009). Robotic surgery has improved precision, accuracy, tremor correction, haptic feedback, etc., resulting in successful surgeries compared to conventional surgery without robot assistance (Boyraz et al., 2019). The robotic equipments, which are commonly used as assistants to enhance the ergonomics of doctors during surgeries, are generally employed in the manipulation and fixation of tools such as light and camera systems. This thesis is about designing a robotic manipulator for holding and maneuvering an endoscope, which aims to assist the surgeon during endoscopic pituitary gland surgeries. The problem definition and aim of the thesis are presented in the following sections.

1.1. Problem Definition

The pituitary gland, located at the base of the brain, serves as the body's primary endocrine organ, regulating many essential physiological processes by producing and releasing various hormones (Barkhoudarian & Kelly, 2017). Serious health problems can arise for people when this organ becomes dysfunctional by various reasons such as tumors. Surgery is one of the treatment methods against tumors, and different approaches can be applied depending on the location and size of the tumor (Arafah & Nasrallah, 2001). One of the treatments is open transcranial surgery, which based on creating an opening in the skull and inverting in the pituitary gland using various surgical instruments. Another approach is transsphenoidal surgery, which is classified as a type of

minimally invasive surgery (MIS) by inserting surgical tools through the nasal cavity (Komotar et al., 2011). While transsphenoidal surgeries date back to beginning of the 20th centuries, use of endoscope during the pituitary surgery for imaging the tumors date back only 1990s (Senior et al., 2008).

During a transsphenoidal surgery, an endoscope is used as the camera. The Endoscope is manipulated such that it passes through the nostril and nasal cavity as shown in Figure 1.1. At the same time, the surgeon uses several special tools to operate on the tissues. Due to the need for both the endoscope and the other tools to be manipulated by the surgeon, and the resulting surgical procedures lasting 2-4 hours, the surgeon's ergonomics is negatively affected during the operation. As seen in Figure 1.2, while the surgeon is holding the endoscope with one hand, she/he is holding a surgical tool with the other hand. One of the most significant problems is muscle fatigue, which increases the risk of the operation (Schöb et al., 2016).

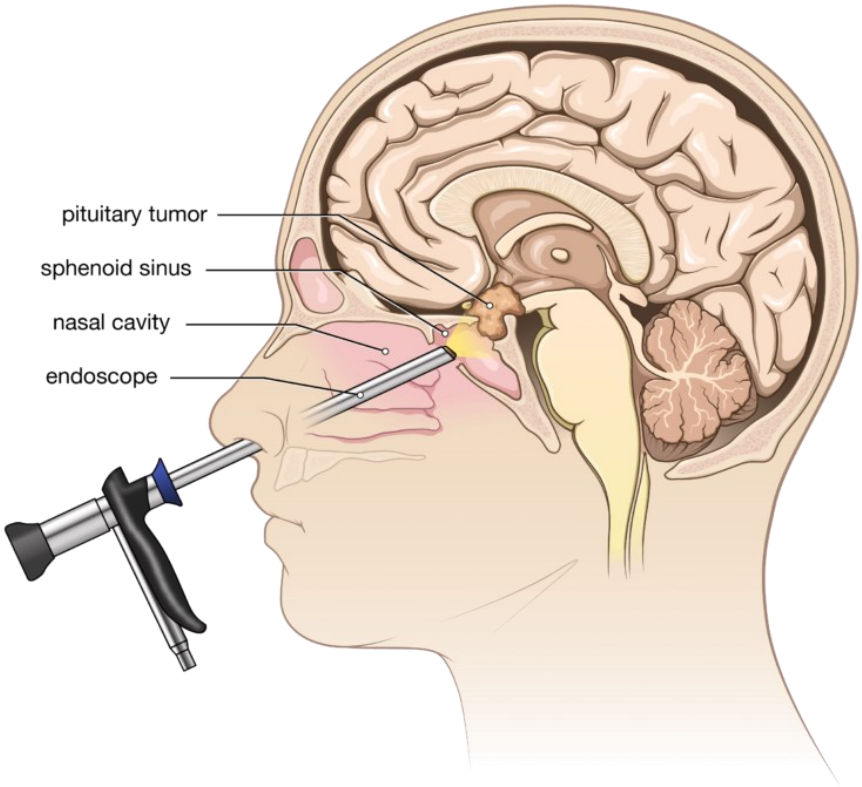

Figure 1.1. Endoscope location and pituitary tumor
(Source: Goodman Campbell Brain and Spine, n.d.)

Figure 1.2. Hands of surgeon and assistant during the MIS operation
(Source: Dede et al., 2017)

There are various methods in order to eliminate these disadvantageous situations mentioned above. Current methods are to have an assistant to hold the endoscope or to use an endoscope stabilizer. However, if the assistant holds the endoscope, which is one of these conventional methods, there may be coordination and communication problems with the surgeon. Using the endoscope stabilizer does not allow to easily change the view angle.

Dede et al. (2017) introduced the "NeuRoboScope" as a teleoperation robot system for endoscopic pituitary surgery. The system called “NeuRoboScope – Robot assisted endoscope control that can be controlled by the surgical tools”, consists of a passive arm and an active arm. The passive arm, which has an active arm attached to it, is manually positioned by the surgeon from the surgical area. Slave component of the teleoperation system is the active arm.

1.2. Aim and Scope of the Thesis

In order to eliminate the problems mentioned above, the thesis aims to design a manipulator as an active arm of the mentioned teleoperation system that meet the following requirements: the manipulator must have 3 degrees of freedom (dofs) 2R1T (R: rotation, T: translation) motion pattern with a remote center of motion (RCM), which is the pivot point at the tip of a nostril. Apart from this, it must not negatively affect the surgeon’s bedside workspace and must not contain parasitic motions.

In Chapter 2, a literature review about minimal invasive surgeries and the robotic equipment used in these surgeries is presented. Conceptual designs with serial and hybrid kinematic structures with RCM and 2R1T motion patterns were evaluated and an appropriate one is selected in Chapter 3. In Chapter 4, the kinematic analysis and balancing solution of the selected manipulator is presented. In Chapter 5, the constructional design, manufacturing of the manipulator parts and prototype assembly are presented. Finally, tests of the manipulator and conclusion of the thesis are given in Chapter 6.

CHAPTER 2

LITERATURE SURVEY

This chapter is divided into three parts: first, the robotic equipments used in MIS operations are examined. The second part is about the RCM mechanisms used in medical operations. The third part is about static balancing.

2.1 Use of Robotic Equipment in MIS Operations

Minimally invasive surgery (MIS) operations are defined as 'entering the body through the anatomical opening, body cavity or skin with the minimum damage to entrance' (Mariani & Pêgo-Fernandes, 2013). Instruments with various end effectors are inserted through the small incision and the surgeon uses these instruments by maneuvering outside the body with his/her hands.

Using robotic equipment in MIS operations has many advantages over traditional MIS operations. One of the advantages of performing surgical operations assisted with robotic systems is more precision and geometric accuracy. Another important one is that the surgeon does not have to keep his/her hand at a fixed pose for a long time during the operation. Also, human sterilization is limited, but the manipulator can be sterilized thoroughly, reducing the risk of infection. Another advantage is that it reduces recovery time since the operation is performed through a small incision (Lanfranco et al., 2004).

The first MIS supported by a robot occurred in 1991 and is applied clinically to patients. This robotic system, called probot, could remove tissue from patients first. Clinical trials were performed manually powered and then under computer control (Davies et al., 1996).

The first commercial robot used in MIS was AESOP (Automated Endoscope System for Optimal Positioning). This robot is the first notable product of the US Medical Robotics Company (established in 1990) and is a system that holds an endoscopic camera to eliminate some disadvantages and difficulties caused by the surgeon's hands such as fatigue and shaking. In 1993, the first clinical trial of AESOP was conducted in a laparoscopic cholecystectomy operation (Kuo & Dai, 2009).

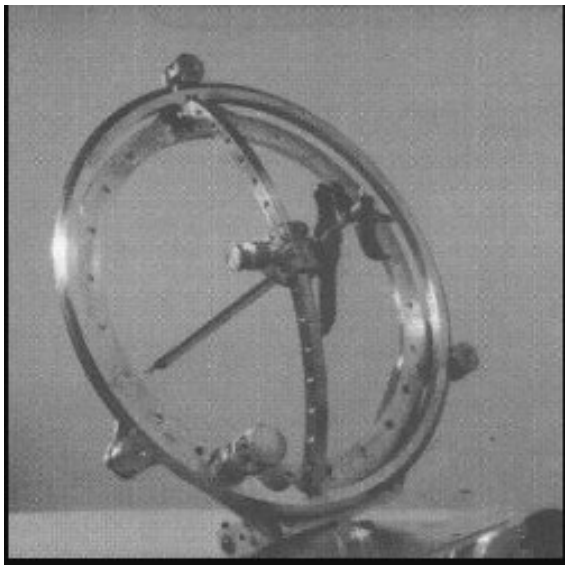

Figure 2.1. Probot
(Source: Davies et al., 1996)

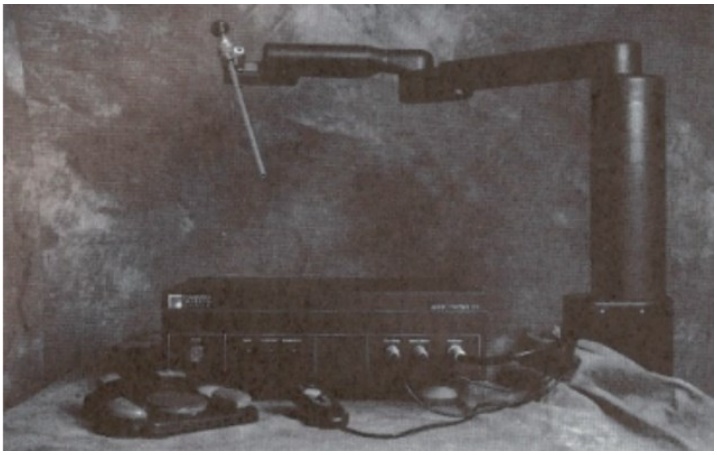

Figure 2.2. AESOP
(Source: Sackier & Wang, 1996)

In the literature, robotic systems with master-slave structures, such as Zeus and da Vinci are the most prominent ones. They have multiple arms for different purposes such as holding light, camera and surgical tools operated remotely from the console and have video-assisted visualization and computer enhancement (Pal et al., 2011).

2.2 RCM Mechanisms Used in Medical Operations

Many different types of manipulators are used in minimally invasive operations. The robotic systems used in these operations must have enough performance for accuracy,

precision and stability. Moreover, because of the nature of MIS, a remote center of motion (RCM) is required for this type of surgical operation. The RCM is a kinematic feature that provides rotation and sliding of the end-effector of the mechanism around a certain point without any physical contact between the end-effector and the point. RCM mechanisms are designed to hold and manipulate tools or endoscopic cameras in robot-assisted surgical operations. They are widely used in MIS and other robot-assisted surgeries (Zong et al., 2008).

Many mechanisms in the literature can be used as endoscope holder manipulators for MIS. Also, many different RCM types, such as circular tracking arc, parallelogram, spherical linkage, parallel manipulators, isocenters, synchronous belt transformation, etc., can be used (Kuo & Dai, 2009). These mechanisms can have serial, parallel or hybrid kinematic structure.

Circular tracking arc mechanisms consist of a circular arc used as a frame and a sliding link. The pivot point is the center of the circular arc. The most straightforward configuration with 1-dof (1R) is shown in Figure 2.3. If the circular arc can rotate about an axis on the plane of the circular arc, then the mechanism has 2 DOF (2R), as shown in Figure 2.4.

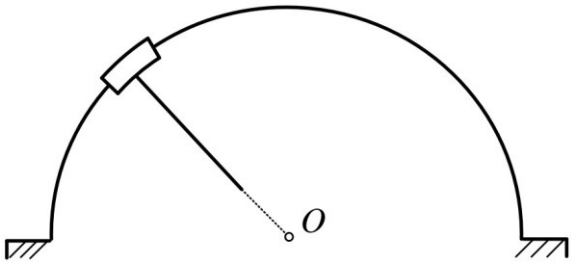

Figure 2.3. 1-dof RCM circular tracking arc

(Source: Kuo, Dai, & Dasgupta, 2012)

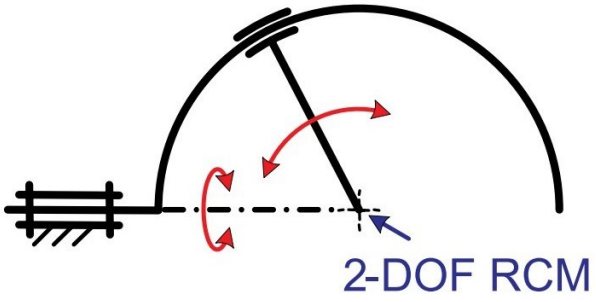

Figure 2.4. 2-dof RCM circular tracking arc

(Source: Zong et al., 2008)

In the literature, there are also 3-dof RCM mechanisms based on circular arc tracking. If a prismatic joint is placed on the sliding part, which travels through the circular arc within the direction of the axis perpendicular to the arc, 3-dof can be obtained around the pivot point. An example of this can be seen in Figure 2.5.

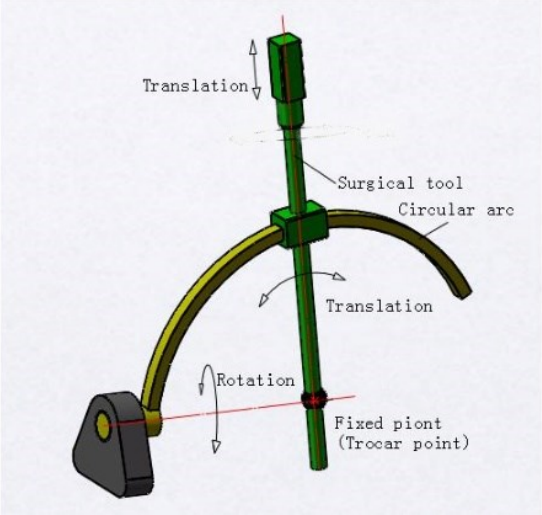

Figure 2.5. 3-dof circular tracking arc RCM mechanism
(Source: Yun-ping & Fan, 2015)

Also, parallelogram-based RCM mechanisms are widely used. Parallelograms provide one dof around a pivot point and different types of parallelograms can be constructed. Most simple planar parallelogram-based RCM linkages consist of 5 moving links and 8 or 7 joints, as shown in Figure 2.6. Figure 2.6-a and b are single-dof over-constrained mechanisms. In general, such RCM mechanisms have many advantages, such as a wide range of motion, a simple structure, and actuation can be performed by a motor located on the base. However, the singularity of parallelogram connections and lack of absolute rigidity caused by too many revolute joints are disadvantages (Kuo & Dai, 2009).

In parallelogram-based mechanisms, just like in circular arc mechanisms, it is sufficient to provide a construction in which the base link can rotate around an extended axis, to achieve a second dof. In this way, 2-dof can be obtained around the pivot point, as in Figure 2.7.

To get the third dof around RCM, a prismatic joint can be added in series on the distal link. In Figure 2.8, a 3-dof (2R1T) parallelogram-based mechanism is shown, where the translational motion through the pivot point is provided by a doubled-slider crank mechanism.

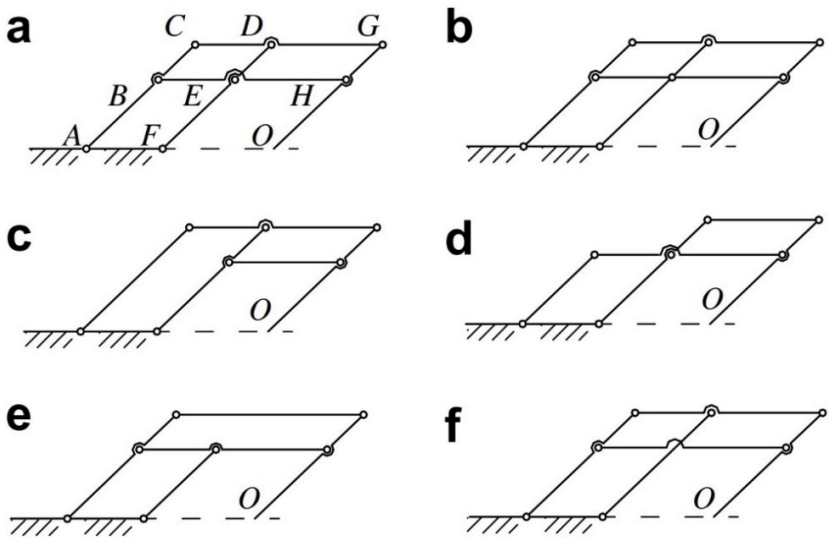

Figure 2.6. 1-dof RCM parallelogram in different configurations

(Source: Xu, Pei,& Yu, 2007)

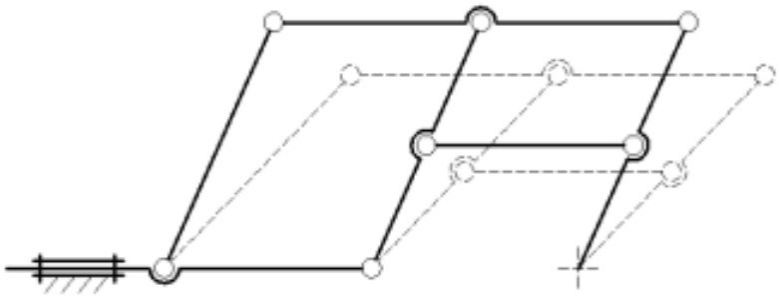

Figure 2.7. 2-dof RCM parallelogram-based mechanism

(Source: Chen et al., 2015)

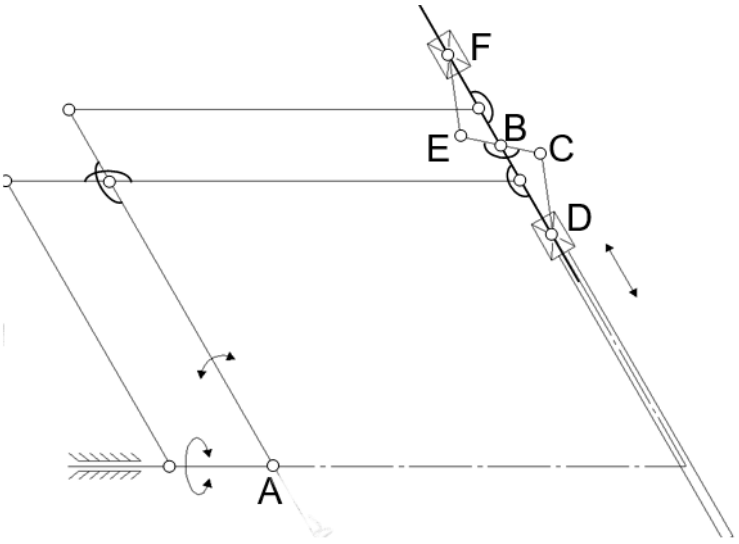

Figure 2.8. 3-dof (2R1T) RCM mechanism based on parallelogram

Another approach to obtain an RCM mechanism is using spherical linkages where all the joint axes intersect a certain point in space. The intersection point of all joint axes refers to the pivot point (Kuo & Dai, 2009). One of the patented examples is the 5-bar spherical linkage used in endoscopy operation as shown in Figure 2.9.

Synchronous belt transmission is a remote center of motion mechanism with the same kinematic structure as the parallelogram RCM mechanisms. It can be seen in Figure 2.10, which has 1-dof RCM. However, because of constructional issues, parallelogram mechanisms are more suitable for obtaining a 2-dof RCM.

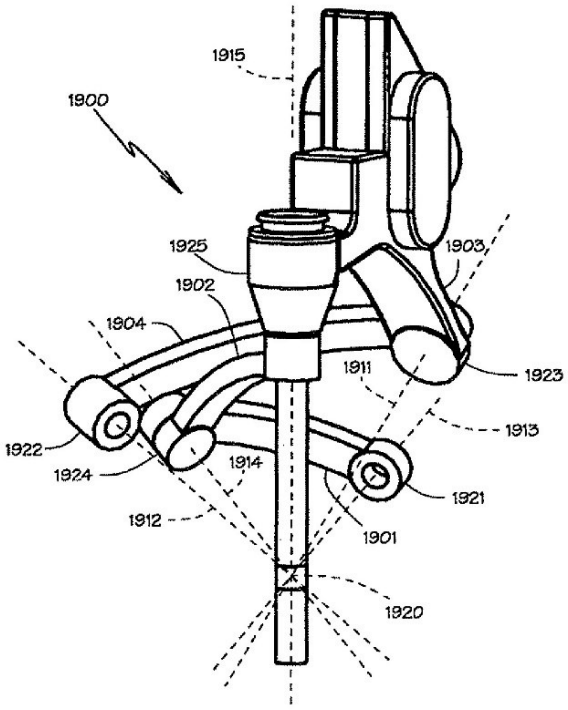

Figure 2.9. 5R spherical linkage for endoscopy
(Source: Schena, 2007)

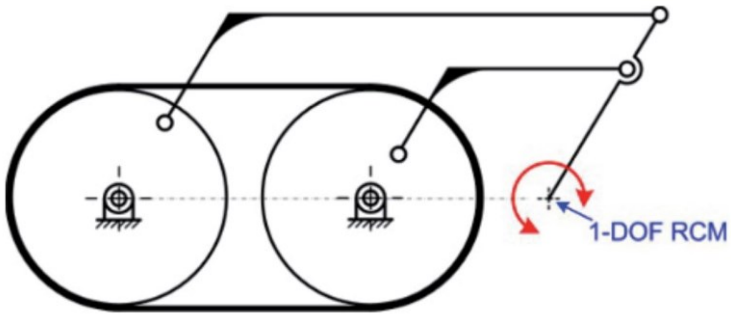

Figure 2.10. 1-DOF RCM design with synchronous-belt
(Source: Kuo & Dai, 2009)

The RCM mechanisms mentioned above mostly have hybrid and serial kinematic structure. Apart from this, RCM can also be obtained with parallel mechanisms. The use of parallel manipulators has some advantages and disadvantages. Pivot flexibility and increasing maneuverability are advantages. But there are disadvantages, such as complex control algorithms and tautening because of having more joints in general. Due to these adverse effects, they cannot be preferred for some medical and minimally invasive surgery applications (Kuo & Dai, 2009).

An example of a parallel manipulator with RCM to be used in the MIS operations can be given as a study by Yaşır et al. (2020). The kinematic structure of the manipulator consists of 3 legs (2URRR-URR) as shown in Figure 2.11. The three leg planes intersect along a line, which intersects a base plane at the pivot point. The manipulator has a mechanical RCM and a 2R1T motion pattern.

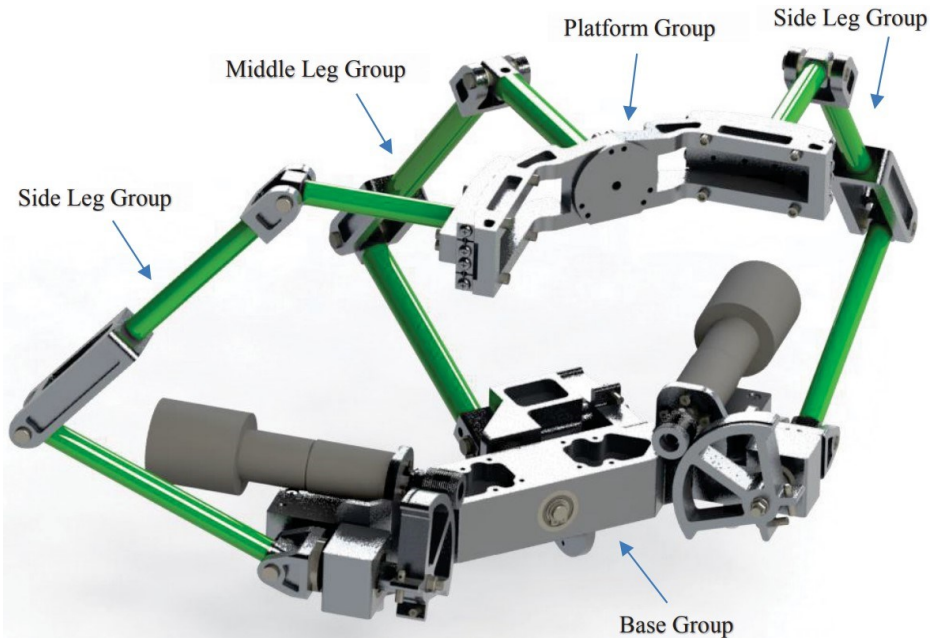

Figure 2.11. 2URRR-URR parallel mechanism with RCM for minimally invasive transnasal surgery applications (Source: Yaşır et al., 2020)

Figure 2.12 shows another example of the parallel mechanism with RCM used in MIS operations; this mechanism assists the surgeon during prostate biopsies. It is designed to be used with one hand. It has three limbs, two UPPR and a virtual UP limb, and has a 2R1T motion pattern. 2-dof provides the attitude adjustments around the RCM point, and the remaining dof feeds the needle through the RCM point (Jiang et al., 2023).

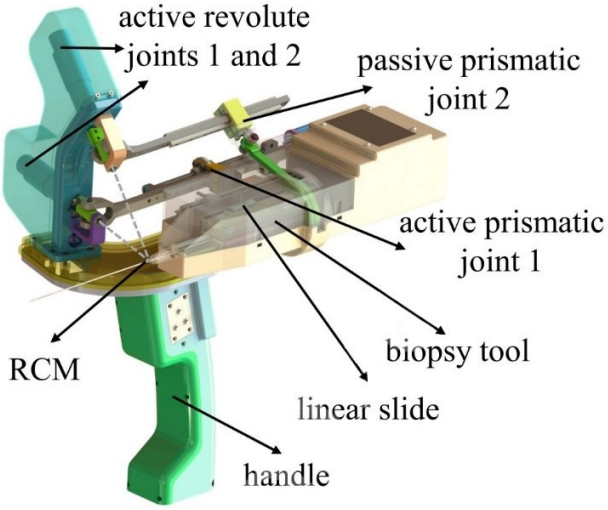

Figure 2.12. 2UPPR-UP parallel RCM mechanism
(Source: Jiang et al., 2023)

2.3 Balancing

The last topic to be discussed in the literature is balancing. Dynamic balancing may be required for a mechanism which works at high acceleration. Surgical robots work in relatively small workspaces and do not work with high accelerations. Also, it must maintain its position when the power supply to the actuators is interrupted for a safe and successful operation. Hence a statically balanced manipulator is enough to meet the specified requirements. Statically balancing a system requires at least two different potential energy storage elements that move so that the sum of their potential energy remains constant. These elements can be either spring or mass (Herder, 2001).

Also, another topic of interest is the inherently balanced mechanism design, which refers to setting kinematic parameters and mass distribution to meet static or dynamic balancing conditions during the kinematic design of the mechanism. This topic is examined separately as subsection 2.3.1.

In the literature, there are many different studies that enrich and diversify the balancing principles and methods for different types of mechanisms. There is no unanimous categorization of these methods, so balancing methods are examined with unreferenced categorization.

Balancing a mechanism by the addition of mass and inertia is one of the most well-known methods in the literature. In this method, the distribution of mass of the mechanism is manipulated to meet the required balancing condition by locating extra

masses at certain positions. The use of counter-mass is simple and can balance any mechanism theoretically, but for a feasible balancing solution, the design process must be considered. Another method can be defined as a hybrid approach that uses both counter masses and springs. Basically, using springs instead of counter masses reduces the total mass of the mechanism, which is used in many applications when the total mass is a concern (Agrawal & Fattah, 2004). An example of a hybrid method is the balancing of one leg of a parallel manipulator by using two counter masses and one spring, as shown in Figure 2.13.

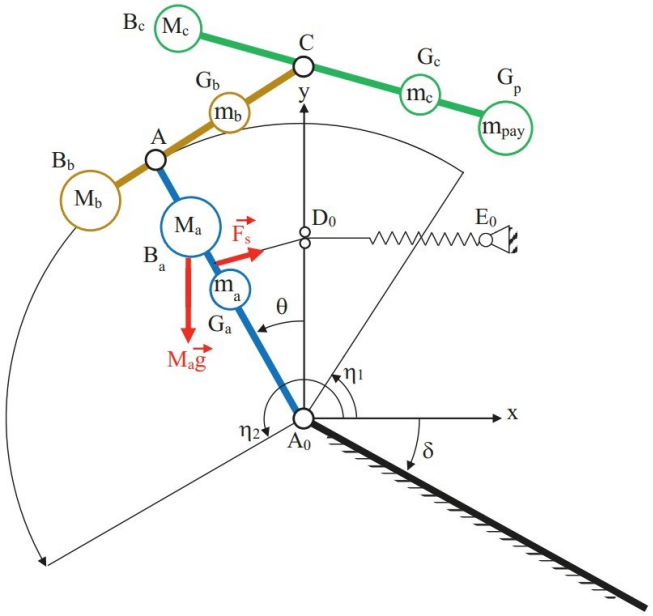

Figure 2.13. Balancing one leg of the parallel manipulator by using two counter masses and a spring (Source: Yaşır et al., 2019)

Another method is using duplicated mechanisms. Due to mirror symmetry, common CoM remains stationary. It is basically based on opposite movements of the links of the mechanism. The mechanism that is balanced in this way is found successful in areas such as different types of agricultural and automatic machines (Arakelian et al., 2005; Arakelian et al., 2000). As an example, balancing a double pendulum using mirror symmetric mechanisms is shown in Figure 2.14.

There are many other methods besides these methods: balancing linkages by using a cam mechanism and balancing by using auxiliary mechanisms such as parallelograms and pantographs. For more information about these methods, studies by Arakelian and

Smith about the history and types of balancing theory can be examined (Arakelian et al., 2000; Arakelian et al., 2005)

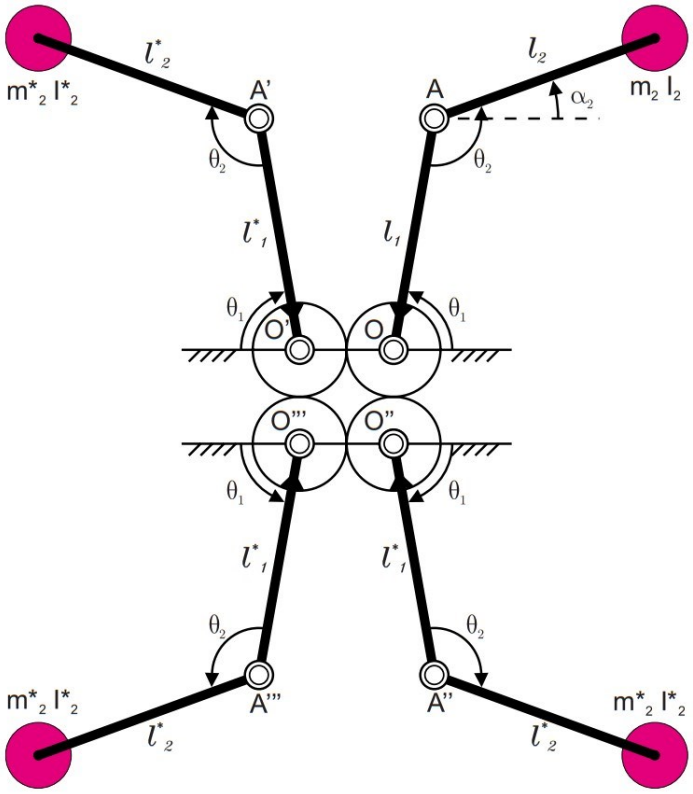

Figure 2.14. Balancing a double pendulum by using mirror symmetric mechanism duplicates (Source: Van der Wijk et al., 2009)

2.3.1 Inherent Balancing

It is important to consider balancing approaches during the design. Methods based on mass/inertia addition after the design of the mechanism may have disadvantages, such as having more mass and inertia than desired design and result not achieving a balancing at the desired level. Designing a mechanism by finding mass and length parameters in the design process is possible by various methods to ensure the balancing. The term inherently balanced mechanism means contributing all elements of mechanism to both motion and balance (Van der Wijk, 2014).

The theory used for designing a balancing mechanism during design goes back over 100 years. One of the oldest studies can be considered as the study of Fischer about principal vectors to provide to fix a common center of mass of all moving links at a point. The method is based on a balancing mechanism relative to each link with respect to a

point on the link, which is called the principal point. After that, the required balancing conditions are derived by using equations of the vector loop of principle points and the structural loop of the mechanism (Arakelian et al., 2000). Fischer used the method of principal vectors to understand the muscle forces of some parts of the human body, such as the leg and arm. Another study of Fisher is on the use of his methods for mechanisms to investigate shaking forces occurring on the base of a slider-crank mechanism and derive the necessary condition for shaking force balancing. Also, he applied this method to complex linkages with 6-to-20 links (van der Wijk & Herder, 2012).

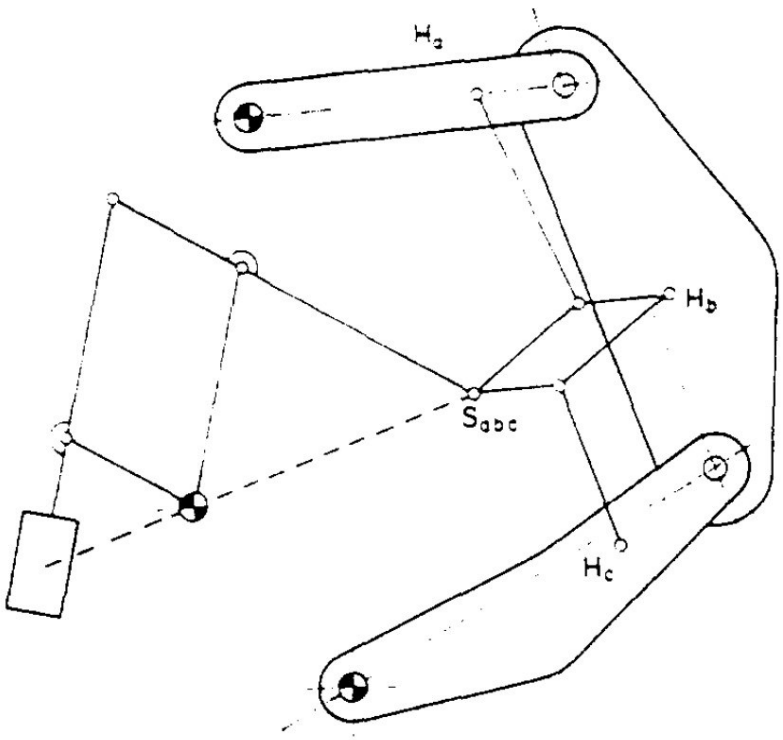

Figure 2.15. Keeping stationary CoM of a four-bar linkage by using pantograph and counter-mass,(Source: Hilpert, 1968)

The principle vector method has been applied by many other researchers and has become an approach for many studies, such as investigating shaking forces of a four-cylinder motor, finding a new method for investigating the CoM of linkages and more complex mechanisms, tracing CoM for linkages and etc. (Agrawal & Fattah, 2004). One of the important studies is keeping CoM of a four-bar linkage stationary with respect to its base by using a pantograph which is shown in Figure 2.15 and in this study conducted by Hilpert (1968), the principal vector method was used. Another important study is the

works of Agrawal and Fattah (2004), which is a hybrid method for gravity balancing of spatial robotic manipulators that include springs and auxiliary links and parallelograms as depicted in Figure 2.16. The methodology is applicable for n-link spatial serial manipulators and it demonstrated for 2- and 3-dof manipulators.

Figure 2.16. Gravity balanced two dof spatial serial manipulator
(Source: Agrawal & Fattah, 2004)

Van der Wijk and Herder (2009) show that Hilpert's approach can be applied to a delta robot. They show four possible solutions to obtain the stationary CoM for a force balanced delta robot. Figure 2.17-i shows a pantograph with counter-mass and other auxiliary linkages that can be used to keep CoM stationary. Figure 2.17-ii provides a solution with three counter masses and a pantograph with counter mass. Figure 2.17-iii demonstrates balancing in a conventional way, adding counter masses to each moving

link without adding any auxiliary linkage in the mechanism. Lastly, in Figure 2.17-iv, each leg is balanced with a 3D pantograph with counter mass.

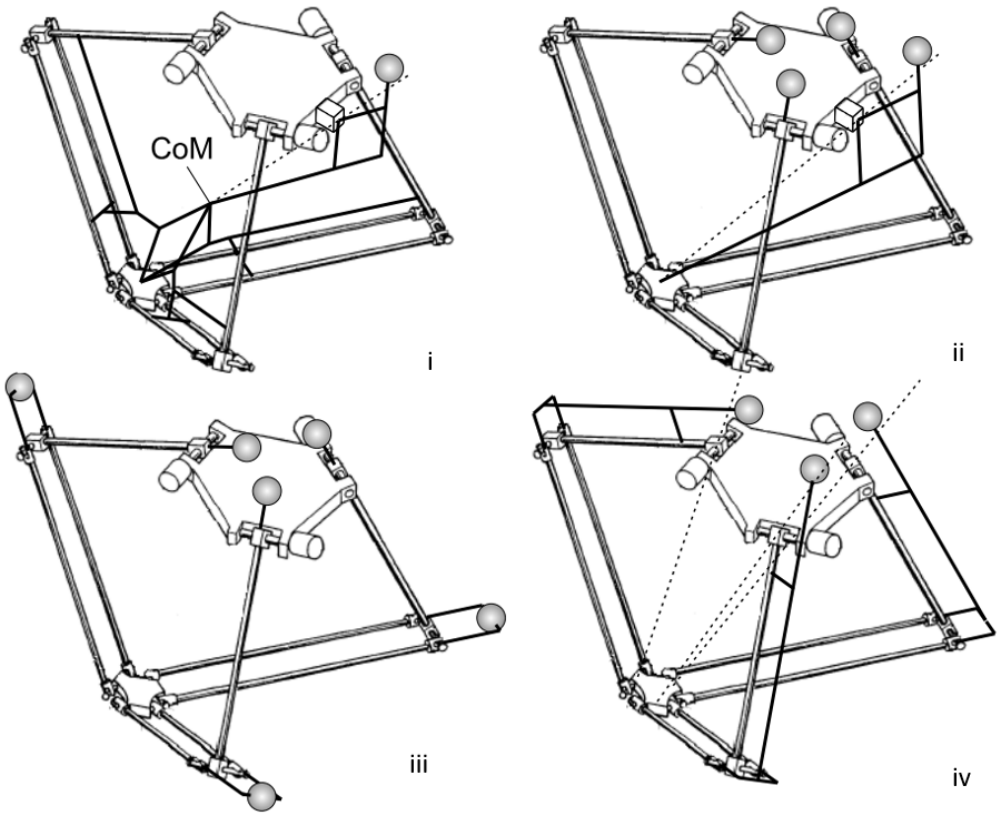

Figure 2.17. Force balancing options for a delta robot
(Source: van der Wijk & Herder, 2009)

Van der Wijk and Herder (2010) developed a more comprehensive method based on linear momentum by modifying the Fischer's approach that derives principal points and dimensions. This method is applied on three and five-body serial chains and is based on adding auxiliary links to construct parallelograms and pantographs in kinematic design in order to keep the CoM stationary with respect to the base. Figure 2.18 shows a force-balanced planar five-link serial chain.

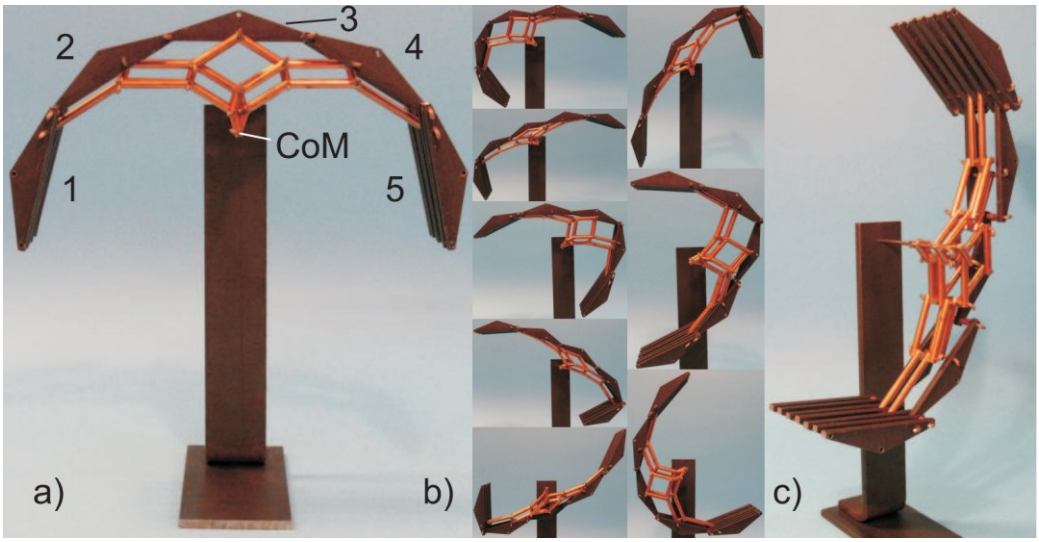

Figure 2.18. Force balancing planar five-body serial chain

(Source: van der Wijk & Herder, 2010)

CHAPTER 3

CONCEPTUAL DESIGN

In this chapter, mainly mechanically constrained RCM kinematic structures are addressed. The suitability of serial and hybrid kinematic structures are discussed. Additionally, some options for static balancing are evaluated. At the end of the chapter, the selected kinematic structure and the parameterized static balancing solution are given.

3.1. RCM Mechanism Design

RCM is mandatory for a mechanism to be used in MIS. RCM can be obtained in three ways: mechanically constrained, passive joints, and programmable (Sadeghian et al., 2019)

Programmable RCM uses a controller to obtain RCM around a specific point. While programmable RCM provides freedom in design, it makes the controller more complex, and in case of emergency such as electronic failure, it creates a weakness in security which is a problem for MIS.

Another way to obtain RCM is to locate a passive joint on a pivot point that provides predetermined freedom(s) around it. Also, using passive RCM provides flexibility in design, but it may cause tautening specifically for translational joints.

A manipulator with mechanical RCM is obtained by kinematically constraining the end effector to move around the pivot point. While they are safer than programmable RCMs, they provide more effortless movement than RCMs obtained by passive joints. An essential disadvantage of it is offering a limited design space. In the literature, there are many different types of RCM mechanisms such as circular tracking arc, parallelogram, spherical linkage, parallel manipulators, isocenters, synchronous belt transformation, etc. (Kuo & Dai, 2009).

In order to obtain 2R1T motion pattern, various RCM types and their kinematic structures are examined. Parallel mechanism solutions are classified by Yaşır and Kiper (2018). Her, only hybrid and serial kinematic structures will be examined. In this section, s refers to serial and p refers to parallel.

3.1.1. Serial Structure (s-s-s)

Serial manipulators have serial kinematic chains, linking each link to a frame or neighbor link by a single joint. Each actuation on joints is made independently and refers to a specific motion in the workspace. Significant advantages of this type of mechanism are as follows. Since it is decoupled, it is easy to control and has simpler kinematic and dynamic equations compared to mechanisms with parallel or hybrid kinematic structures.

3.1.1.1. Circular Tracking Arc

The circular tracking arc is a three-degree-of-freedom (dof) serial mechanism with kinematic structure R-R-P (R: revolute joint, P: prismatic joint) from base to end effector, respectively. As can be seen in Figure 3.1, the mechanism that has 2-dof RCM at point C, rotates the whole mechanism around the x-axis by the first revolute joint (point A0). In contrast, the second revolute joint (point A) provides rotation at point C on the axis perpendicular to the paper. The prismatic joint (point B) provides translational motion through point C. For more information about circular tracking arc and other 1-dof RCM mechanisms, the study of Zong can be examined. (Zong et al., 2008)

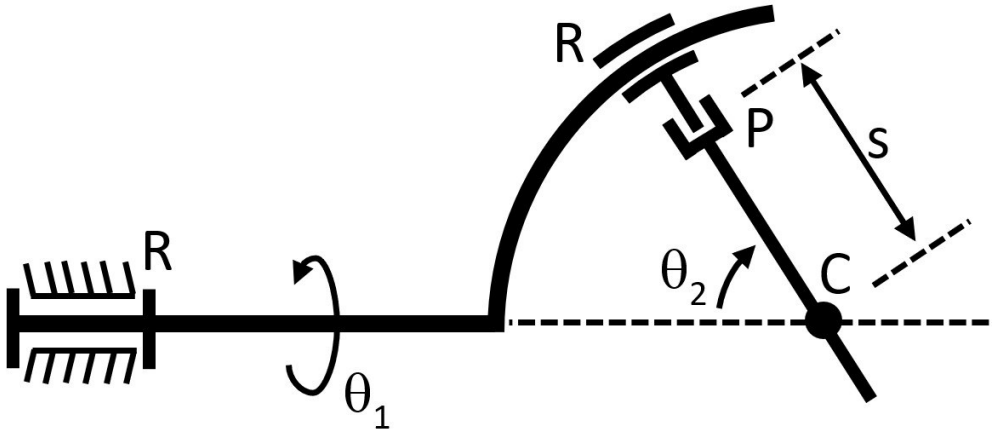

Figure 3.1. Circular Tracking Arc

3.1.1.2. Modified Circular Tracking Arc

Although the modified circular tracking arc has precisely the same kinematics as above, several changes must be made because of the working space criteria. The

mechanism must be located on the top of the patient's head, and the endoscope entrance must be done from under the head, as seen in Figure 3.2; the alpha angle indicates the entry angle of the endoscope.

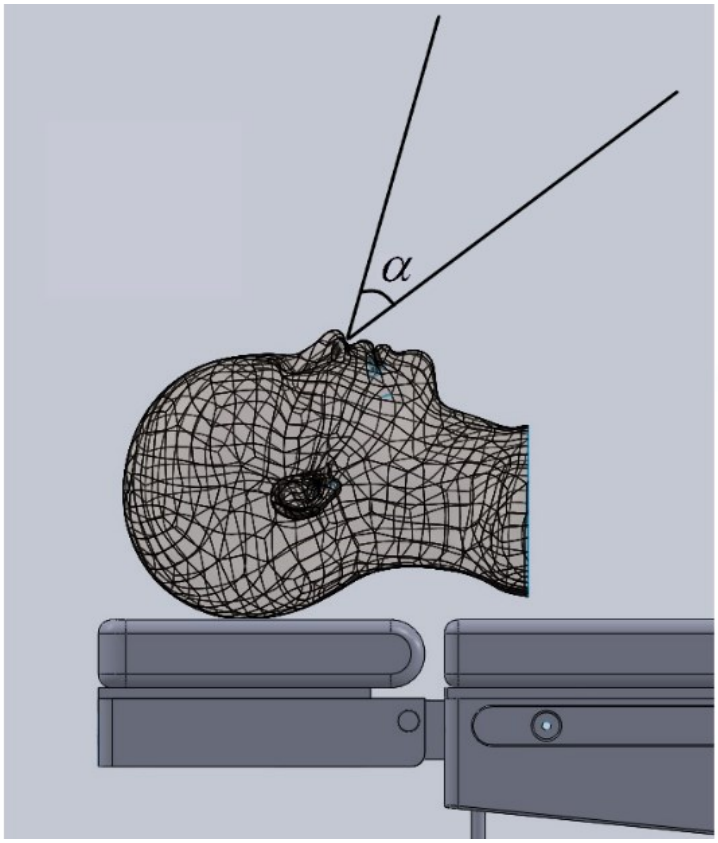

Figure 3.2. Head Model and Entrance Angles of Endoscope

The Circular tracking arc mechanism consists of 3 links and the third link is changed to meet the abovementioned criteria. The revised circular tracking arc can be seen in Figure 3.3.

3.1.2 Hybrid Structures

The hybrid kinematic structure is composed of both serial and parallel structures. In this type of mechanism with the advantages of two different structures, RCM is based on a parallel mechanism. All possible combinations are discussed, and feasible ones are listed below.

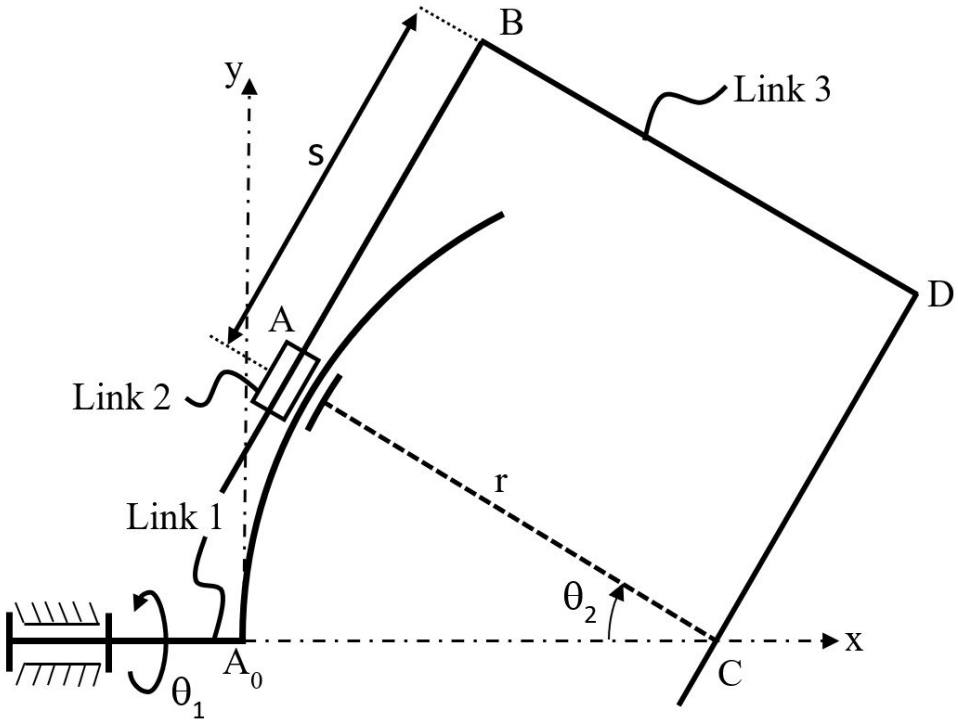

Figure 3.3. Modified Circular Tracking Arc

3.1.2.1 s-p-p structure

As seen in Figure 3.4, the first revolute joint is actuated by an actuator that serially connects the base and remaining parts. The second rotation is provided by a parallelogram RCM that connects the axis of the whole mechanism with the translational joint. A coupled slider-crank mechanism is selected for the last dof in this configuration. The first and second rotation values are represented by θ1 and θ2, respectively, while the translational value is represented by s. Generally balancing, sliding masses are more difficult to balance than rotating masses. So, using a symmetrically coupled slider crank along the endoscope axis, is one of the solutions that can be used.

3.1.2.2. p-p-p structure

This configuration is based on the execution of each dof by a closed-loop mechanism. When the manipulator mentioned above is discussed, if the actuator connects to a closed loop mechanism such as a four-bar linkage which provides rotational motion along the first axis, the s-p-p manipulator becomes p-p-p. Instead of using the first revolute joint on the first axis in the s-p-p configuration specified in Figure 3.4, a four-

bar linkage placed on a plane that intersects the plane where the parallelogram is located will give a p-p-p configuration.

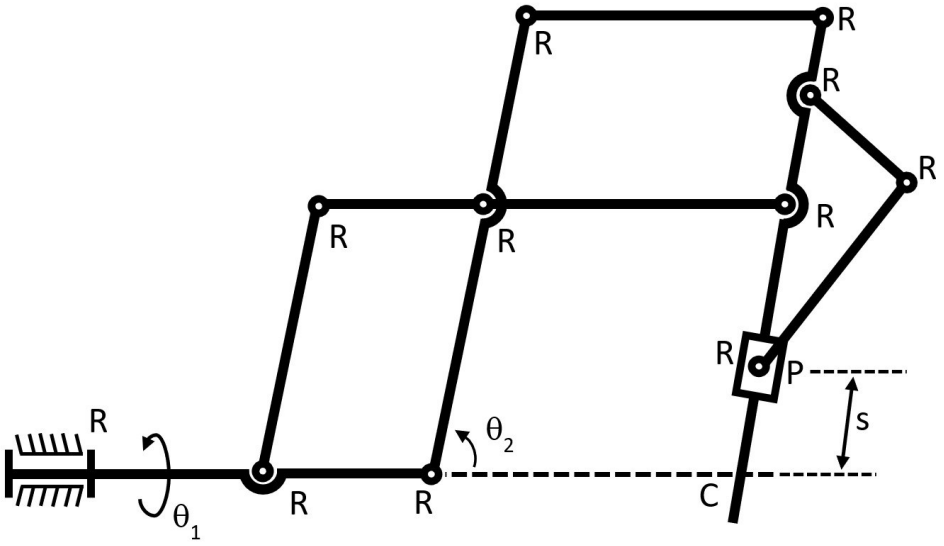

Figure 3.4. Combination of s-p-p, an example of RCM Hybrid Mechanism

3.1.2.3 s-2p structure

In this configuration, two translational actuators will move simultaneously inside the parallelogram RCM, which becomes 2-dof, as shown in Figure 3.5. Therefore, while this parallelogram provides a rotation about an axis that is perpendicular to the paper, which is denoted by θ2, it also glides endoscope by the amount of s along pivot point C. Rotation about 1st axis, which refers to θ1, is performed by the first motor which is connected serially, as mentioned configurations above. Also, in Figure 3.6, a prototype of this configuration can be seen (Davies et al., 2000).

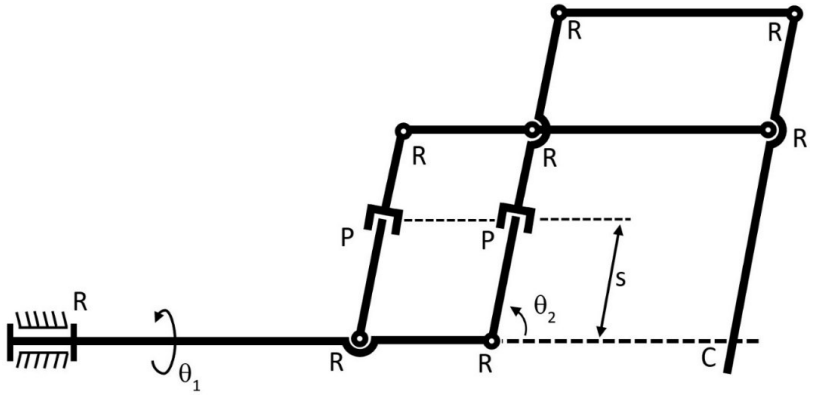

Figure 3.5. Configuration of s-2p with parallelogram based RCM

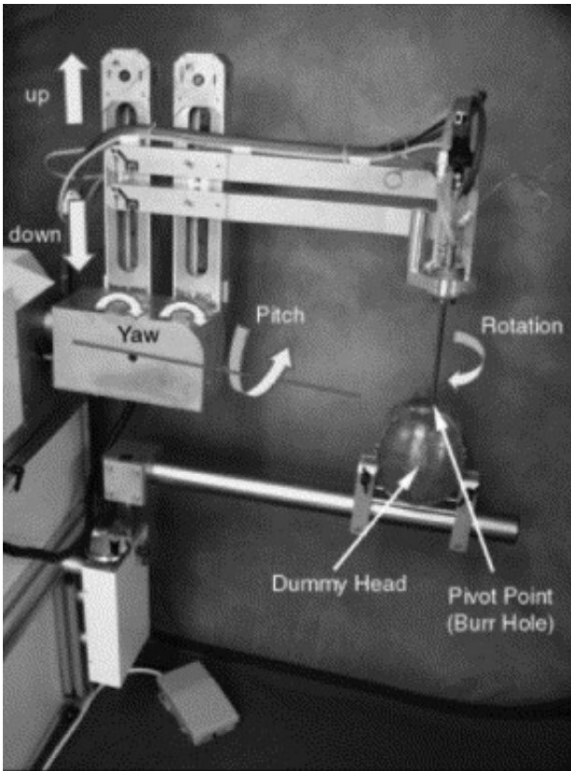

Figure 3.6. Neurobot
(Source: Davies et al., 2000)

3.1.2.4. s-p-s structure

Configuration of s-p-s is comprising serially connected first rotational (refers to θ1) and translational joint (refers to s). Rotation freedom between two joints is created by the parallelogram that provides RCM as mentioned mechanisms above. An example of this is shown in Figure 3.7. Adding a serial sliding joint to the mechanism has adverse effects on balancing. Therefore, a closed-loop mechanism can provide a translational motion instead of directly connecting to a linear actuator. An example of using a closed loop for translational dof can be the symmetrically coupled slider-crank mechanism in the s-p-p section mentioned above.

3.1.2.5 p-p-s structure

As mentioned in the p-p-p section, If the first rotation is performed by a closed-loop mechanism rather than directly connected to an actuator, the configuration will be changed from s-p-s to p-p-s.

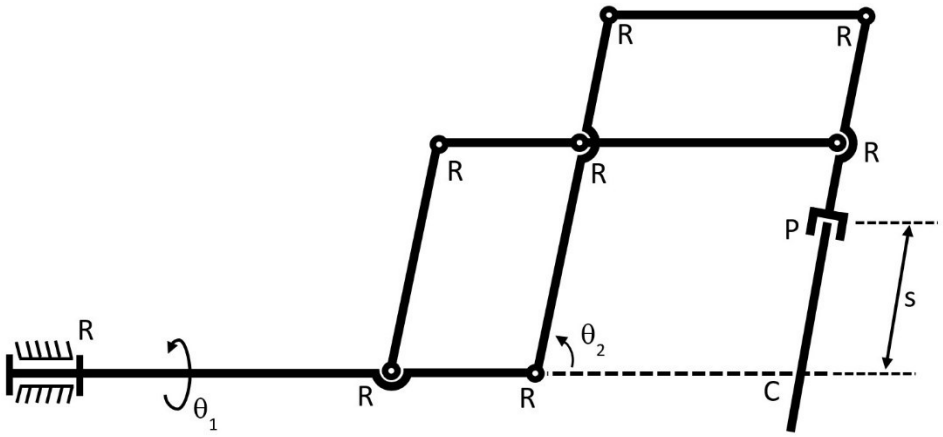

Figure 3.7. Combination of s-p-s with parallelogram based RCM

3.1.2.6 Remaining combinations: p-s-s, 2p-s, p-s-p, s-s-p

Since the parallelogram-based RCM mechanisms require a parallelogram for the second rotation about the pivot point, a serial joint for the second dof is impossible to construct. Thus, p-s-s, p-s-p, and s-s-p are not suitable to design. Also, parallelogram-based RCM 2p-s configuration is impossible to obtain because being parallelogram is one dof.

3.1.3 RCM with passive joint (pRCM)

RCM with a passive joint uses a passive joint with specific dof(s) according to the desired motion pattern on the pivot point. While this type of RCM provides flexibility during the kinematic design, forces exerted on the passive joint may cause problems.

3.1.3.1. $\lambda = 5$ Design

One of the RCM mechanisms that can be obtained using passive joints is shown in Figure 3.8. While the sum of each freedom is 8, there are three dofs (2R1T) because of SP (spherical and translational) passive joint at the pivot point. Here λ stands for the mechanism space dimension. For $\lambda = 5 < 6$, we have an over-constrained mechanism. The mechanism with $\lambda = 5$ design uses a parallelogram joint (PA) which has one dof. In the mechanism with serial kinematic structure, three dofs are RRP, represented by θ_1, θ_2, and s, respectively.

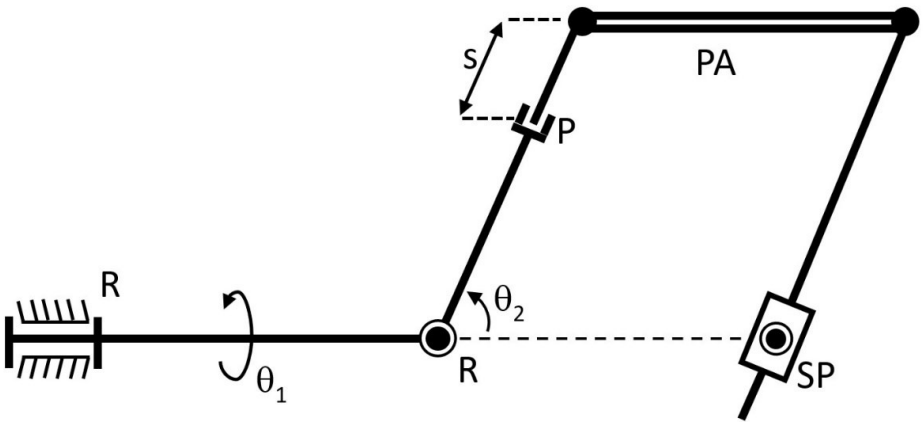

Figure 3.8. An example of using passive joint, λ = 5 Design

3.1.3.2. λ = 6 Design

Another pRCM mechanism can be designed, as shown in Figure 3.9. For this mechanism, the sum of each joint dof is 9, while there are 3-dof around the pivot point, as in the λ = 5 design. In the mechanism, which has a serial structure, all the active joints are prismatic, and the passive joints are the universal joint (U) and SP joint.

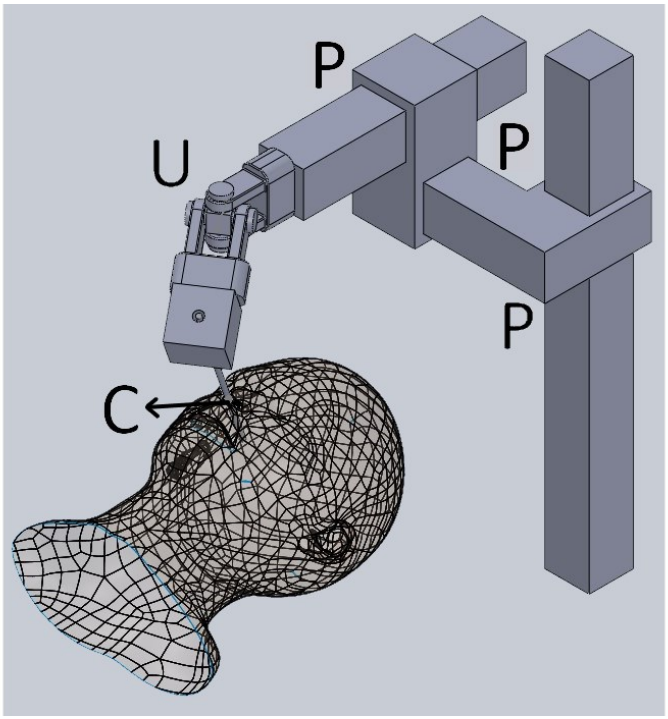

Figure 3.9. An example of using passive joint, λ = 6 Design

Evaluating all design alternatives presented in this section, the serial solution depicted in Figure 3.3 is selected for the detailed design considering its simple kinematic structure and ease of balancing. In the following section, we address alternative balancing solutions.

3.2. Balancing Options

As specified in section 2.3, only static balancing options are focused on. Also, the planned design is expected to have a serial or hybrid kinematic structure to be compared with the previously designed parallel manipulator by Yaşır et al. (2020). Various balancing methods are discussed for hybrid and serial kinematic structures.

3.2.1 5R Design

The planar 5R mechanism, which is shown in Figure 3.10, has 2-dofs. A directly connected actuator provides rotation (θ_1) about first axis. The second rotation and translation are based on 2-dofs of the 5R mechanism, which are θ_2 and θ_3. The below mechanism has pRCM, a passive joint located on the pivot point with 4-dof (3R1T). One of the disadvantage of this mechanism is the control of the 5R planar mechanism, which should be driven by two different actuators and the minimization of the loads exerted on the 3R1T passive joint.

3.2.2 Symmetric Mechanism

Using a symmetric mechanism is one of the primary methods that can be used if the constraints related to mass and workspace are flexible. In Figure 3.11, the rotation about first axis is provided in the same way as mentioned above examples. Rotation about the second axis is performed by a coupled slider-crank mechanism that is symmetric about the first axis. Also, translational motion is based on a symmetric coupled slider-crank mechanism. This configuration is not suitable as it does not satisfy the design requirements regarding mass and working space.

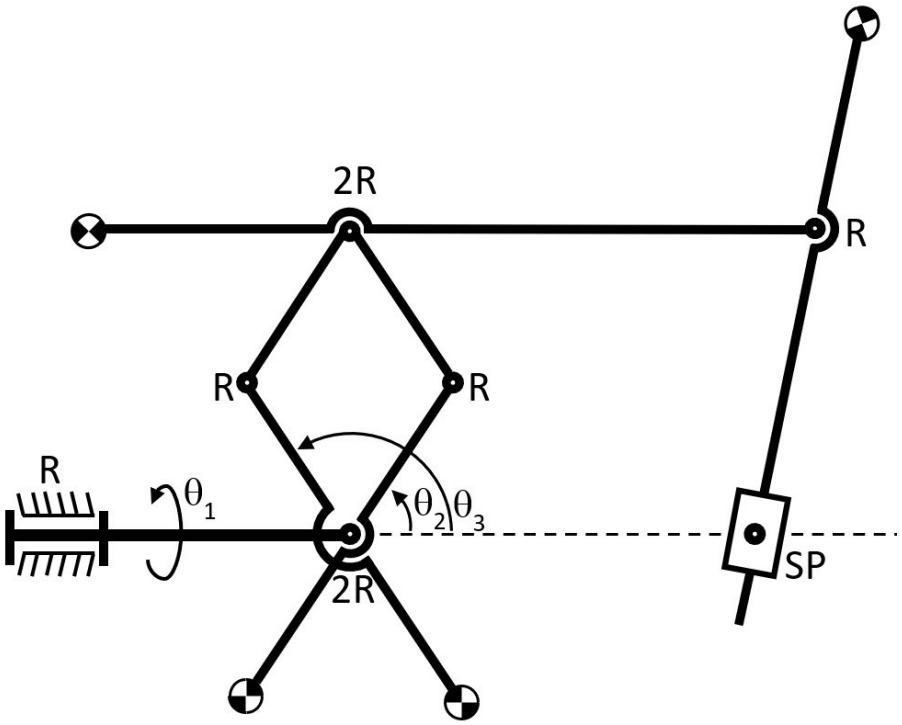

Figure 3.10. Using 5R solution

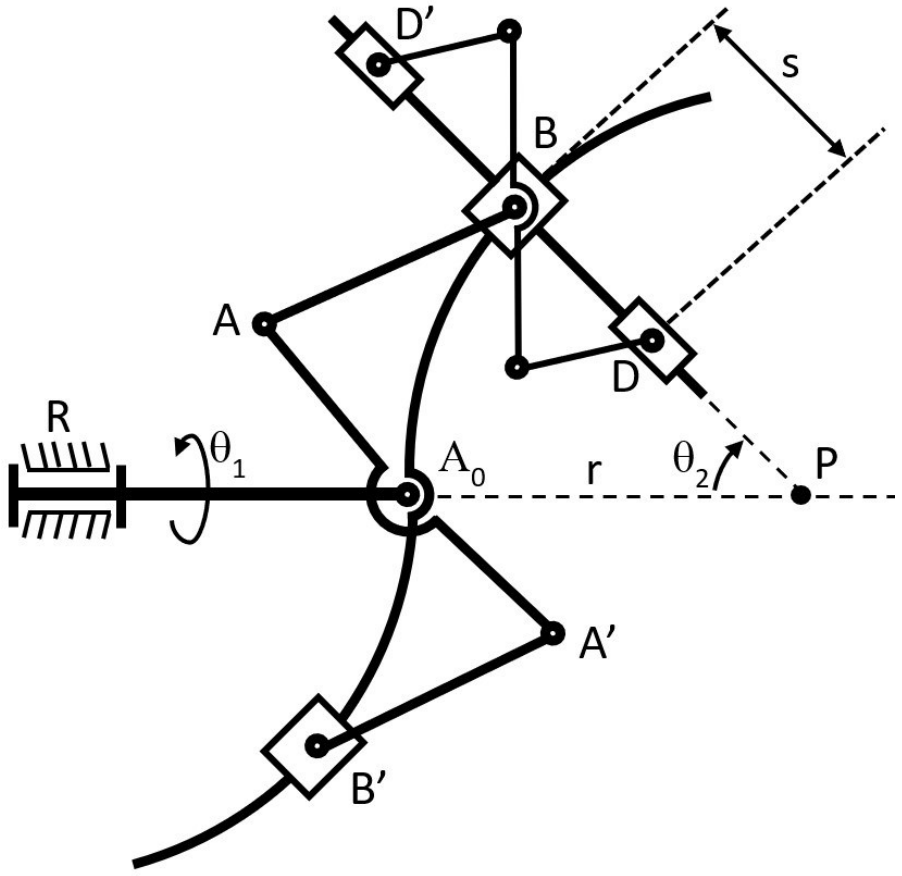

Figure 3.11. Symmetrical RCM mechanism

3.2.3 Using Passive Closed Loops

Serial mechanisms are usually balanced by considering each relatively moving mass individually. One of the simplest examples of this can be shown as the balancing of a 2R or 3R robotic arm. So, one of the methods that can be used in the circular arc-based mechanism shown in Figure 3.3 is to balance each mass by using passive closed loops. The moving masses of the mechanism can be balanced in two ways: by using springs or masses.

3.2.3.1. Balancing Using Springs

The general solution for spring balancing is shown in Figure 3.12. This solution has two different closed loops, and each loop balances a specific part of the mechanism. The primary mechanism, which is R-R-P, consists of 3 links. The mass of link 2 is denoted by m_2 and it can be traced by a single dof mechanism. Therefore, it can be balanced by using a parallelogram and spring which are represented in orange. Link 3 can be traced by a 2-dof linkage and mass of it is denoted by m_3. So, link 3 can be balanced by using a pantograph and two springs which are shown in blue in Figure 3.12. While E_0, G_0, and F_0 are points where one end of a spring is connected to the fixed link, whereas E, G, and F are the points where the other end is connected to the links of the passive closed loops. Thus, the closed loop of link 2-parallelogram and link 3-pantograph has a stationary CoM xy-plane. In order to statically balance these two closed loops around the x axis, counter masses for both of them can be used. Remain link is not statically balanced around the x axis is the circular arc (link 1) and it can be balanced using either mass or spring.

3.2.3.2 Balancing Using Counter-Mass

First, a statically balanced mechanism requires force balancing during motion which requires rate of change of linear momentum to be zero, as shown in equation 3.1.

$$\vec{F}_{net} = \frac{d\vec{P}}{dt} = \vec{0} \tag{3.1}$$

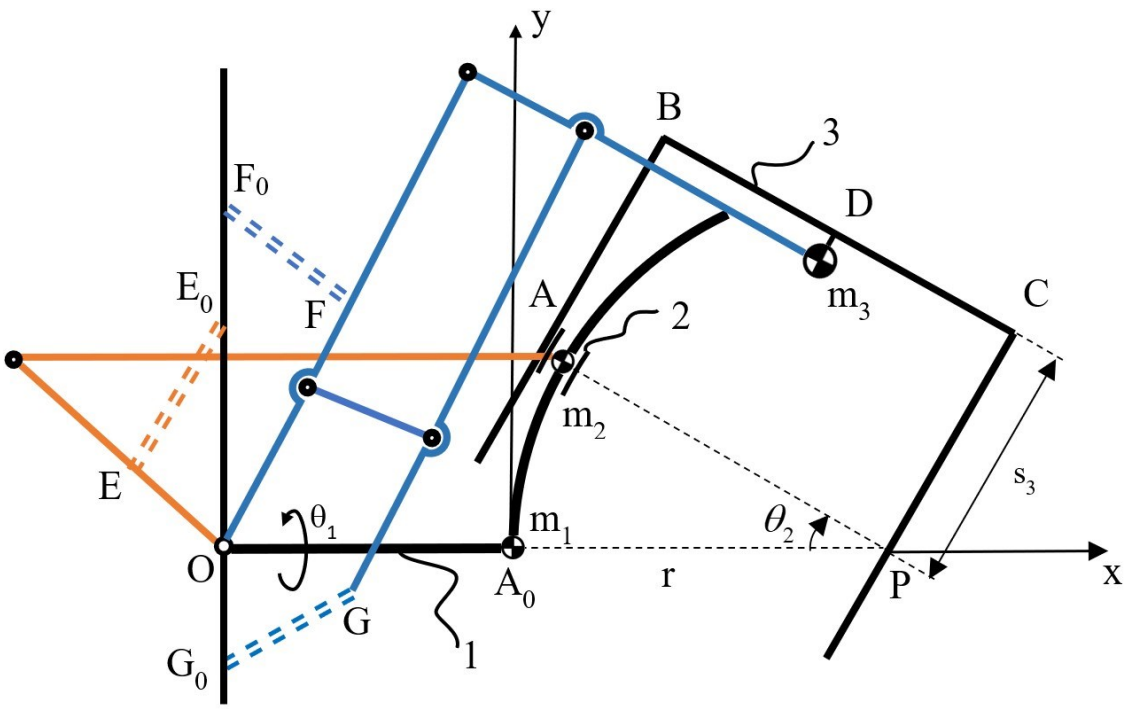

Figure 3.12. General solution of the spring balancing

Another way to reach static balancing is by writing the potential energy equation of each link and equating the sum of the change in potential energy to zero, called gravity compensation in literature (Lu et al., 2011). The equation 3.2 explains the gravity-compensated mechanism, where U is the total potential energy.

$$\frac{dU}{dt} = 0 \tag{3.2}$$

The pantograph mechanism is a planar 2-dof mechanism that tracks CoM of three masses. This mechanism is pivoted on the ground at a point O. Various methodologies can achieve static balancing around that point, such as linear momentum, potential energy equations, etc. The important thing is connecting the manipulator with the mechanism, making construction so that the center of the fixed joint O and the pivot point must be aligned on the same axis as the first motor shaft. All parametrization and derivations are made based on Figure 3.13.

The location of the CoM of each link and the combination of link and external masses are symbolized as points that are symbolized as follows. M_3 and M_4 refer to locations of CoM of shortest two links; M_c and M_e refer to positions of CoM of the longest two links with counter masses and endoscope mass respectively. Also, m_3 and m_4 are

masses of shortest links as seen in Figure 3.13, m_e and m_c are masses of longest two links with endoscope and counter mass respectively. Lastly, naming of lengths that defines distances between CoM and joints as follows. $|OC| = a_4$, $|OB| = a_3$, $|OM_4| = l_4$, $|OM_3| = l_3$, $|CM_c| = l_c$ and $|BM_e| = l_e$.

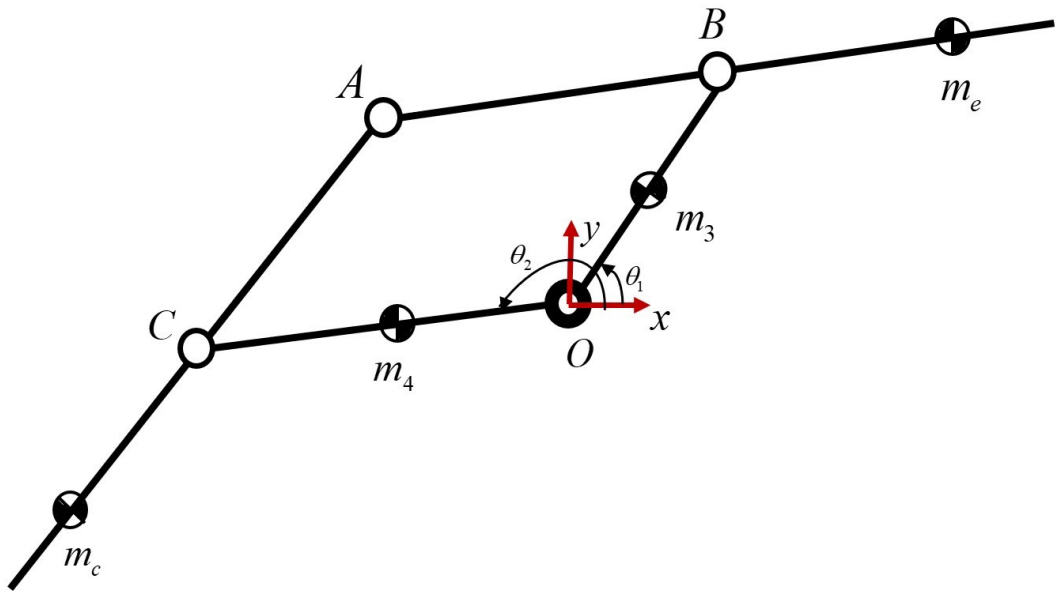

Figure 3.13. Pantograph sketch

Both total potential energy and linear momentum approaches mentioned above give the same balancing condition for gravity compensation. Throughout the derivation, sθ refers to sin(θ) and cθ refers to cos(θ). Total potential energy of the parallelogram can be written as equation 3.3. By rearranging equation 3.3, equation 3.4 is obtained.

$$\sum U = \mathrm{m}_3 l_3 \mathrm{s}\theta_1 + \mathrm{m}_4 l_4 \mathrm{s}\theta_2 + \mathrm{m}_e a_3 \mathrm{s}\theta_1 - \mathrm{m}_e l_e \mathrm{s}\theta_2 + \mathrm{m}_c a_4 \mathrm{s}\theta_2 - \mathrm{m}_c l_c \mathrm{s}\theta_1 \tag{3.3}$$

$$\sum U = [\mathrm{m}_3 l_3 + \mathrm{m}_e a_3 - \mathrm{m}_c l_c]\mathrm{s}\theta_1 + [\mathrm{m}_4 l_4 + \mathrm{m}_c a_4 - \mathrm{m}_e l_e]\mathrm{s}\theta_2 \tag{3.4}$$

Since the total potential energy must be constant, values in square brackets in the equation 3.3, must be equal to zero. Therefore, balancing conditions for the pantograph can be derived as equation 3.5.

$$m_c l_c = m_3 l_3 + m_e a_3 \tag{3.5}$$

$$m_e l_e = m_4 l_4 + m_c a_4 \theta_2 \tag{3.6}$$

Let m_t denote the total mass which slides on the circular arc. The parallelogram is a planar one-dof mechanism that can track CoM through a circular arc. Two of the links of this mechanism are links of the RCM mechanism. All parametrization and derivations are realized according to Figure 3.14, where only the two balancing links are shown.

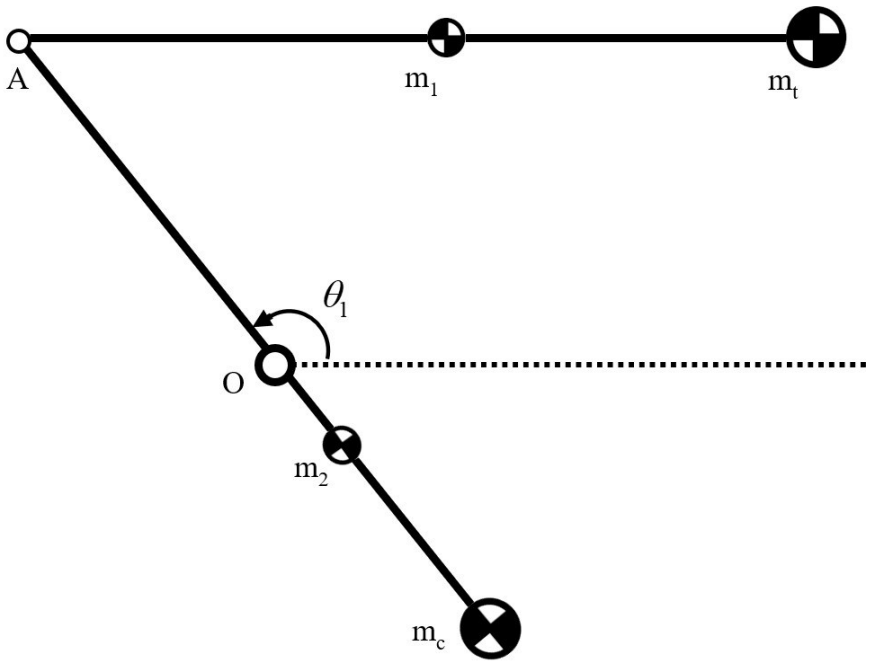

Figure 3.14. Sketch of the parallelogram links

Since a parallelogram has one dof, all masses were modeled separately. The coordinates of each CoM are symbolized as a point named as follows. M_1, M_2, M_c and M_t refer to locations of CoM of link1, link2, counter mass and target mass respectively. All length parameters (distance between the CoM and joints) represented as $|OA| = l_a$, $|OM_c| = l_c$, $|OM_2| = l_2$, $|AM_1| = l_1$, $|AM_t| = a_1$ and $|AM_c| = a_2$. Also, mass parameters for link 1, link 2, counter mass and target mass are m_1, m_2, m_c, m_t.

While both linear momentum and potential energy equations give the same results for the pantograph, they give different balancing conditions for the parallelogram. Since gravity compensation is desired, potential energy equations are enough to obtain

balancing conditions. Based on Figure 3.14, total potential energy of the links can be written as equation 3.7

$$\sum U = [(\mathrm{m}_1 + \mathrm{m}_t)l_a - (l_2\mathrm{m}_2 + l_c\mathrm{m}_c)] \tag{3.7}$$

Since the total potential energy must be constant, values in square brackets in the equation 3.7, must be equal to zero. Therefore, balancing condition for the parallelogram can be derived as equation 3.8.

$$l_c\mathrm{m}_c = (\mathrm{m}_1 + \mathrm{m}_t)l_a - l_2\mathrm{m}_2 \tag{3.8}$$

Balancing conditions of the pantograph and parallelogram mechanism given by equations 3.5, 3.6 and 3.8. These equations have many parameters to optimize, link and mass parameters are selected by considering total mass and working space criteria.

3.2.4 Selected Kinematic Structure and Balancing Solution

The kinematic structure of the mechanism is selected as modified circular tracking arc (s-s-s). Derivation of the balancing conditions of the mechanism is performed during the kinematic analysis. Basically, the manipulator consists of three different links that perform relative motion to each other. These are links a, b and c in the kinematic scheme shown in Figure 3.15.

Joint parameters for the mechanism are θ_1, θ_2 and s can be expressed as follows: the first dof is rotation about x-axis of the whole mechanism, second dof is rotation of link 2 and link 3 about the pivot point (C) and the remaining dof is translation of link 3 along the tangent to the circular arc.

Balancing of the mechanism is simply tracking all moving links by auxiliary linkages and balancing each auxiliary linkage itself around the first revolute joint axis. While there are two links for position and orientation changes which are link 2 and link 3, there is one link to just orientation changes which is link 1. A pantograph can trace link 3, and a parallelogram for link 2. Therefore, a parallelogram and pantograph are used for the gravity compensation for these links. Remain link 1 is not balanced by another

linkage. It's constructional design is performed so that the mass center of link 1 is located on the A_0, as shown in Figure 3.16.

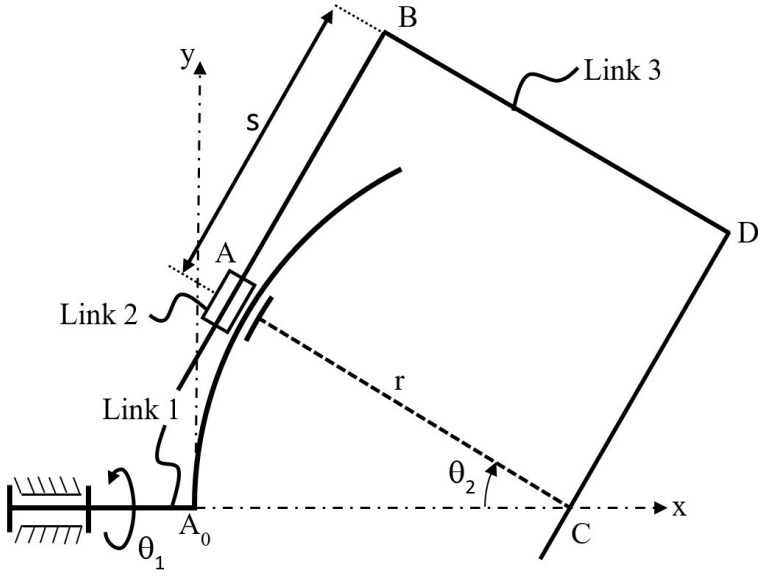

Figure 3.15. Modified circular tracking arc

All links and mass parameters for the auxiliary linkages as shown in Figure 3.16. Location of the CoM of the auxiliary links are M_i and their masses m_i for i = 1, …, 6. Link lengths are $|JA| = |OP| = a_1$, $|JM_1| = b_1$, $|JM_{C1}| = a_2$, $|OJ| = |PA| = r$, $|OM_2| = b_2$, $|OM_{C1}| = b_{C1}$, $|OI| = |HG| = a_3$, $|OM_3| = b_3$, $|OG| = |HI| = a_4$, $|OM_4| = b_4$, $|IM_5| = b_5$, $|GM_{C2}| = b_{C2}$, $|IE| = b_e$.

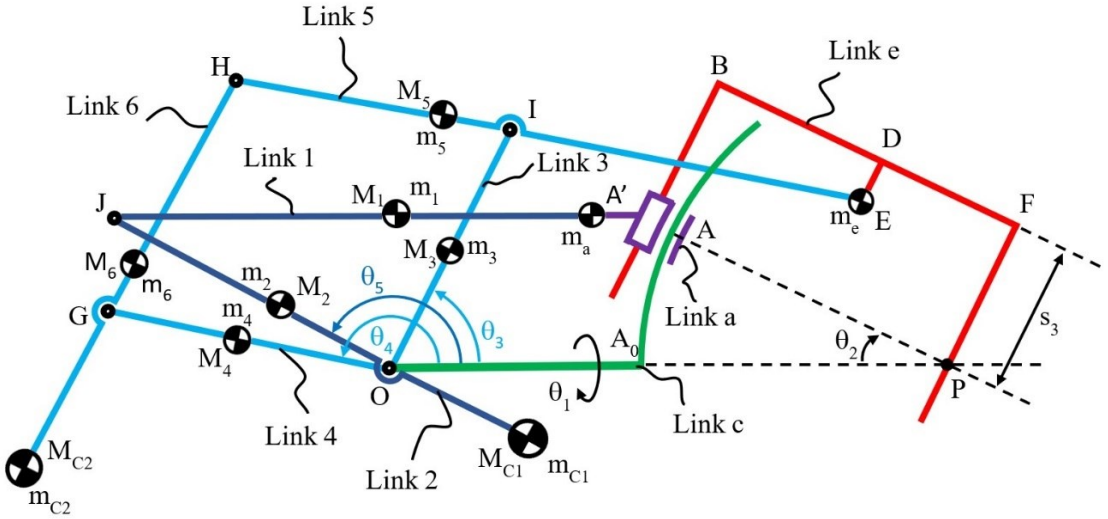

Figure 3.16. Kinematic scheme of counter mass solution for balancing the whole mechanism

For pantograph, only masses to be used in the balancing solution are shown in Figure 3.17, where only the pantograph and the RRP mechanism are presented.

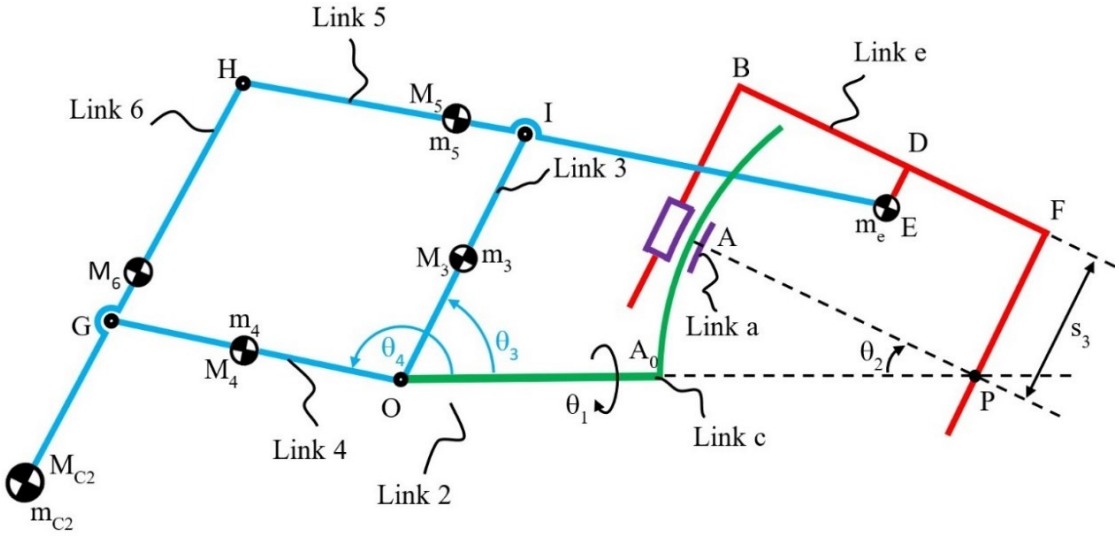

Figure 3.17. Kinematic scheme of the pantograph and RRP mechanism

The total potential energy of the pantograph and link e can be written in equation 3.9. By rearranging this equation, equation 3.10 is obtained.

$$\sum U = \mathrm{m}_3 b_3 \mathrm{s}\theta_3 + \mathrm{m}_4 b_4 \mathrm{s}\theta_4 + \mathrm{m}_e[a_3 \mathrm{s}\theta_3 - \mathrm{b}_e \mathrm{s}\theta_4] + \mathrm{m}_5[a_3 \mathrm{s}\theta_3 + \mathrm{b}_5 \mathrm{s}\theta_4] + \mathrm{m}_6[\mathrm{a}_4 \mathrm{s}\theta_4 + b_6 \mathrm{s}\theta_3] + \mathrm{m}_{c2}[\mathrm{a}_4 \mathrm{s}\theta_4 - \mathrm{b}_{c2} \mathrm{s}\theta_3] \tag{3.9}$$

$$\sum U = \mathrm{s}\theta_3[\mathrm{m}_3 b_3 + \mathrm{m}_e a_3 + \mathrm{m}_5 a_3 + \mathrm{m}_6 \mathrm{b}_6 - \mathrm{m}_{c2} \mathrm{b}_{c2}] + \mathrm{s}\theta_4[\mathrm{m}_4 b_4 - \mathrm{m}_e b_e + \mathrm{m}_5 b_5 + \mathrm{m}_6 a_4 + \mathrm{m}_{c2} a_4] \tag{3.10}$$

For the gravity compensation, potential energy must be constant through the motion of the mechanism. So, potential energy is not a function of joint parameters. Therefore, balancing conditions can be drawn from equation 3.10, as 3.11 and 3.12.

$$\mathrm{m}_3 b_3 + \mathrm{m}_e a_3 + \mathrm{m}_5 a_3 + \mathrm{m}_6 \mathrm{b}_6 - \mathrm{m}_{c2} \mathrm{b}_{c2} = 0 \tag{3.11}$$

$$\mathrm{m}_4 b_4 - \mathrm{m}_e b_e + \mathrm{m}_5 b_5 + \mathrm{m}_6 a_4 + \mathrm{m}_{c2} a_4 = 0 \tag{3.12}$$

For parallelogram balancing, isolated kinematic scheme can necessary kinematic parameters as shown in Figure 3.18. An important thing about kinematic scheme of the parallelogram is A′ and A are intended to be the same point, but in constructional design some amount of deviation occurred between them. Due to this offset, parallelogram solution will be valid for partially balancing. This offset can be compensated by friction during motion of the mechanism.

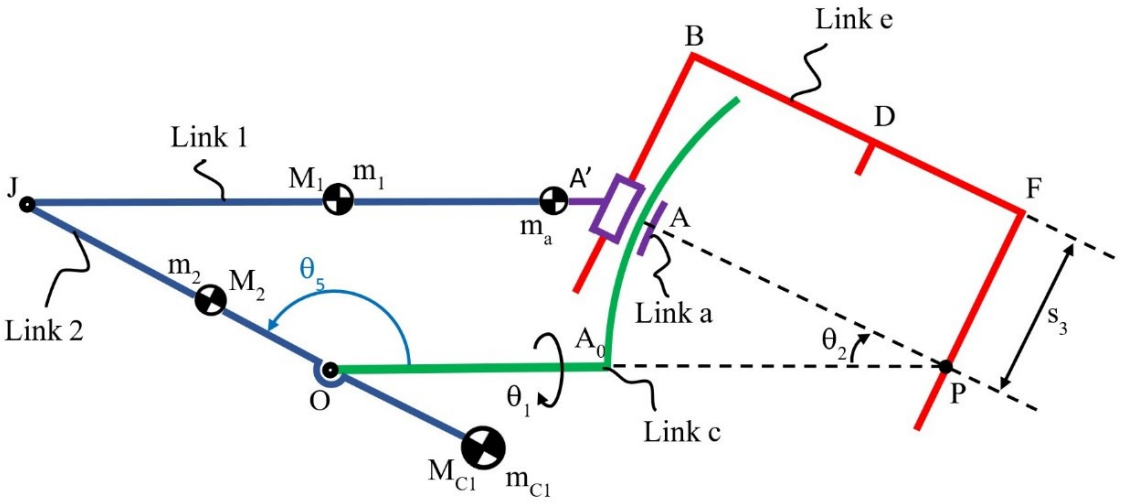

Figure 3.18. Kinematic scheme of the parallelogram and RRP mechanism

The total potential energy of the parallelogram and link a can be written as equation 3.13. By rearranging this equation, equation 3.14 is obtained.

$$\sum U = -\mathrm{m}_{C1} b_{C1} \mathrm{s}\theta_5 - \mathrm{m}_2 b_2 \mathrm{s}\theta_5 + (\mathrm{m}_1 + \mathrm{m}_a)\mathrm{r}\mathrm{s}\theta_5 \tag{3.12}$$

$$\sum U = \mathrm{s}\theta_5[-\mathrm{m}_{C1} b_{C1} - \mathrm{m}_2 b_2 + (\mathrm{m}_1 + \mathrm{m}_a)\mathrm{r}] \tag{3.13}$$

Just as in the pantograph, for the gravity compensation; potential energy must be constant through the motion of the mechanism. Therefore, balancing conditions can be drawn from equation 3.13, as 3.14.

$$-\mathrm{m}_{C1} b_{C1} - \mathrm{m}_2 b_2 + (\mathrm{m}_1 + \mathrm{m}_a)\mathrm{r} = 0 \tag{3.14}$$

Gravity compensation of both pantograph and parallelogram are performed in the MS Excel which are shown in Figure 3.19 and Figure 3.20. CoMs of these isolated parts of the mechanism are kept in a specified position to provide gravity compensation. These positions are origin for the pantograph and a point on the x-axis with variable value with respect to the θ_5. Calculated parameters are positions and values of the counter masses. These parameters are calculated from the free parameters, which refer to other lengths and masses of remaining links. The outputs of the Excel solutions are performed to obtain a balanced pantograph or parallelogram; therefore, obtaining suitable kinematic parameters is an optimization process. Kinematic parameters for both of them are evaluated by considering total mass and working space criteria of the manipulator.

link parameters [m]		distance parameters [m]		mass parameters [kg]		calculated parameters		Joint Parameters			
a_3	0.2	b_3	0.1	m_3	0.2	$m_{c2}b_{c2}$ [kgm	0.29	θ_3	118		2.05949
a_4	0.22	b_4	0.11	m_4	0.2	m_{c2} [kg]	1.372727	θ_4	208		3.63028
a_5	0.52	b_5	-0.1	m_5	0.3	b_{c2} [m]	0.211258	BALANCING CONDITIONS			
a_6	0.41126	b_6	-0.1	m_6	0.3	deg2rad		$m_4b_4 - m_eb_e + m_5b_5 + m_6a_4 + m_{C2}a_4 = 0$			
		b_e	0.3	m_e	1.2	0.017453		$m_3b_3 + m_3a_3 + m_5a_3 + m_6b_6 - m_{C2}b_{C2} = 0$			

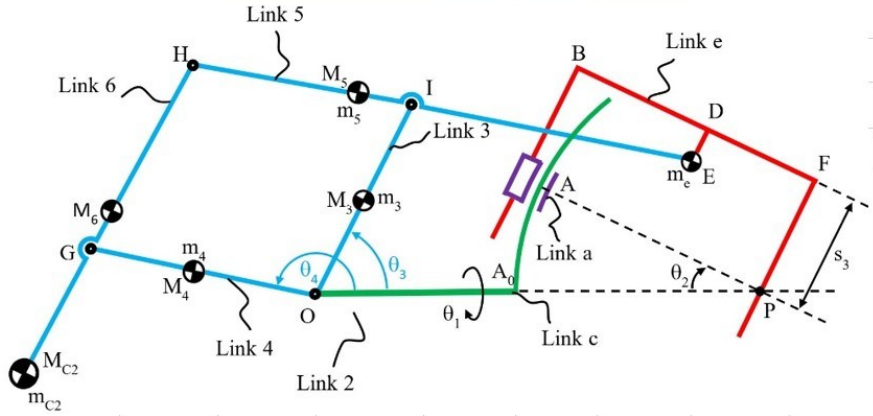

LINK PARAMETERS

$|OI| = |HG| = a_3,\ |OG| = |HI| = a_4$

$|OM_3| = b_3,\ |OM_4| = b_4$

$|OM_1| = b_{c1},\ |GM_{c2}| = b_{c2}$

$|GM_6| = b_6,\ |IM_5| = b_5,\ |IE| = b_e$

	O	G	H	I	E	M_{C2}	M_3	M_4	M_5	M_6	CoM
x	0	-0.194248	-0.2881428	-0.09389	0.17099	-0.09507	-0.046947	-0.09712	-0.0056	-0.1473	0
y	0	-0.103284	0.0733058	0.17659	0.31743	-0.28981	0.088295	-0.05164	0.22354	-0.19158	-6E-17

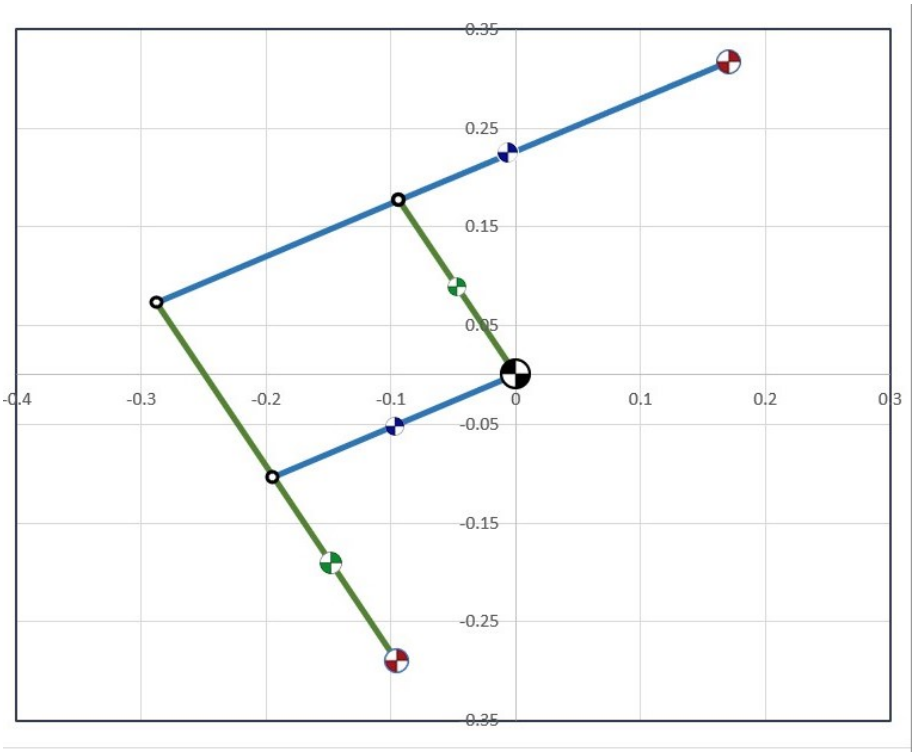

Figure 3.19. Excel solution for the pantograph balancing

Link Parameters [m]	
a_1	0.6
r	0.27
a_2	0.65
Distance Parameters [m]	
b_1	0.3
b_2	-0.07
Mass Parameters [kg]	
m_1	0.6
m_2	0.7
m_a	1.7
Calculated Parameters	
$m_{c1}b_{c1}$ [kgm]	0.572
b_{c1} [m]	0.38
m_{c1} [kg]	1.50526316
Joint Parameters [deg]	
θ_5	120
2.0943951	

LINK PARAMETERS

$$|JM_1| = b_1, \quad |OM_2| = b_2$$

$$|JA| = |OP| = a_1$$

$$|OM_{C1}| = b_{C1}$$

$$|OJ| = |PA| = r,$$

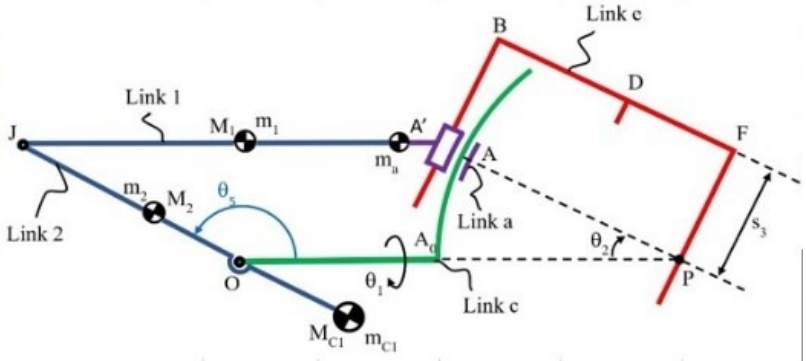

	O	J	A	M_1	M_2	M_{C1}	CoM
x	0	-0.135	0.465	0.165	0.035	0.19	0.26636
y	0	0.233826859	0.23383	0.23383	-0.06062	-0.32909	1.2E-17

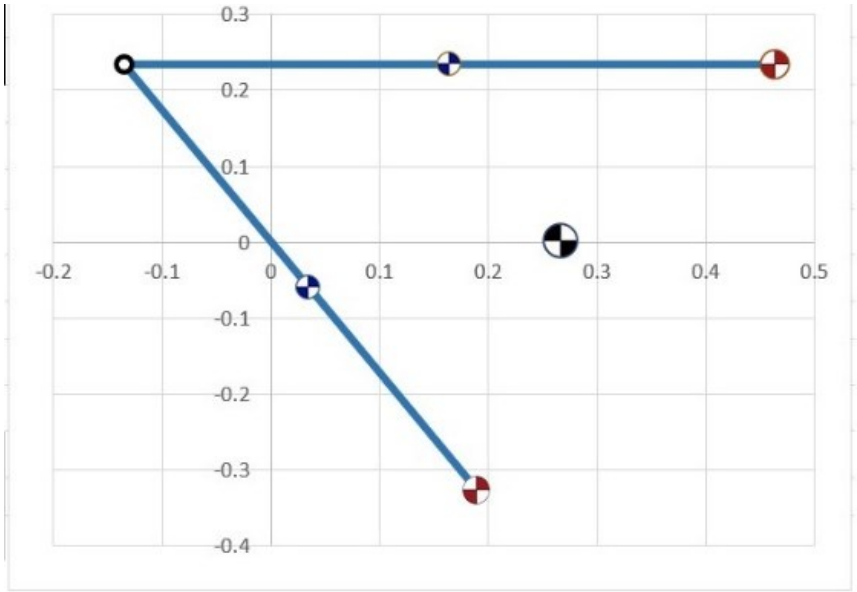

BALANCING CONDITION

$$m_{C1}b_{C1} = (m_1 + m_a)r - m_2 b_2$$

Figure 3.20. Excel solution for the parallelogram balancing

CHAPTER 4

CONSTRUCTIONAL DESIGN

In this chapter, the constructional design of the manipulator is examined through figures of CAD designs in Solidworks. The design of the manipulator is explained through joint designs, actuation groups design and auxiliary linkages design. The manipulator is divided into six sub-assembles: Base, radial rail, radial carriage, linear carriage, parallelogram and pantograph, as shown in Figure 4.1. Also, the isometric and front views of the manipulator can be seen in Figure 4.2.

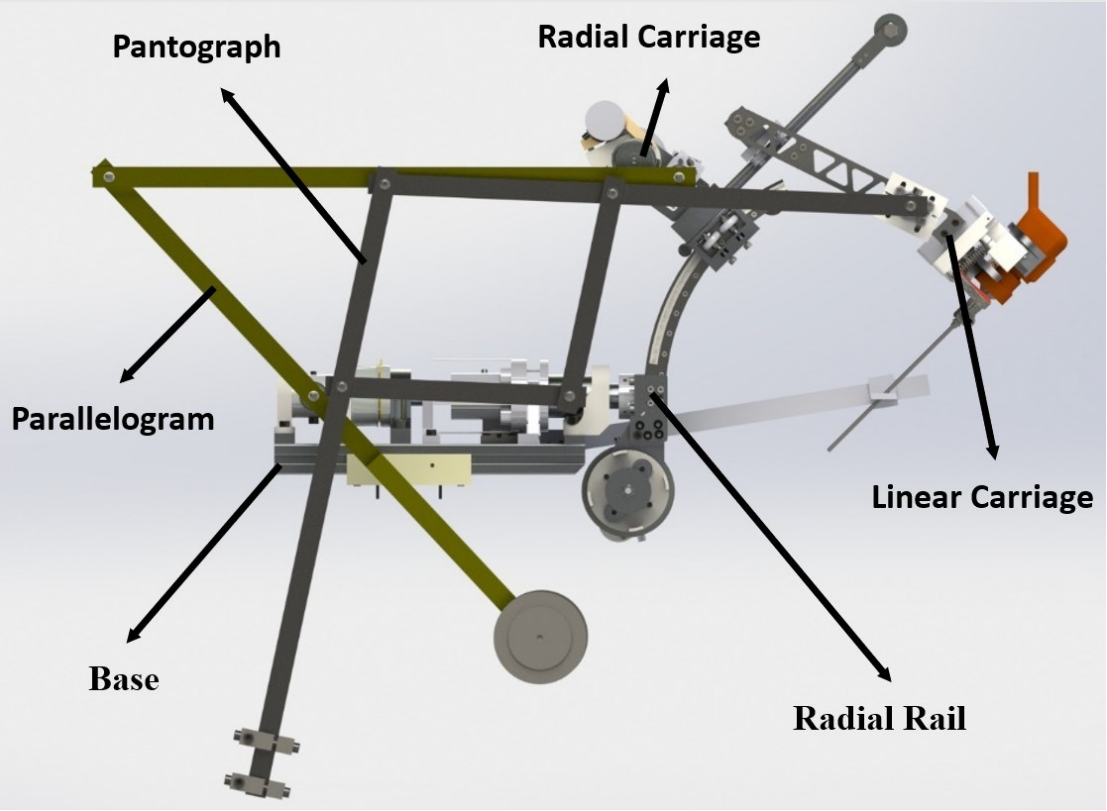

Figure 4.1. Side view of the whole mechanism with sub-assemblies

4.1. Joint Constructions

In this section, joint designs of the RRP mechanism are examined. The first rotational dof provides relative motion between the base and the radial rail, the second

rotational dof between the radial rail and the radial carriage, and finally, the translational dof between the linear carriage and the radial carriage.

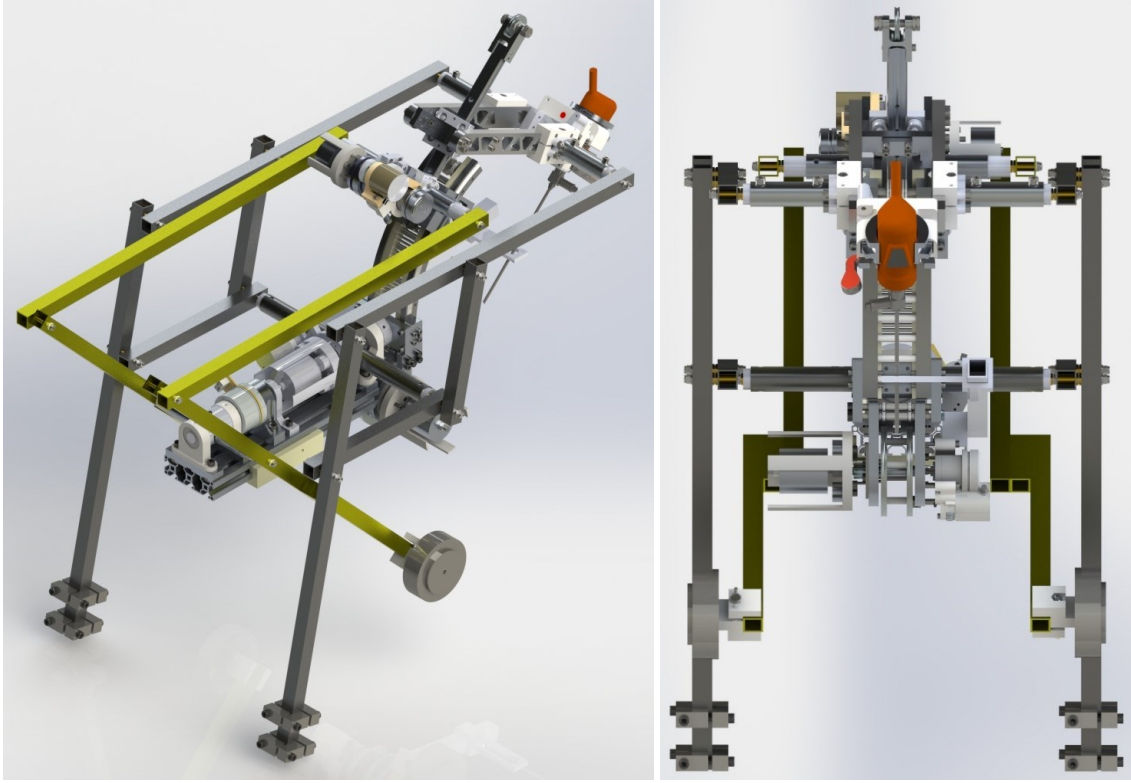

Figure 4.2. Isometric and front views of the mechanism

4.1.1. First Joint (R)

The first revolute joint is rotating the whole mechanism around the first motor axis and actuated by first motor. This joint is constructed between the base and radial rail connected to each other using a coupling. As shown in Figure 4.3, the parallelogram shaft housing, first motor, spring system and pantograph shaft housing are fastened to the aluminum frame from left to right respectively. Also radial rail is located at the end of the base. The rotational dof enables the whole mechanism to rotate about first motor axis by ±20°. Both end positions for the joint is shown in Figure 4.4.

The motor is directly mounted to the spring system; from there it is mounted to the pantograph housing and finally to the radial rail. Throughout the first motor axis, assembly between the motor shaft and radial rail are secured with bearings from 3 different places to achieve minimum deflection as shown in Figure 4.5.

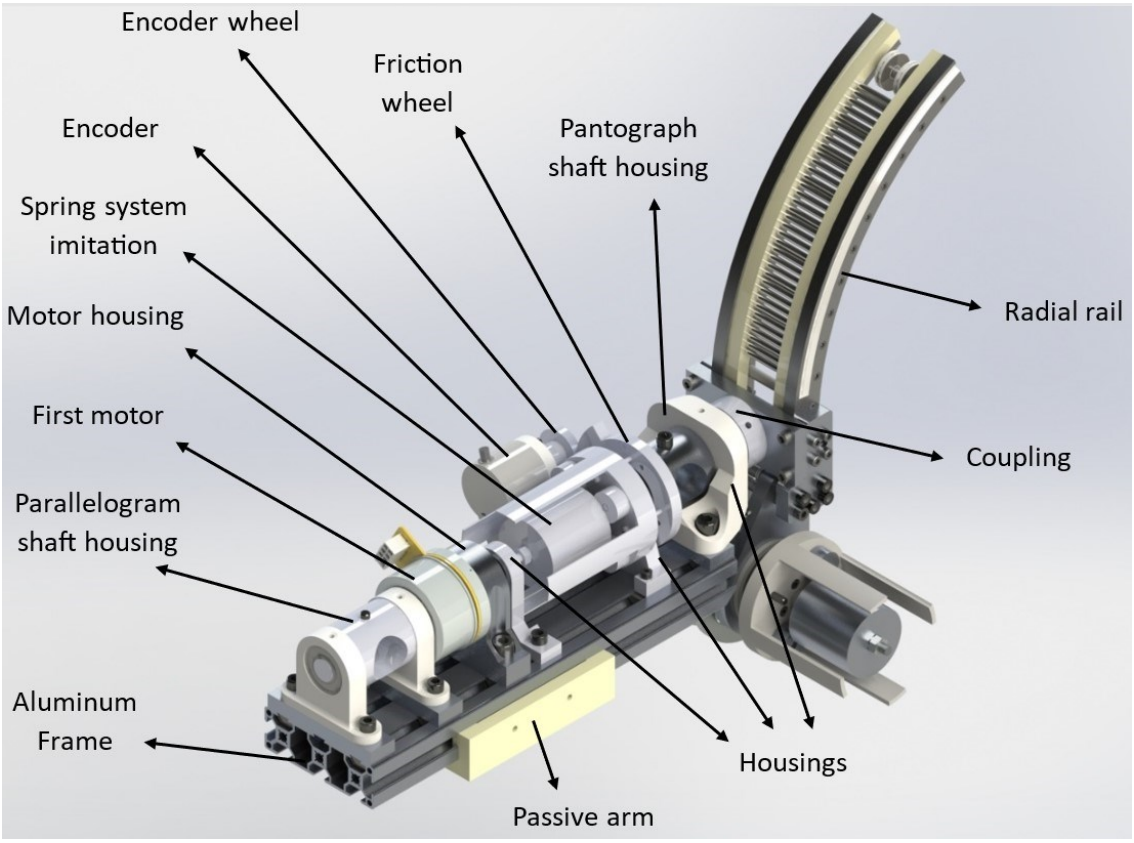

Figure 4.3.Assembly of base and radial rail

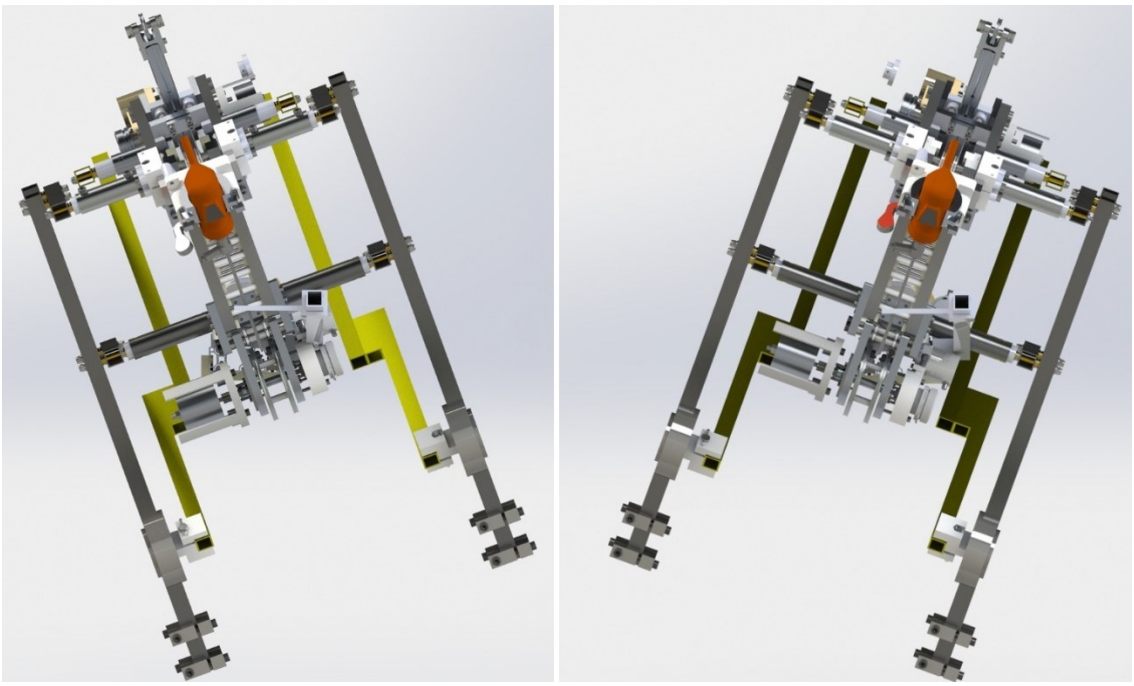

Figure 4.4. Motion range of the first revolute joint by ±20°

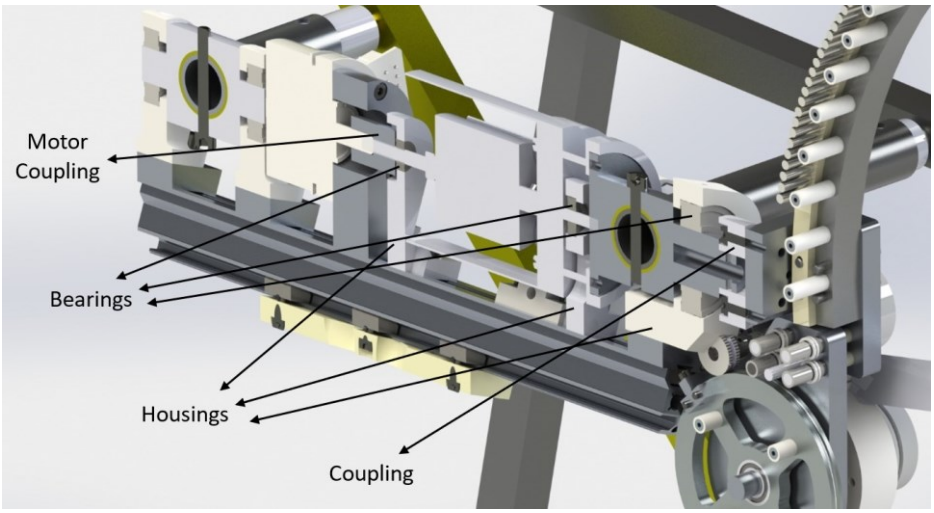

Figure 4.5. Construction of the first joint

4.1.2. Second Joint (R)

The second revolute joint actuation is performed by the second motor and the range of the motion of the joint can be seen in Figure 4.6. Between two positions radial carriage changes its orientation by 40°. Construction of the joint consists of two parts: radial rail and radial carriage. Isometric view of the assembly of these two parts is shown in Figure 4.9. This figure shows all parts of radial rail and carriage. The actuation of this joint is discussed in Section 4.4.2.

The contact between these two parts occurs between the wheels of the radial carriage and the channels on the outward faces of the aluminum cases on both sides of the radial rail, as shown in Figure 4.7. In theory, each wheel has two-point contact with the channel from both faces. For four wheels, 8 point contacts occur. Also, as seen in Figure 4.8, the positioning of the wheels along the rotation axis can be changed by tightening and loosening the screws on the radial car. Each wheel is adjusted separately to achieve minimum mechanical gap and friction between the radial rail and radial car.

4.1.3. Third Joint (P)

The third joint is translational and actuated by the third motor. The motion range of 110 mm of the joint can be seen in Figure 4.10. Construction of the third joint is formed by two commercial products: linear rail and carriage. There are steel rods on both sides of the aluminum linear rail and the linear car is mounted so that surface contacts between

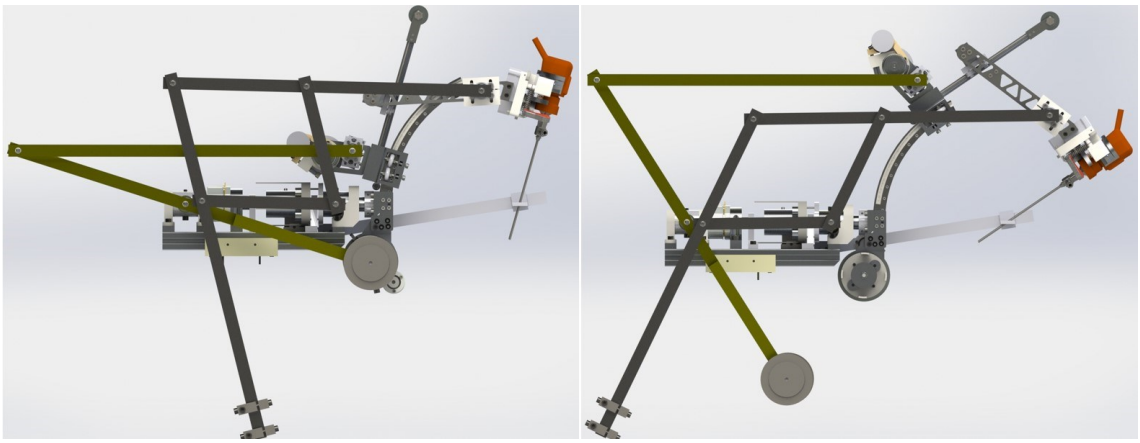

Figure 4.6. Range of motion of the second revolute joint

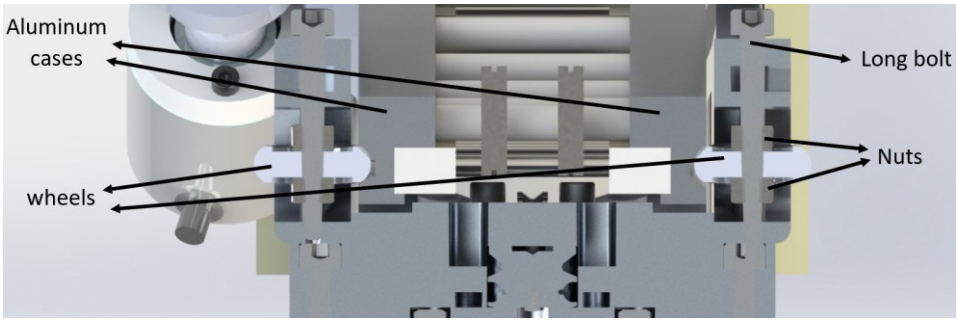

Figure 4.7. Cross section view of the 2nd revolute joint

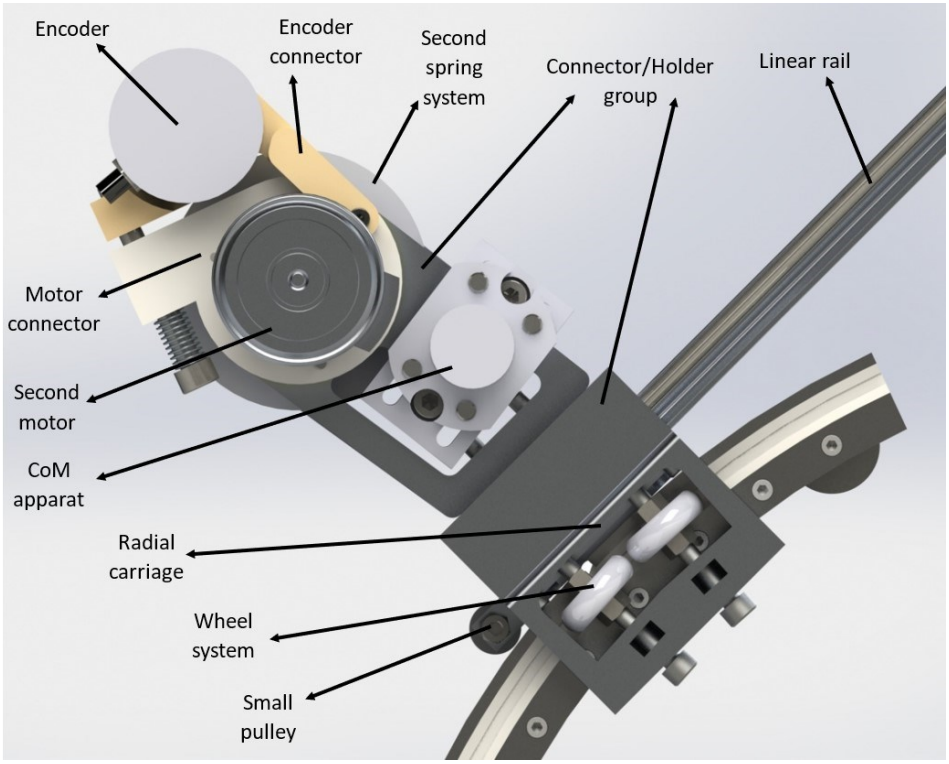

Figure 4.8. Side view of the radial carriage

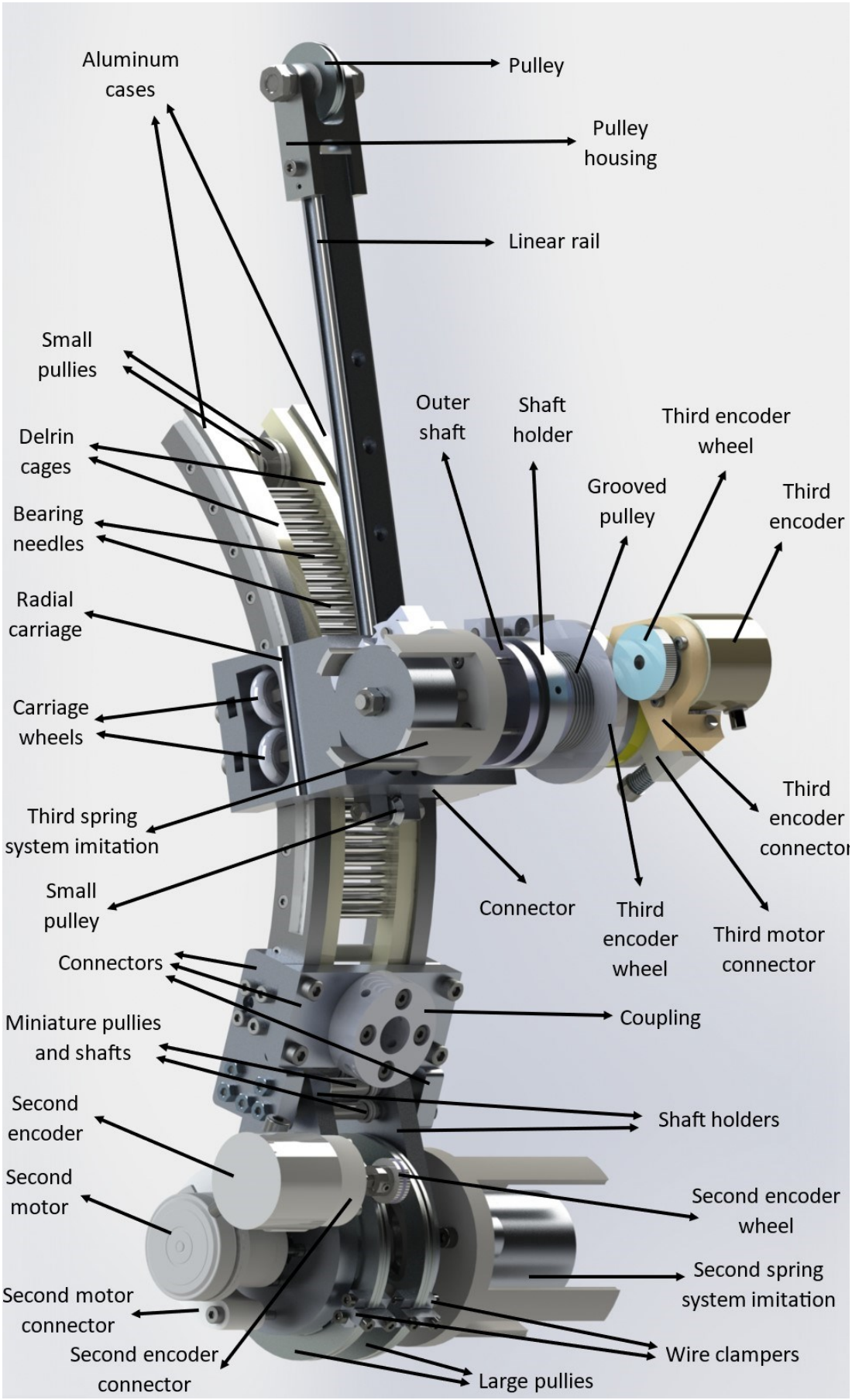

Figure 4.9. Assembly of radial rail and radial carriage

wheels and rods occur as depicted in Figure 4.11. Also, this joint can be adjusted by bolts to reduce mechanical gap and friction between the parts.

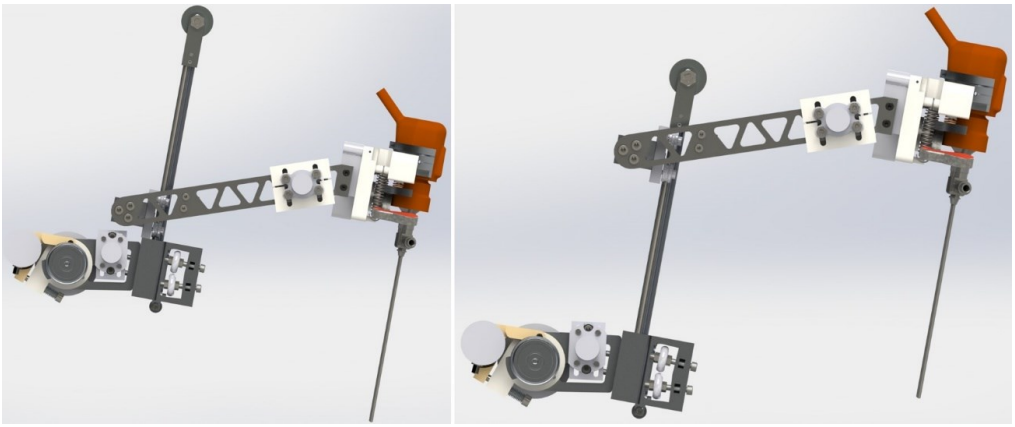

Figure 4.10. Range of motion of the third joint

This joint provides a linear relative movement between the joint linear carriage and the radial carriage. Assembly of the radial carriage and linear rail is shown in Figure 4.12. The actuation of the third joint is discussed in Section 4.4.3.

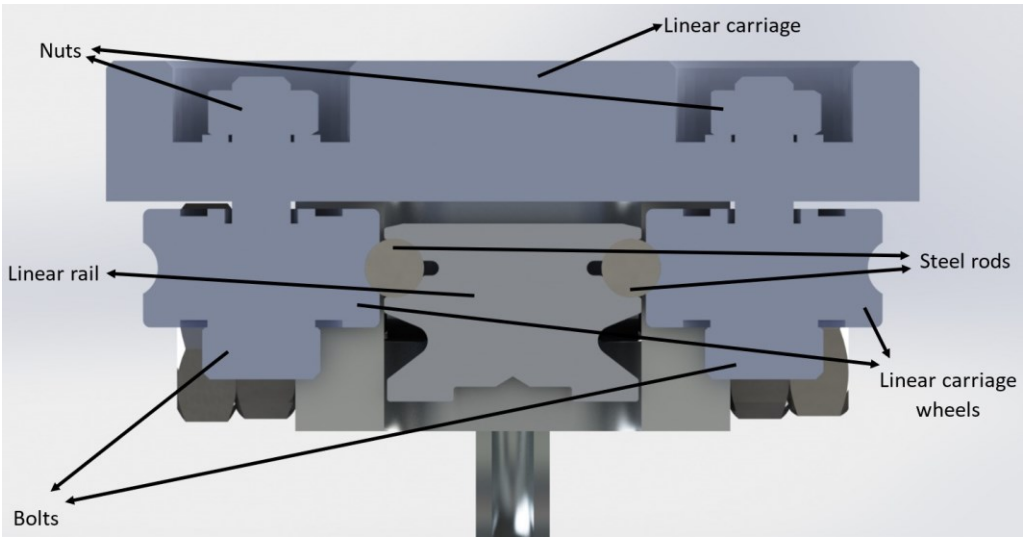

Figure 4.11. Cross section view of third joint

4.2. Actuation Group Constructions

The joints mentioned in Section 4.1 are active, i.e. actuated. All joints of the mechanism in the auxiliary linkages are passive. This section examines the actuation groups designed for these actuated joints.

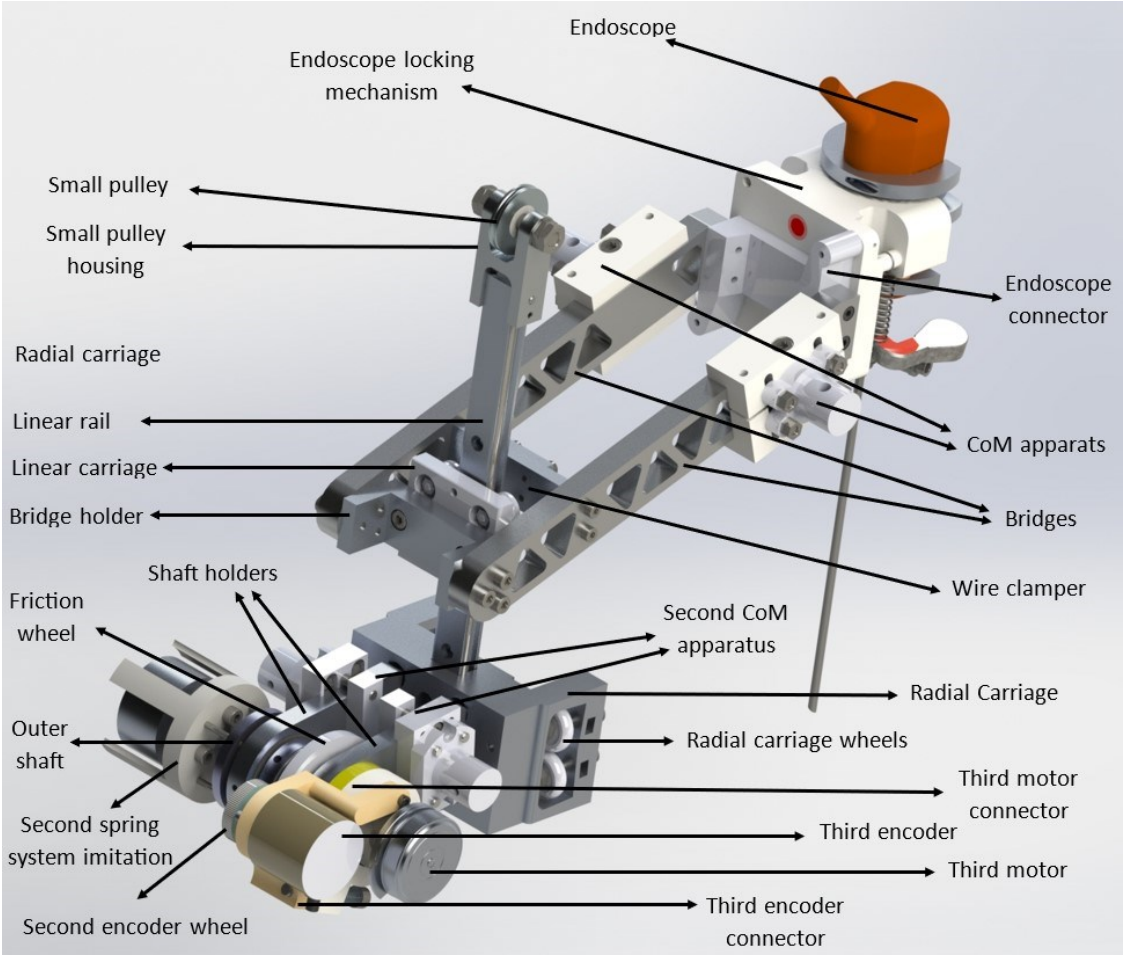

Figure 4.12. Assembly of radial carriage and linear carriage

Among the actuator groups; the first actuator group has a different construction compared to the second and third groups. In the first actuator group, the motor shaft is directly connected to the spring group and the spring group is connected to the radial rail by means of a coupling. In other actuator groups, the motor shaft is connected to the inner shaft, then the inner shaft is connected to the spring system. The spring system output is fastened to the outer shaft, and the outer shaft is connected to the pulley. The rotation of the inner and outer shafts is independent of the bearing between them. This construction is made in order to realize a balancing solution working in the plane by pulling the center of gravity of the moving masses to the symmetry axis of the radial rail.

4.2.1. Actuation of the First DoF

The first actuator group is mounted on an aluminum sigma profile. The first element of the first actuator group is the first motor (Figure 4.13). The motor shaft is connected to the input shaft of the spring system with a coupling. Output bolts of the spring system are connected to the pantograph shaft housing, then the right end of the housing is mounted to the radial rail with another designed coupling. The transmission of power from the motor to the radial rail is shown by arrows in Figure 4.13.

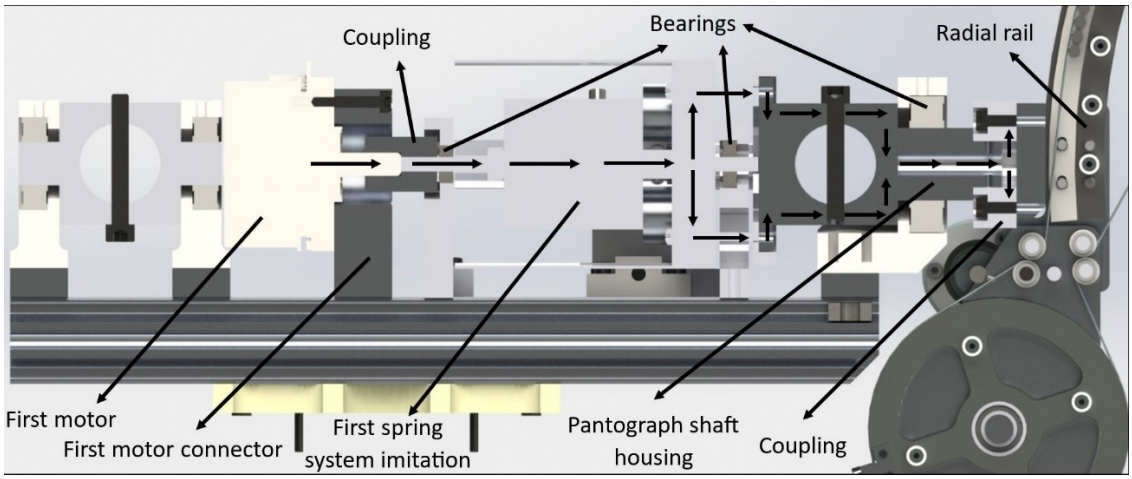

Figure 4.13. Cross section side view of the first actuation group

4.2.2. Actuation of the Second DoF

The second dof is driven by cable. The motor shaft is connected to the inner shaft with a set screw, the inner shaft is connected to the input shaft of the spring system with

a coupling, and the output screws of the spring system are fastened to the outer shaft. Finally, it is mounted to the pulley. One end of the tensioned cable is fixed on the pulley and it can move in both directions together with the pulley. Transformation of power from the second motor to the pulley is shown in Figure 4.14 with white arrows.

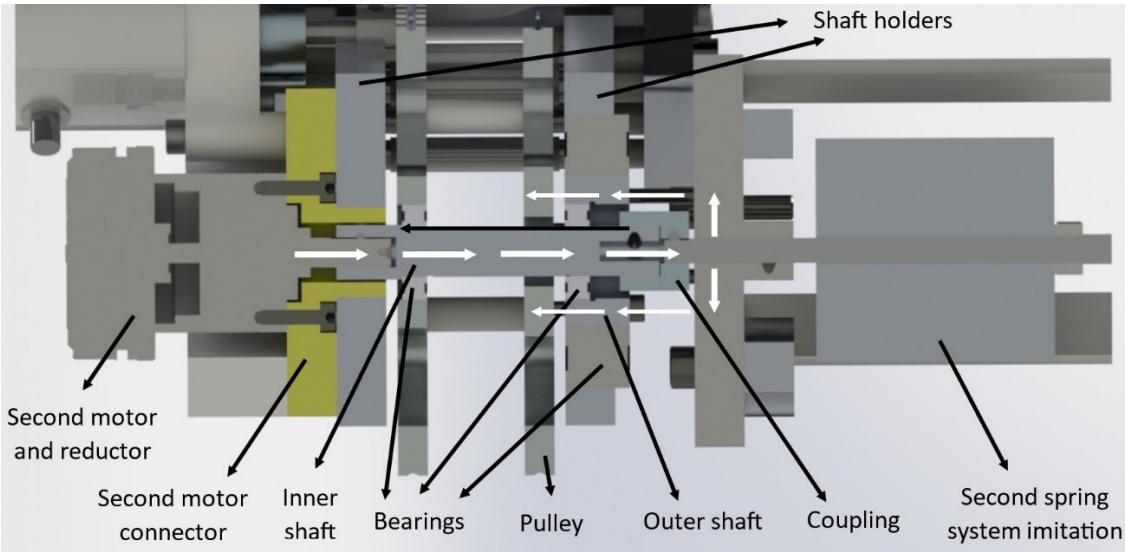

Figure 4.14. Cross section side view of the second actuation group

The cable is secured at two different points along its path; initially, it is affixed to the large pulley using a clamp, and subsequently, it is threaded through the holes on the radial carriage and fixed in place under tension, as depicted in Figure 4.15. Also path of the cable is as follows; one end of the cable is secured to the large pulley, then it extends towards the radial carriage, making contact with the bearing needles. This process is facilitated by the miniature pulleys, as shown in Figure 4.15, to avoid part collisions. Upon exiting the radial carriage, the cable extends to the pulley at the terminus of the radial rail, then returns to the large pulley with the assistance of additional miniature pullies.

4.2.3. Actuation of the Third DoF

The third actuator group is cable driven, just like the second actuator. The main difference between them is the diameter of the pulleys and the placement of the motor and the spring system. Power transforms from the motor shaft to the inner shaft and from there to the spring system. Moreover, from the spring system, it is transferred to the outer

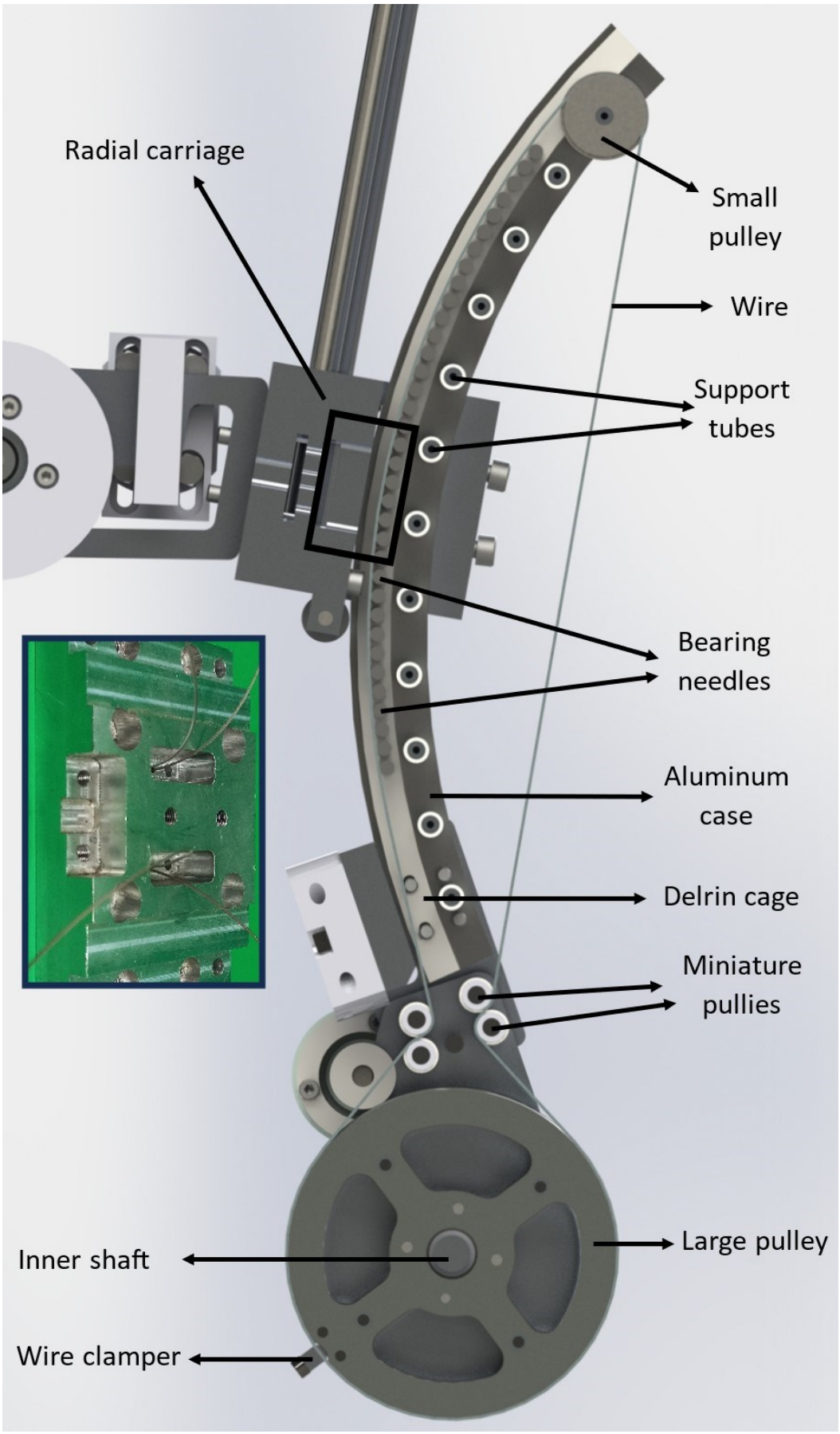

Figure 4.15. Cable path for the second actuation

shaft and then to the grooved pulley, thanks to the output screws of the system. Power transmission is shown by white arrows in
Figure 4.16.

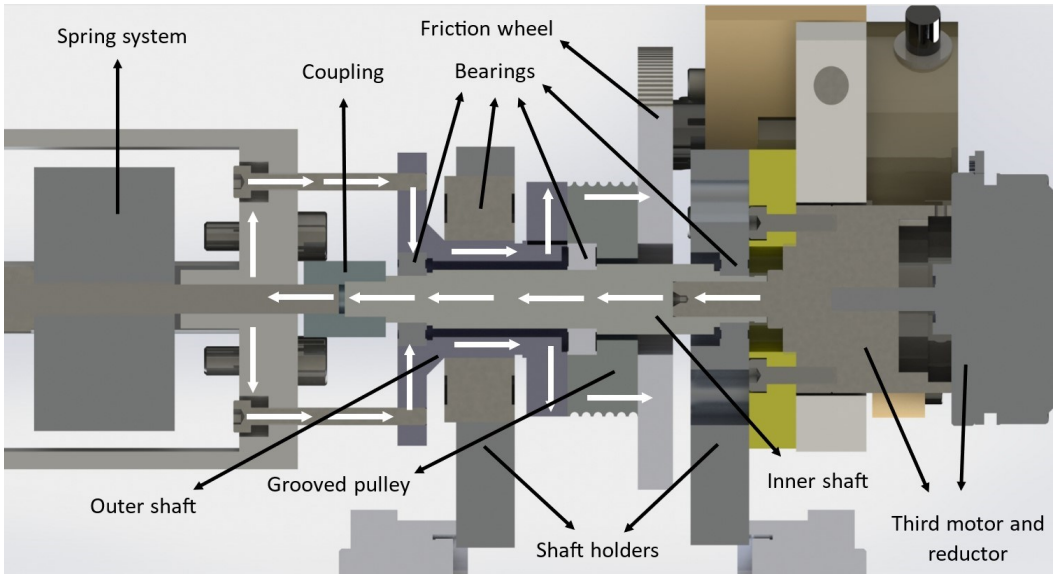

Figure 4.16. Cross section side view of the third actuation group

The final joint, a prismatic joint, is also actuated by a cable. One end of the cable is wound around a grooved pulley that is concentric with the motor shaft, effectively preventing slippage between the rope and reel. The other end of the rope is secured to the linear carriage by a cable clamp that is screwed into the bridges, as depicted in Figure 4.17. The rope, anchored to the grooved pulley, extends to the pulley located at the end of the linear rail, and then proceeds to a small pulley attached to the radial carriage. Finally, it loops back to the grooved pulley, thereby completing its path.

4.3. Auxiliary Linkage Constructions

All links utilized in the parallelogram and pantograph are constructed from 20×20 aluminum box profiles with a wall thickness of 1.5 mm. To assemble brass housings, aluminum profiles are drilled at appropriate locations, ensuring a tight fit. Both auxiliary mechanisms comprise revolute joints. The design involves placing brass housing inside aluminum box profiles and tightening the steel shafts with fiber nuts from both sides. To reduce friction, a polyoxymethylene (POM) washer is placed between the housing faces meeting each other. Construction of a revolute joint is shown in Figure 4.18.

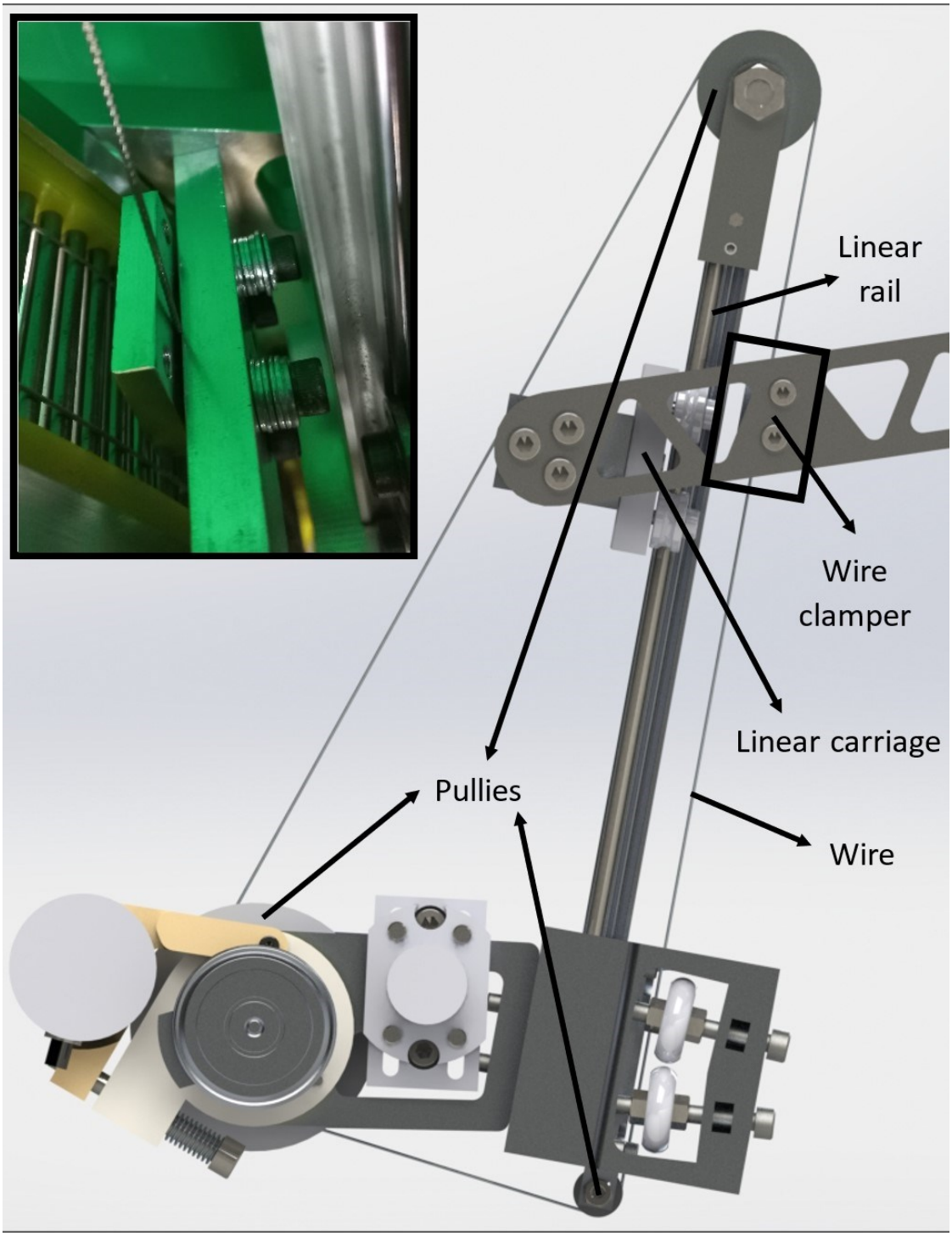

Figure 4.17. Cable path for the third actuation

Aside from these aspects that are specific to the parallelogram and pantograph, additional connecting structures are discussed in the forthcoming subsections, including base connections, radial and linear carriage connections, and counter-masses**.**

4.3. Auxiliary Linkage Constructions

All links utilized in the parallelogram and pantograph are constructed from 20×20 aluminum box profiles with a wall thickness of 1.5 mm. To assemble brass housings, aluminum profiles are drilled at appropriate locations, ensuring a tight fit. Both auxiliary mechanisms comprise revolute joints. The design involves placing brass housing inside aluminum box profiles and tightening the steel shafts with fiber nuts from both sides. In order to reduce friction, a polyoxymethylene (POM) washer is placed between the housing faces meeting each other. Construction of a revolute joint is shown in Figure 4.18. Aside from these aspects that are specific to the parallelogram and pantograph, additional connecting structures are discussed in the forthcoming subsections, including base connections, radial and linear carriage connections, and counter-masses**.**

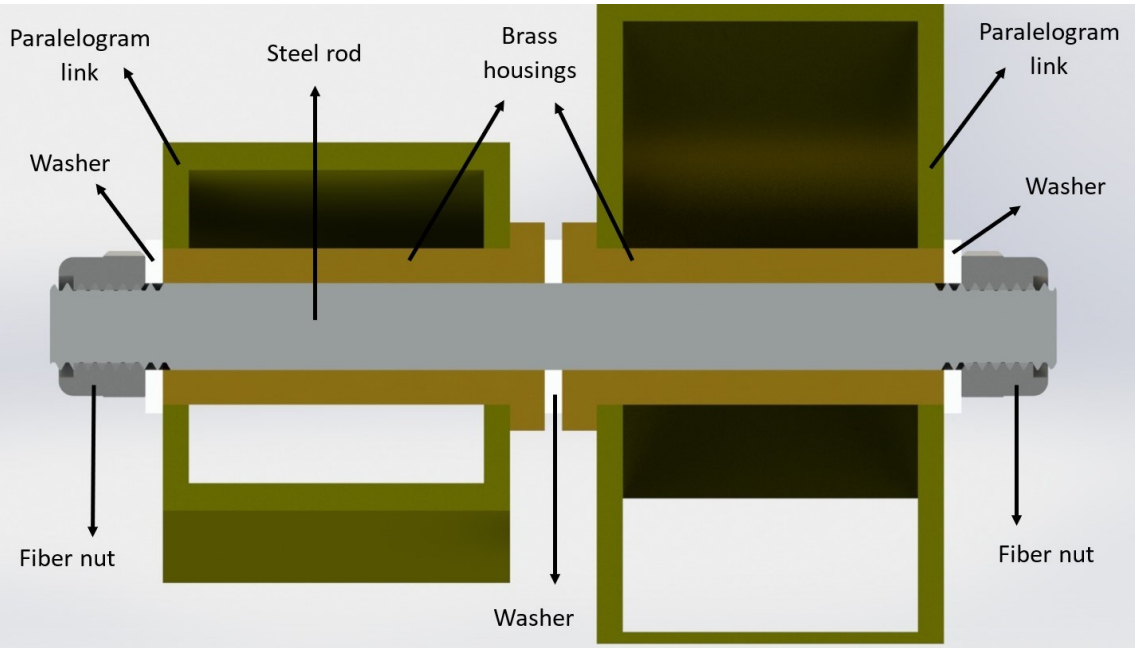

Figure 4.18. Cross section side view of the 2R construction

4.3.1. Pantograph

The pantograph and base connection, installed on an aluminum pipe, incorporates 2R joint configurations on both of right and left sides. It is attached to the pantograph shaft with a centrally located screw, thereby permitting rotation along the axis of the first motor shaft. Figure 4.19 depicts the entire assembly and the mirror-symmetrical 2R joint configurations located at the bottom right and left within the frame. Fundamentally, the components used are not different from those mentioned earlier in revolute joint construction. While there is a revolute joint between the aluminum pipe and a link of the pantograph, two links of the pantograph also include a revolute joint between them. As depicted in Figure 4.19, from left to center on the steel rod, which is tightened by a nut, there are two pantograph links with a brass housing in them. Friction is decreased by utilizing a plastic washer between the brass housings. A brass housing has also been inserted into the POM hollow tube embedded in the aluminum pipe. Plastic washers are employed on both sides, with a steel washer positioned in the center to reduce further friction between the aluminum pipe and the brass housings of the middle link.

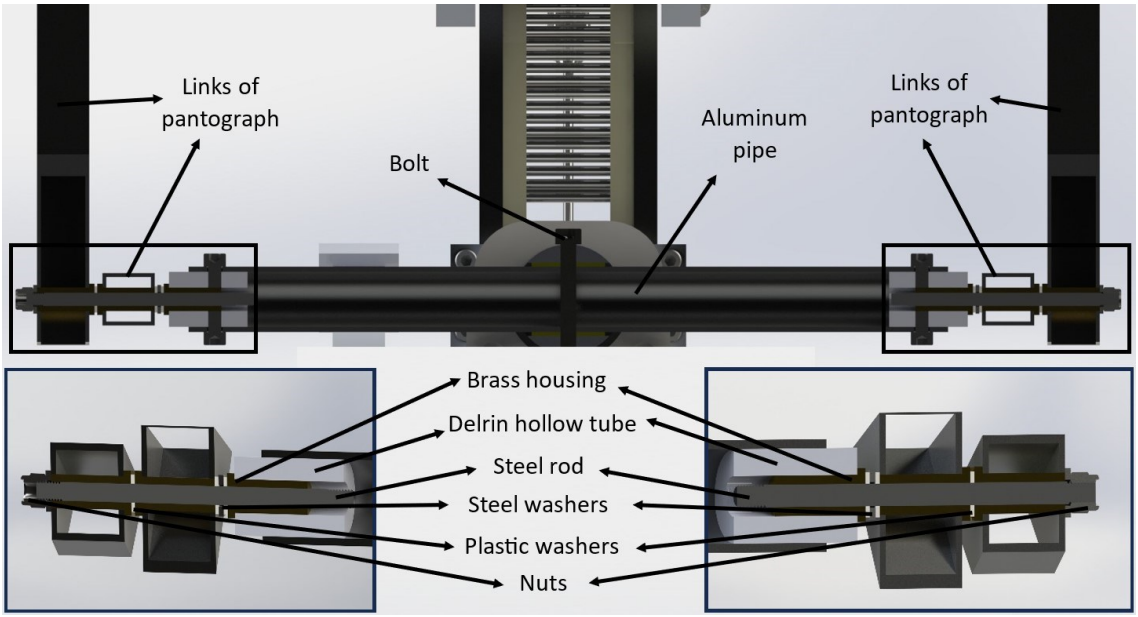

Figure 4.19. Cross section of the main shaft and 2R construction of the pantograph

The connection between the linear carriage and the pantograph, attached to the right and left bridges via a Center of Mass (CoM) apparatus, comprises two mirror-symmetrical components. The CoM apparatus is a device affixed to the bridges and can

be positioned over the center of mass of the entire linear carriage. As seen in Figure 4.20, one end of the aluminum pipe is attached to the coupling half of the CoM apparatus via a bolt. Inside the other end of the aluminum pipe, a PLA cylinder is inserted, into which a brass housing is embedded. A steel rod is placed concentrically with the brass housing. To the left of the steel rod, another brass housing is embedded within the pantograph link. The entire assembly is tightened using fiber nuts on both the right and left sides.

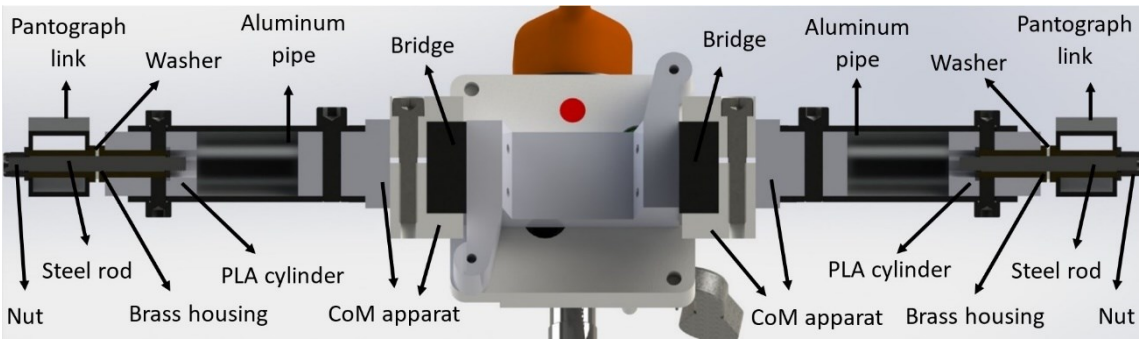

Figure 4.20. Cross section view of the linear carriage and pantograph connection

4.3.2. Parallelogram

The connection between the parallelogram and the base is depicted in Figure 4.21. This structure is constructed on an aluminum pipe, just as other connection constructions mentioned above. There are revolute joints with a single dof on both sides of the aluminum pipe, which is affixed in the center of the parallelogram shaft housing with a screw. From the center to both sides; a PLA cylinder inside the aluminum pipe is secured with a screw. A brass housing is nailed into place at the other end of the PLA cylinder. Another brass housing is embedded in the parallelogram link at the other end of the steel rod within the brass housing. The plastic washer situated between the two brass housings serves to reduce friction. The friction within the joint can be adjusted by either tightening or loosening the nut on the steel rod at the end.

The connection between the radial carriage and the parallelogram link is constructed on aluminum pipes connected to the Center of Mass (CoM) apparatus on the right and left shaft holders as depicted in Figure 4.22. From both sides of the aluminum pipe, the coupling half of the CoM apparatus and the PLA cylinder have fastened a bolt. At the other end of the PLA cylinder, a brass housing is embedded. A steel rod, concentric with the brass housing, extends from within this housing, and at the other end of this rod,

a brass housing is nailed into the aluminum link. As previously described, the entire system can be adjusted for tightness by manipulating the nut.

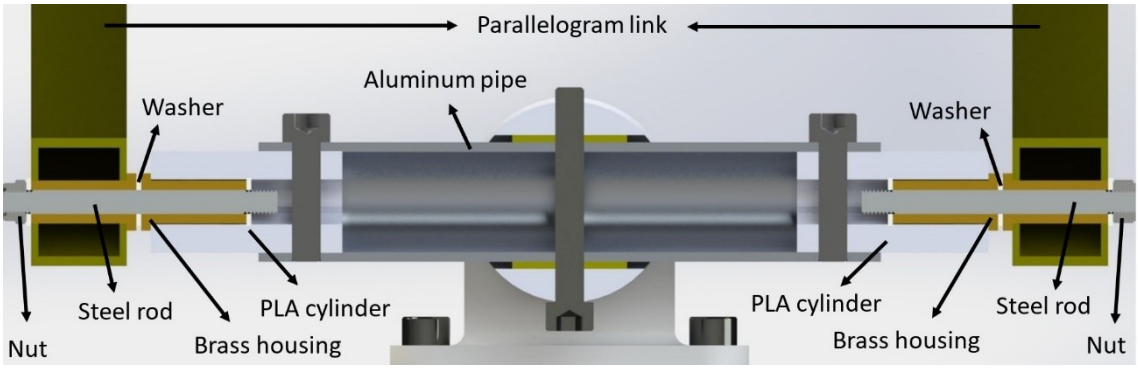

Figure 4.21. Cross section view of the base and parallelogram connection

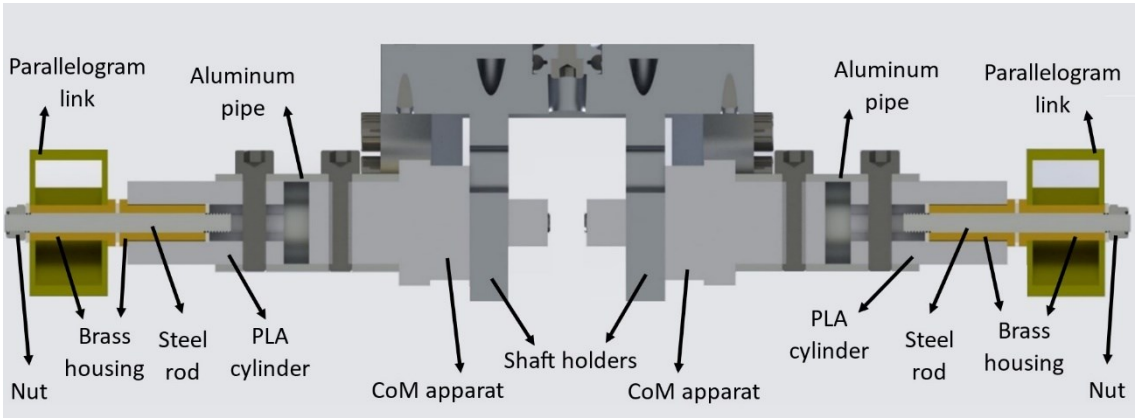

Figure 4.22. Cross section view of the radial carriage and parallelogram connection

CHAPTER 5

MANUFACTURING AND ASSEMBLY

This Chapter is about the production and assembly of the parts of the whole mechanism. The entire assembly is divided into sub-assemblies and discussed. The mechanism is divided into two main parts: the RRP mechanism and the auxiliary linkages. The base, radial rail, radial carriage and linear carriage shown in Figure 5.2, are subassemblies of the RRP mechanism, while the parallelogram and pantograph belong to the auxiliary linkages. Also, every sub-assembly, except the parallelogram and pantograph, is divided into groups, such as the actuation group and the holder/connector group.

As shown in Table 5.1, the balanced RRP mechanism has 4 sub-assemblies and 13 groups. Base (Sub-assembly A) is divided into 4 groups which are A1: Base, A2: Parallelogram Housing Group, A3: First Actuator Group. Radial Rail (Sub-assembly B) includes B1: Connector/Holder Group, B2: Radial Rail Group and B3: Second Actuator Group. Radial Carriage (Sub-assembly C) composed of C1: Holder/Connector Group C2: Radial Carriage Group, C3: Third Actuator Group and C4: First CoM Apparat. Finally Linear Carriage (Sub-assembly D) involves D1: Linear Carriage Group, D2: Second CoM Apparat and C3: Endoscope Group. Auxiliary Linkages composed of the remains; Parallelogram (Sub-assembly E) and Pantograph (Sub-assembly F).

Each component is allocated a unique code, as exemplified in Figure 5.1. The initial letter of the code indicates the sub-assembly to which the part is attributed, while the subsequent numeral signifies the group number of the parts. Furthermore, the digit appearing to the left symbolizes the part number within the designated group. This systematic methodology guarantees precise identification and organization of each component, thereby enabling smooth assembly and enhancing overall performance.

To clarify the previously mentioned code example, let us examine the A3-5 Pantograph Shaft Housing as referenced in Table 5.1. This component is part of the First Actuator Group, which is the third group within the Base (A) sub-assembly. Furthermore, it constitutes the fifth item in the aforementioned group.

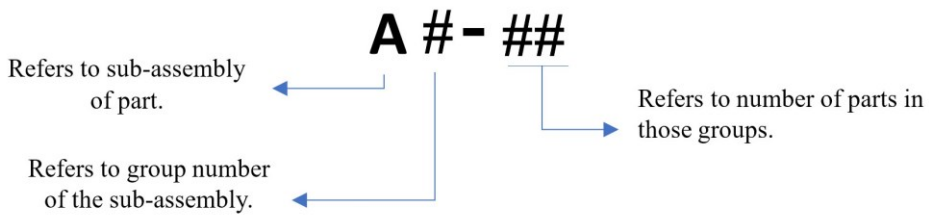

Figure 5.1. Code Expression of a Parts

Table 5.1. Sub-assembly-code and description table

Sub-assembly	Group	Description
A	A1	Base
	A2	Parallelogram Housing
	A3	First Actuator Group
B	B1	Connector/Holder Group
	B2	Radial Rail Group
	B3	Actuator Group
C	C1	Holder/Connector Group
	C2	Radial Carriage Group
	C3	3rd Actuator Group
	C4	1st CoM Apparat
D	D1	Linear Carriage Group
	D2	2nd CoM Apparat
	D3	Endoscope Part
E	-	Parallelogram
F	-	Pantograph

5.1. Base (Sub-assembly A)

The base of the manipulator is the only sub-assembly that does not move. It serves as a link between the passive arm and the manipulator. Within sub-assembly A, there are 15 components subdivided into groups of A1, A2, and A3. Part codes are listed in Table 5.2. Furthermore, the fully assembled representation of sub-assembly A is depicted in Figure 5.3.

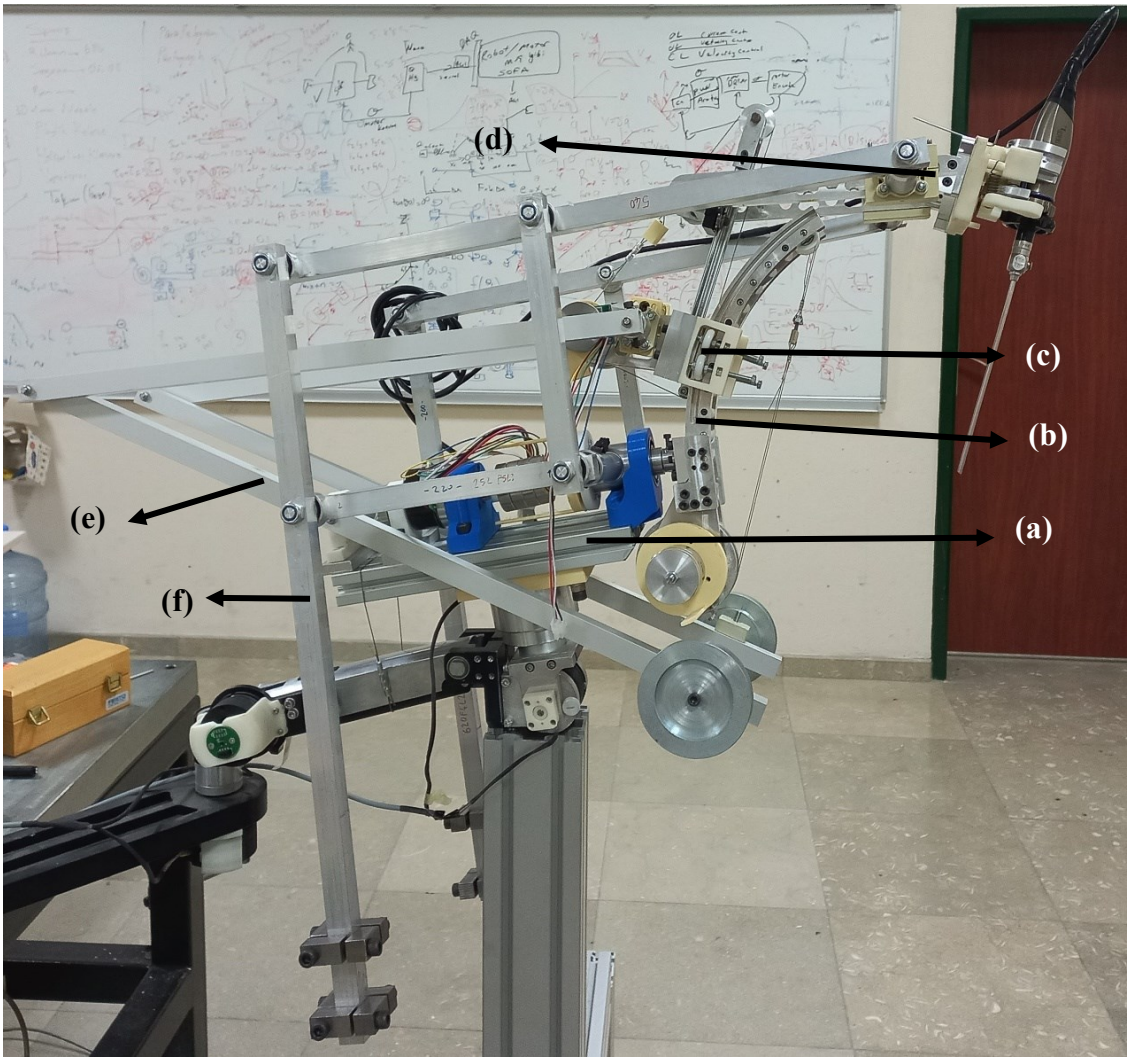

Figure 5.2. Assembly of the RRP mechanism with the balancing linkages (a) base, (b) radial rail, (c) radial carriage, (d) linear carriage, (e) parallelogram and (f) pantograph

Table 5.2. Material list of base (sub-assembly A)

Part Code	Part Name	Material	Number of Parts	Mass (gr)
A1-1	Frame Connector	PLA	1	86.2
A1-2	Sigma Profile Frame	Aluminum	1	576.7
A2-1	Parallelogram Shaft	Aluminum	1	163.1
A2-2	Parallelogram Shaft Housing (Right)	Aluminum	1	48.9
A2-3	Parallelogram Shaft Housing (Left)	Aluminum	1	49.2
A2-4	Bearing 6002zz	Steel	2	28.7
A2-5	Lever for Housings	Aluminum	2	64.9 x 2
A3-1	1st Motor		1	
A3-2	1st Motor Connector		1	72.6
A3-3	1st Motor Coupling	Aluminum	1	16.3
A3-4	Spring System	PLA	1	243.5
A3-5	Pantograph Shaft	Aluminum	1	167.8
A3-6	Pantograph Shaft Housing	PLA	1	179.9
A3-7	Bearing 6005	Steel	1	78.6
A3-8	Friction Wheel	Aluminum	1	20.5
	Socket Head Bolt M4 – 30 mm		3	
	Socket Head Bolt M6 – 40 mm		1	
	Socket Head Bolt M5 – 20 mm		4	
	Socket Head Bolt M3 – 20 mm		4	
	M6 Nut		1	
	Socket Head Bolt M6 – 25 mm		4	
	Socket Head Bolt M8 – 20 mm		2	
	Socket Head Bolt M8 – 25 mm		2	
	Sigma Profile Nut M8		8	
	Socket Head Bolt M3 –20 mm		4	
	Socket Head Bolt M8 – 12 mm		2	
	Socket Head Bolt M8 – 20 mm		4	
	Sigma Profile Nut M8		6	
	Socket Head Bolt M6 – 45 mm		1	

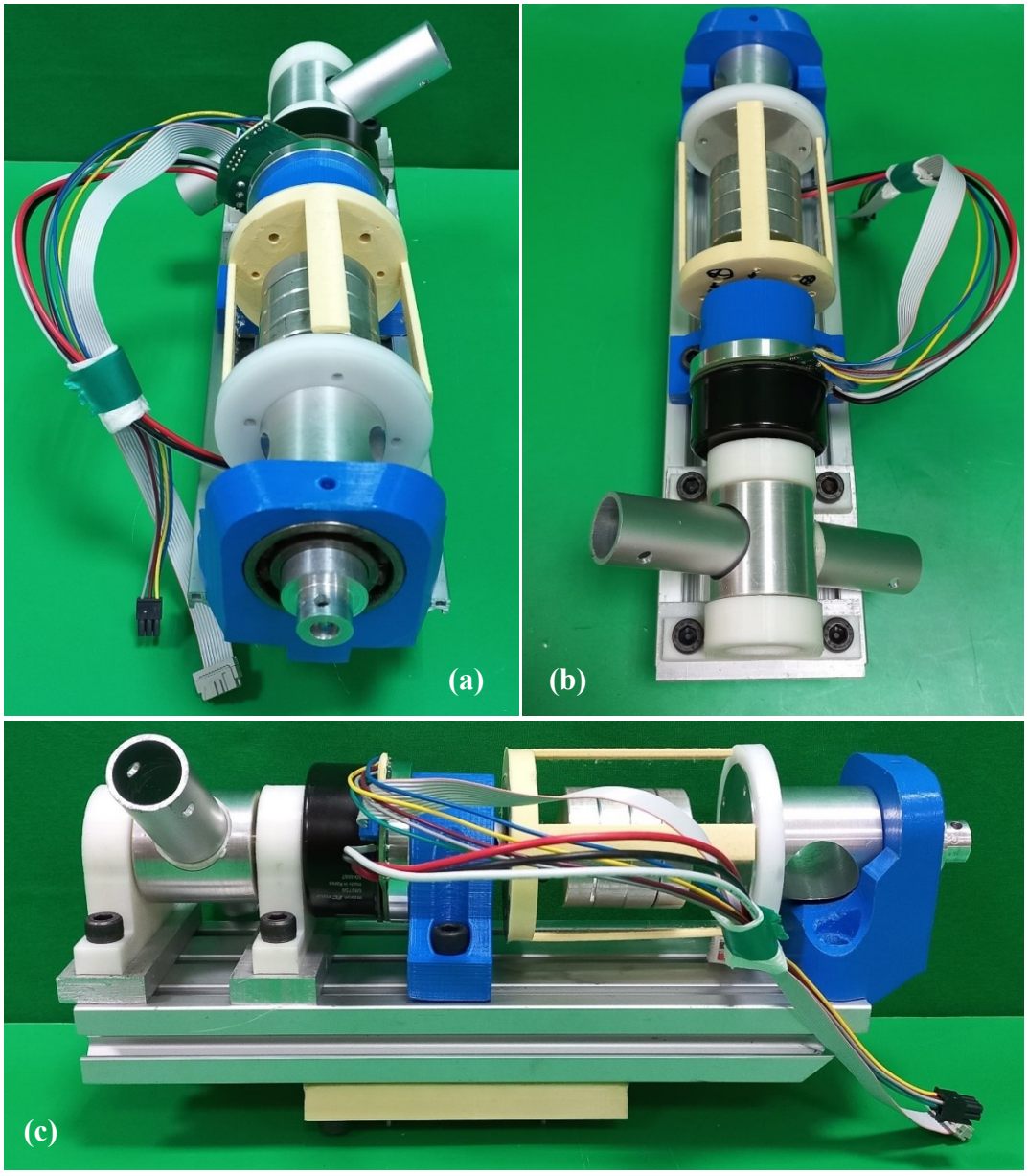

Figure 5.3. Completed assembly of the base sub-assembly with different view (a) view from Front of the base, (b) view from up of the base, (c) side view of the base

5.1.1. Manufacturing of the Base Parts

Entire base assembly is placed on an aluminum sigma profile (A1-2). Also, considering the connection of the base assembly with the passive arm, a frame connector (A1-1) part was designed for fastening passive arm and sigma profile frame. While the supplied sigma profile is machined to get appropriate dimensions to avoid link collision, the A1-2 part is produced using a 3D printer.

In addition, all bearing housings and motor connector on the base are manufactured from PLA by using 3D printer. These parts are parallelogram housings (A2-2: right and A2-3: left), 1st motor connector (A3-2) and pantograph housing (A3-6) as shown in Table 5.2.

Both pantograph and parallelogram housings were designed and manufactured in such a way that bearings are assembled on these parts with an shrink fit. The remaining details on the parts are two bolt holes for A2-2 and A2-3 to fasten it to sigma profile, while there are 3 bolt holes in A3-6 due to the load of RRP mechanism exerted on it. These parts can be seen as two white parts on the left of Base in Figure 5.3(c) and Figure 5.5(j) respectively. Differently from the others, the A3-2 has extra three holes to fasten motor on it as depicted in Figure 5.5(f). Another part on the base assembly is lever for housing (A2-5) which is manufactured from aluminum plate and shown in Figure 5.5(d). The only purpose of this part is making the axis of parallelogram shaft bearing, coincidence with the axis of the first motor shaft.

Before proceeding with the assembly of the base, there are two important parts manufactured from the aluminum by lathe; these are pantograph and parallelogram housings. Manufactured parts as shown in Figure 5.4.

The pantograph and shaft housing are the parts that connect the links of the pantograph and parallelogram to the base. Both parts are manufactured by using similar methods. The manufacturing process of the pantograph and parallelogram shaft housings are examined as follows. First, during the pantograph shaft housing, aluminum cylinder used as raw material is fixed chunk of lathe, then it is machined. Then, holes are drilled by using a CNC milling machine. Main difference between these two parts for manufacturing process is using extra end mill cutter to drill 4 bolt holes on the pantograph shaft housing.

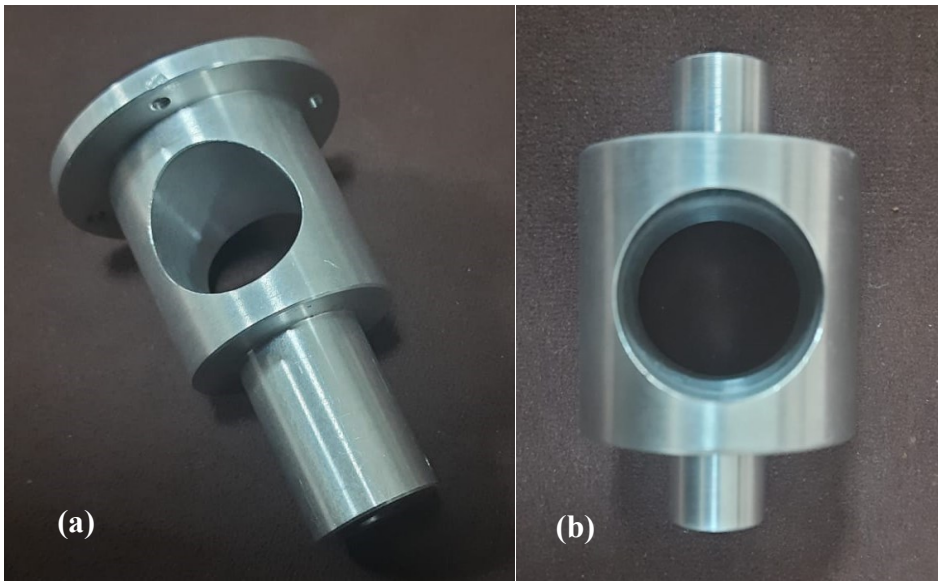

Figure 5.4. Manufactured shaft housings (a) pantograph shaft housing and (b) parallelogram shaft housings

5.1.2 Assembly of the Base (A)

The base sub-assembly consists of three groups: the base (A1) which includes frame connector (A1-1) and the aluminum frame (A1-2), which are mounted each other by bolts. The Parallelogram Housing (A2) indirectly connects to the first motor through the radial rail and the parallelogram, allowing for adjustment of parallelism. It includes the parallelogram shaft (A2-1), left housing (A2-2), and right housing (A2-3). The First Actuator (A3) is responsible for actuation on the first revolute joint and includes the motor (A3-1), connector (A3-2), coupling (A3-3), spring system (A3-4), pantograph shaft (A3-5), and shaft housing (A3-6). The motor and spring system are secured to the aluminum frame, and the pantograph shaft transfers rotational motion, comes from the first motor to the radial rail. Total mass of the Base sub-assembly is 2348.4 gr. All major parts can be seen in Figure 5.5.

5.2. Radial Rail (Sub-assembly B)

The radial rail is an essential component of the overall assembly, consisting of various parts distributed among three main groups: B1 (connector/holder group), B2 (radial rail group), and B3 (actuator group) as depicted in Figure 5.7. B1, B2, B3 groups contain 15, 9 and 16 parts, respectively. All parts of the radial rail is shown in Table 5.3.

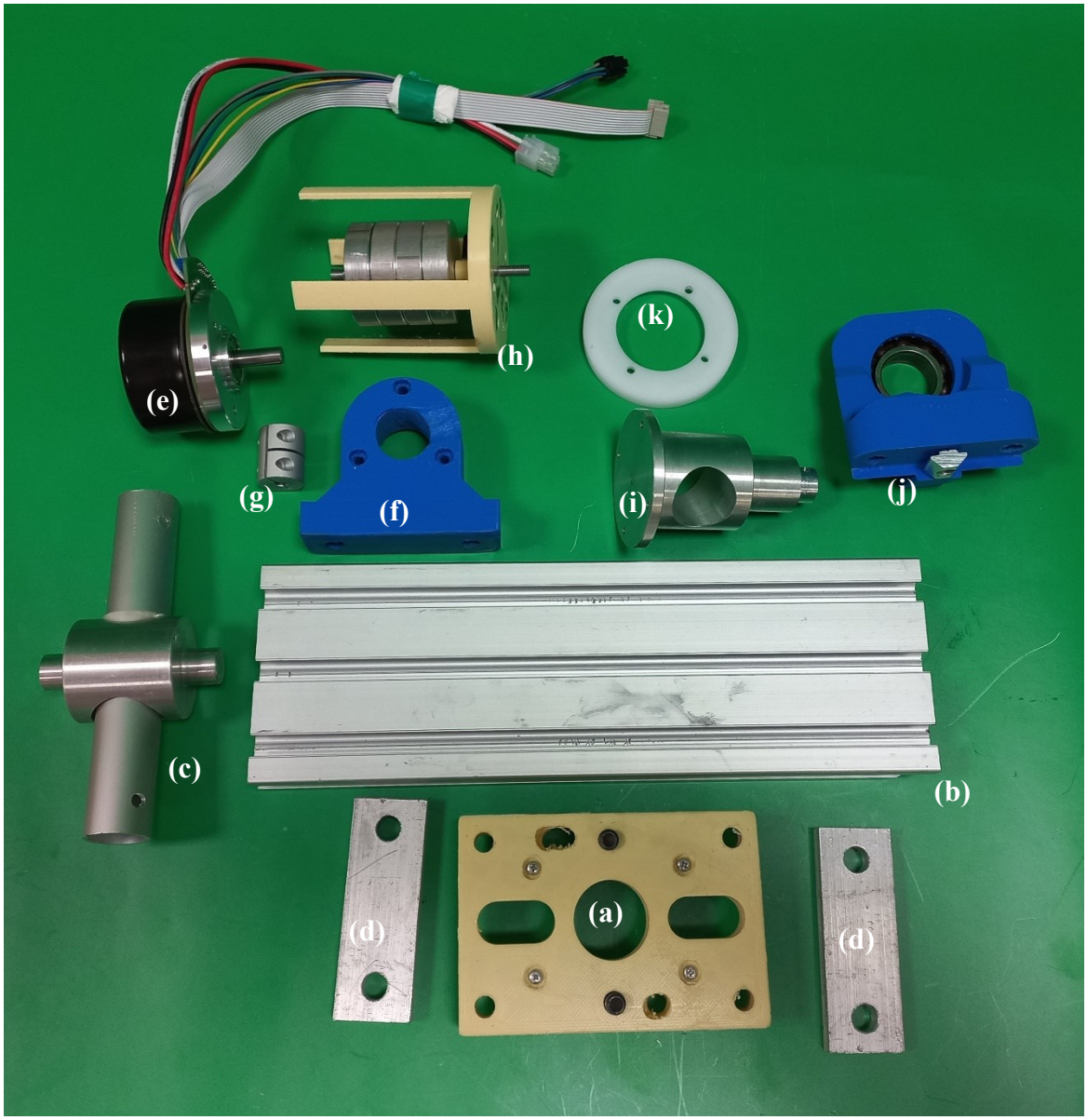

Figure 5.5. All parts of Base assembly (a) A1-1 frame connector, (b) A1-2 sigma profile frame, (c) A2-1 parallelogram shaft, (d) A2-5 lever for housings, I A3-1 first motor, (f) A3-2 first motor connector, (g) A3-3 firsst motor coupling, (h) A3-4 spring system, (i) A3-5 pantograph shaft, (j) A3-6 pantograph shaft housing, (k) A3-7 encoder adjacent wheel

5.2.1. Manufacturing Radial Rail Parts

Shaft holders are parts of the connector/holder group (B1) of sub-assembly radial rail (B) and house the second actuator group installed on the second motor axis. Three holes with a diameter of 5 mm and two holes with 4mm on the upper side of the part must be co-axial when radial rail (B) is constructed. Likewise, since the two parts have mirror symmetry except for hole diameters at the bottom of the parts, the holes must be concentric.

These parts are machined using a CNC milling machine by using SolidCAM software. Holes are drilled first in these parts manufactured from aluminum plates because their center distance between each other is essential. Then, they are machined to form outer geometry. The manufactured shaft holders can be seen in Figure 5.6.

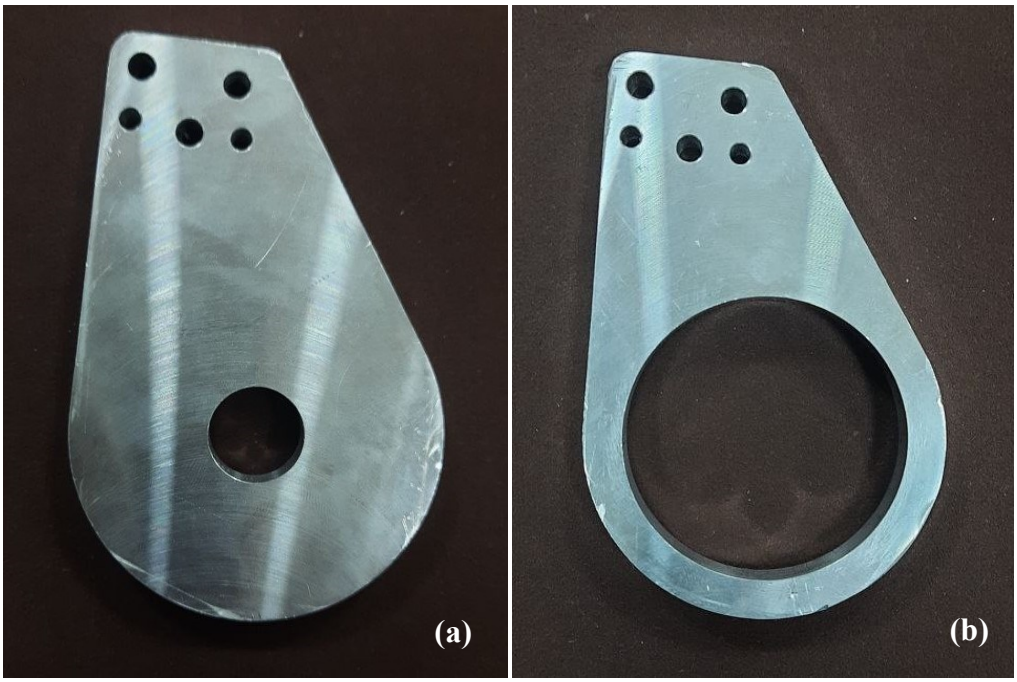

Figure 5.6. Manufactured shaft holders: (a) left shaft holder, (b) right shaft holder

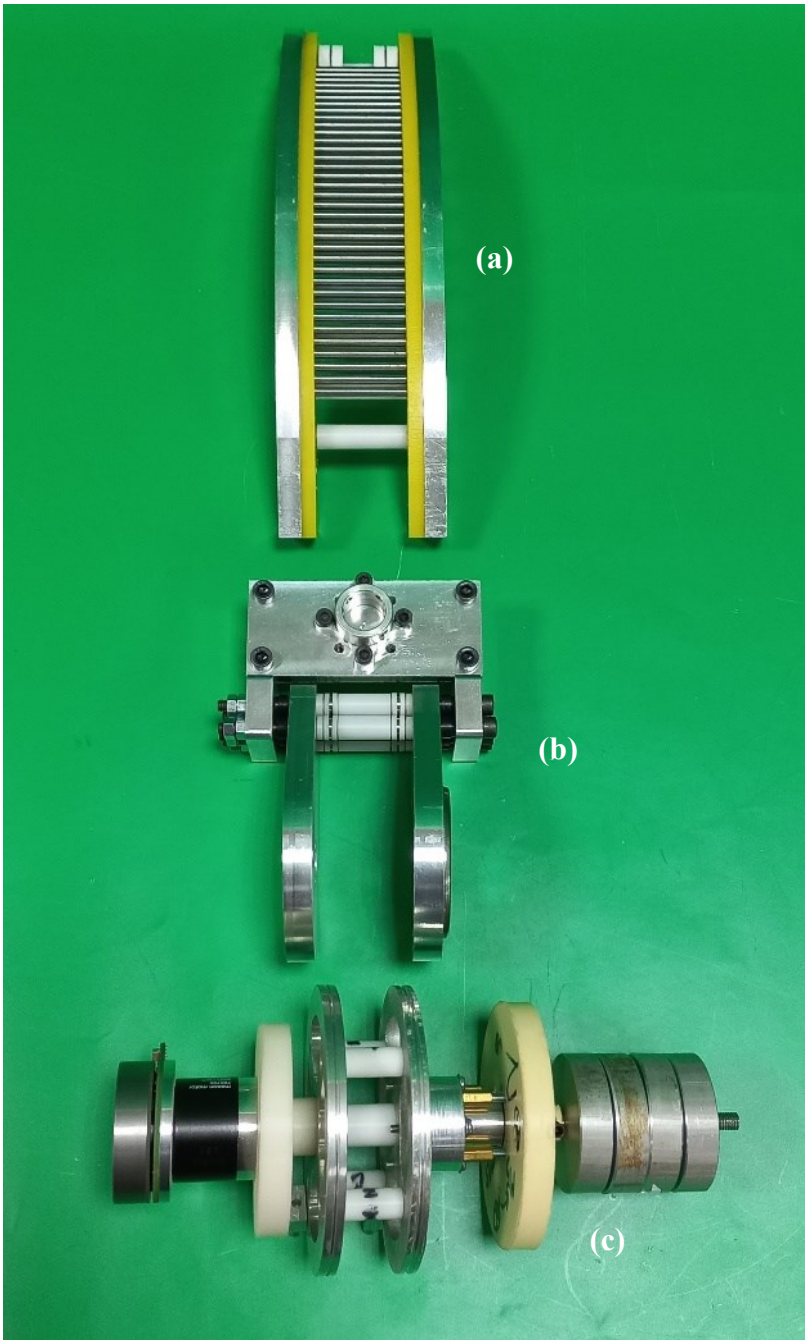

Figure 5.7. Groups of radial rail sub-assembly (a) radial rail group, (b) connector/holder group, (c) actuator group

Table 5.3. Material list of radial rail (sub-assembly B)

Part Code	Part Name	Materials	Number of Parts	Mass (gr)
B1-1	Shaft Coupling	Aluminum	1	9.4
B1-2	Connector Middle	Aluminum	1	92.0
B1-3	Connector Right	Aluminum	1	44.0
B1-4	Connector Left	Aluminum	1	43.6
B1-5	Shaft Holder Right	Aluminum	1	197.2 (/w bearing)
B1-6	Shaft Holder Left	Aluminum	1	139.6
B1-7	M5 Long Bolts	Steel	5	15.4 x 5
B1-8	Small Pulley	Steel	8	0.5 x 8
B1-9	PLA Spacer I	PLA	8	1.2
B1-10	PLA Spacer II	PLA	4	1.2 x 8
B1-11	Teflon Spacer	Teflon	10	0.7 x 5
	M5 Nut		5	
	Socket Head M4 – 30 mm		8	
	Socket Head M4 – 20 mm		4	
	Socket Head M5 –25 mm		4	
B2-1	Radial Case Right	Aluminum	1	592.9 (in total)
B2-2	Radial Case Left	Aluminum	1	
B2-3	Radial Cage Right	POM	1	
B2-4	Radial Cage Left	POM	1	
B2-5	PLA Cage for Support Tube		9	
B2-6	Support Tube	Aluminum	12	
B2-7	Needle	Steel	36	
B2-8	Small Pulley	Aluminum	2	
B2-9	Plastic Spacer Middle		1	
B2-10	Plastic Spacer Side		2	
	Socket Head M3 – 8 mm		24	
	Cable locking part		2	8.5 x 2
B3-1	2nd Motor		1	
B3-2	Motor Connector		1	25.9
B3-3	Inner Shaft		1	12.8
B3-4	Outer Shaft		1	31.6
B3-5	Right Pulley		1	59.1
B3-6	Left Pulley		1	60.6
	Bearing 6002		1	
	Bearing 6006		1	
	Support pipe	Aluminum	4	8.4 x 4 (/w screws)

(cont. on next page)

Table 5.3 (cont.)

B3-7	2nd Spring System			245.1
	Shaft coupling	Aluminum	1	
	Support Tube PLA	PLA	4	4.2 x 4
B3-8	PLA Spacer for Inner Shaft		1	2.0
	Socket Set Screw M3 – 4 mm		2	
	Socket Head Bolt M3 – 5 mm		8	
	Socket Head Bolt M3 – 12 mm		8	
	Socket Head Bolt M3 – 20 mm		8	
	Socket Head Bolt M3 – 25 mm		3	
	Socket Set Screw M4 – 4 mm		3	
	Socket Head Bolt4 – 30 mm		3	
	Socket Head M6 –30 mm		1	

Other parts are right, left and middle connector belongs to the connector/holder group of sub-assembly of radial rail. While right and left connectors are mirror symmetrical parts and in total has 11 holes with varying in 3 different diameters, middle connector has hour holed with 4 mm diameter to mount coupling on it. The manufacturing process of them is examined respectively.

The distance between the hole centers and being co-axial of the opposing holes of the parts are important, so holes for both parts are drilled first. Then, they are machined to create outer geometry of the parts. Aluminum plates are used as raw material. While Figure 5.8(a) shows material removing process to form general shape of part after holes were drilled. During machining, after machining one face of the part is completed, part is fixed again so that machined from other face. Figure 5.8(b) shows the photos of the part before it is fixed again. Finally, manufactured parts can be seen in Figure 5.9.

Aluminum cases are the essential parts of the sub-assembly of radial rail and are parts of the radial rail group (B2). These parts, manufactured from different aluminum blocks, are mirror-symmetrical, and the holes on them must be co-axial to each other. Both parts were manufactured using a CNC milling machine and SolidCAM. The manufacturing process of these parts is examined as follows: first aluminum block is secured to the bed of the milling machine, and it is machined by side mills to get a smaller rectangular shape. This process carried out to get position references of holes must be co-axial. The same process is performed as the first part. After that, holes and channels on the parts are machined using an end mill, as seen in Figure 5.10(a).

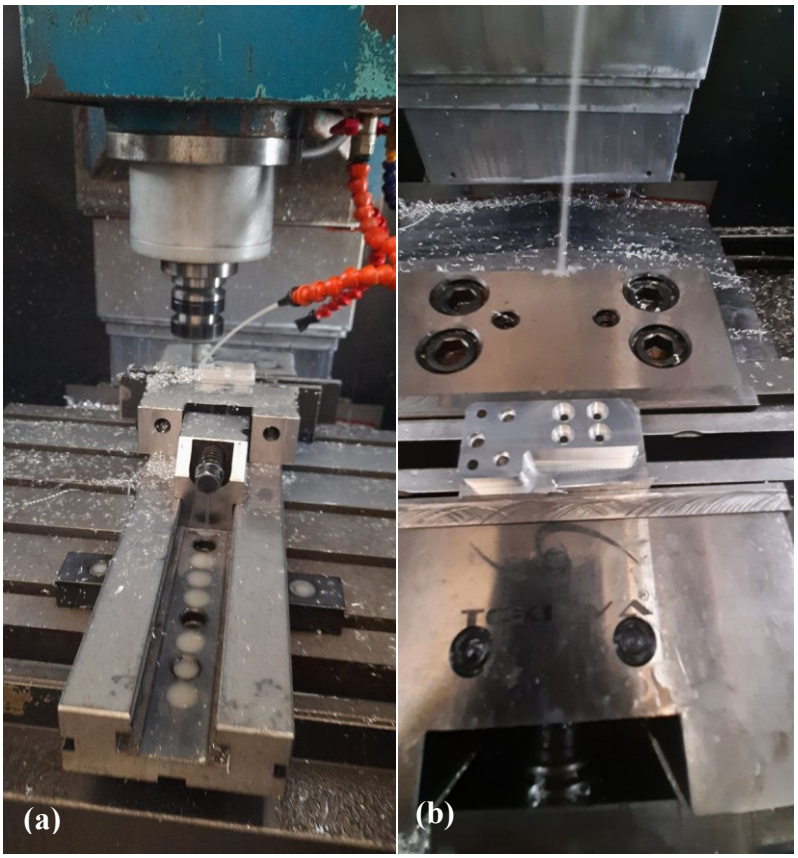

Figure 5.8. Manufacturing process of the connectors (a) Milling process (b) Finishing machining of one face of the left connector

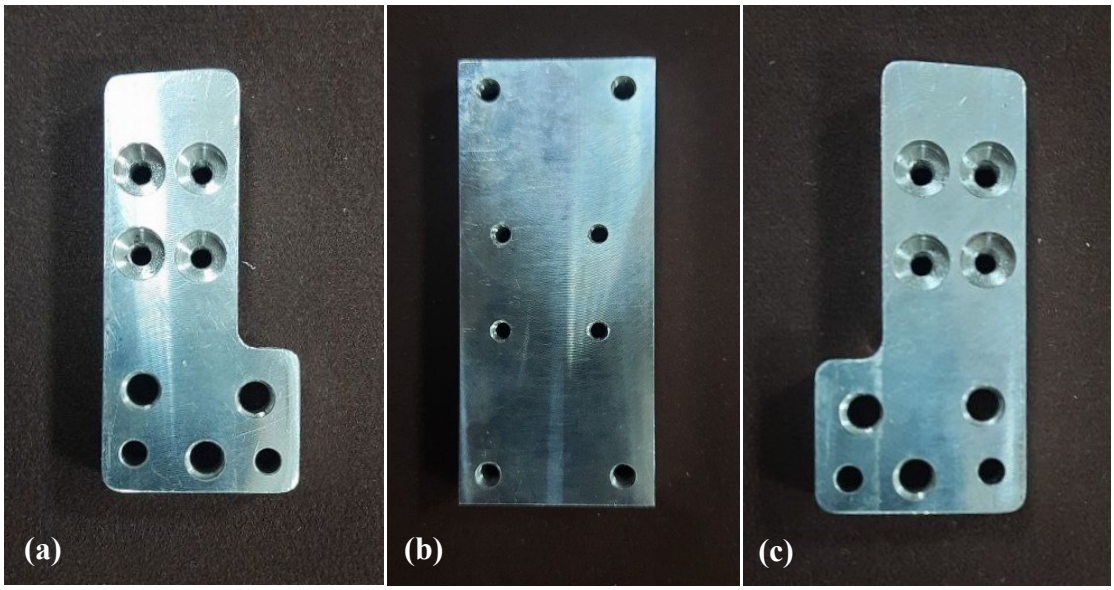

Figure 5.9. Manufactured Connectors (a) Left connector, (b) Middle connector and (c) Right Connector

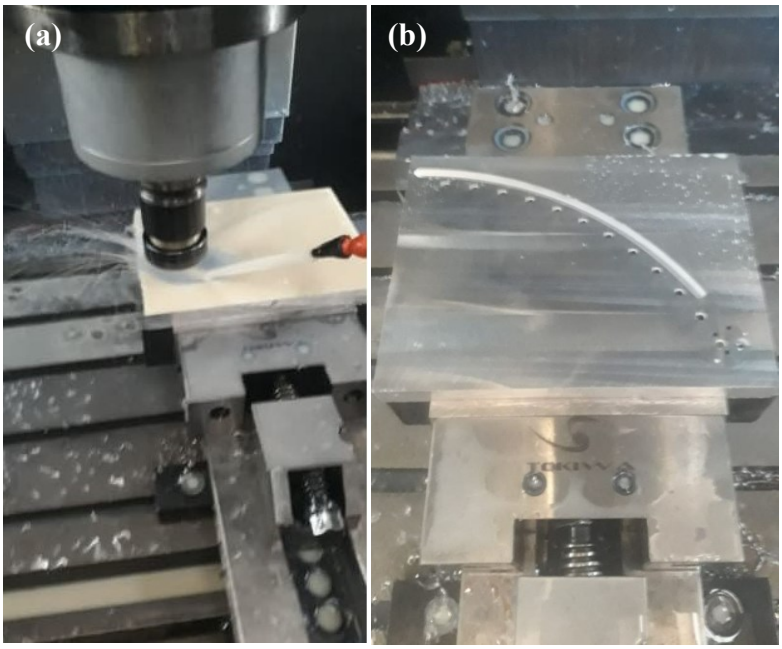

Figure 5.10. Manufacturing process of aluminum case

After drilling holes and machining channels, part can be seen in Figure 5.10(b). Then, by changing fixture type because of interference of router and fixing tools, the outer sides of the part are machined and, then, machined to form outer geometry by side mill. Finally, the metric holes were tapped. Each part has 12 holes with 6- and 5-mm diameters and four with 3.3 mm diameters. The manufactured parts are shown in Figure 5.11.

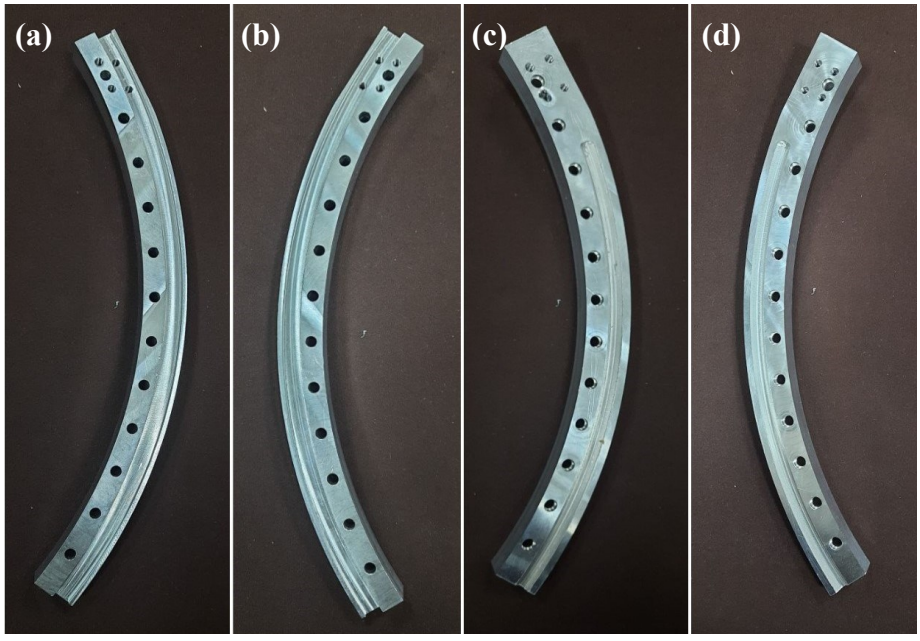

Figure 5.11. Manufactured aluminum cases (a) and (d) left aluminum case, (b) and (c) right aluminum case

The POM cage parts, mounted on the aluminum case, act as housing for bearing needles and provide an appropriate discrete arc path. The important thing about the housing is providing less friction while rotating because of its material. The drilling process is vital since the holes to be drilled are used as housing for the bearing needles. Both ends of the 4 mm diameter bearing needles are round, as shown in Figure 5.12. Therefore, the largest radius of the contacted conical area will be less than 2 mm. First, holes are drilled with an R2 Spherical end mill with 1.9 mm depth which brings a contact circle with a diameter of less than 4 mm.

Figure 5.12. Bearing needles

The right and left parts were manufactured from a single part of raw material using CAM software. They are manufactured from POM plate in dimensions of 350x150x20 mm, as seen in Figure 5.13(c). These parts were manufactured on the same CNC Machine where aluminum parts were manufactured. The machining process of the parts is shown in Figure 5.13(b), and the fixing part can be seen in Figure 5.13(a). Also, 12 pieces of 5 mm diameter aluminum pipes are used as support between two aluminum cases, which are tapped from both ends.

The second actuator group's (B3) inner and outer shafts (B3-3 and B3-4) and right and left pulleys (B3-5 and B3-6) are manufactured from aluminum cylinders. These parts are machined with a lathe first, and then holes are drilled in the CNC milling machine. The motor connector is manufactured from PLA by a 3D printer.

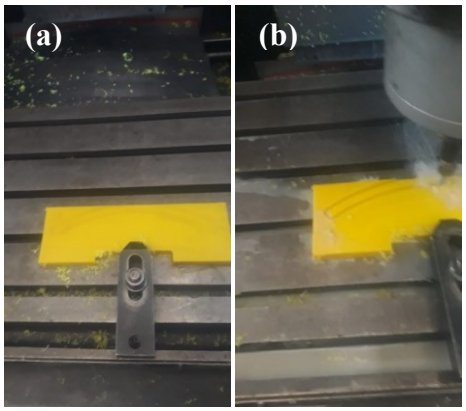

Figure 5.13. Machining POM cages: (a) securing POM plate, (b) machining POM cage

5.2.2. Assembly of Radial Rail (B)

The total mass of the connector/holder group is 646.1 gr, while the total mass of the radial rail is 592.9 gr. The mass of the second actuator group was not measured separately. The total mass of the radial rail is 1934.9 gr. All assembled groups from the top to bottom, are group of radial rail, connector/holder, and 2nd actuator are shown in Figure 5.14.

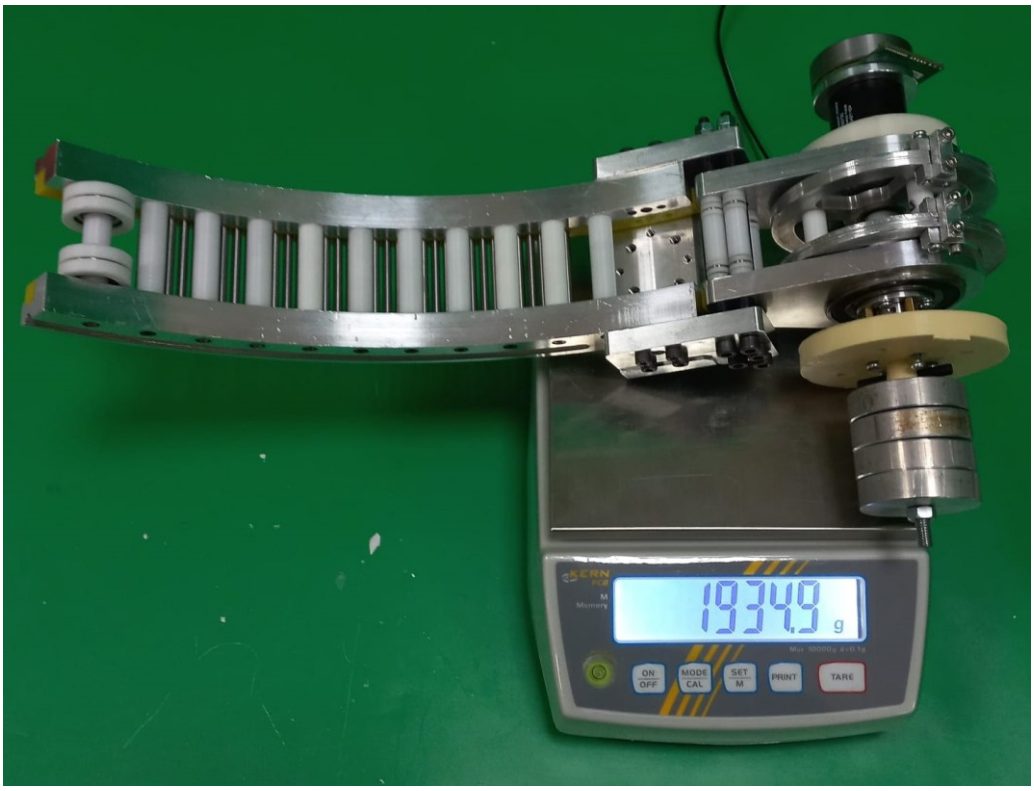

Figure 5.14. Total mass of the radial rail

In the assembly of the connector/holder group (B1), five main parts are used, including the connector middle (B1-2), connector right (B1-3), connector left (B1-4), shaft holder right (B1-5), and shaft holder left (B1-6). These parts are connected and adjusted using various bolts, spacers, and nuts. The purpose of this group is to establish a rigid connection between the first motor and the radial rail and holding second actuator group (B3).

The radial rail group (B2) assembly involves POM cages (B2-3 and B3-4) are mounted in rectangular channel on the aluminum cases (B2-1 and B2-2) and mounting bearing needles (B2-7) to the cages. Support pipes (B2-6) are attached to the aluminum case to secure the bearing needles so that they can rotate but not fall. Pulleys and PLA cylinders (B2-8, B2-9 and B2-10) are also installed on the rail to ensure proper positioning. This group enables the movement of the radial carriage along the rail.

The second actuator group (B3) consists of seven parts, with special attention required during assembly. The third spring system (B3-7) is mounted by a coupling on the inner shaft (B3-3) and output screws of it fastened to the outer shaft (B3-4). Other end of the inner shaft is attached to the second motor (B3-1) shaft. The pullies (B3-5 and B3-6) are mounted on the inner shaft. There is a point to be considered during the installation of the pullies on the inner shaft: one of the shaft holders (B1-5 or B1-6) must be disassembled. After the installation, the pullies and the other end of the outer shaft are fastened, and the assembly is completed.

5.3. Radial Carriage Assembly (Sub-assembly C)

The radial carriage (Subassembly C) comprises four groups: holder/connector group (C1), radial carriage group (C2), third actuator group (C3) and first CoM apparat (C4). As shown in Figure 5.15, The C1 group consists of parts a, b, and c; the C2 group consists of parts d, e, f, g, and h; the C3 consists of parts m, n, o, p, k, j, and l; and lastly, the C4 group consists of parts t, s, and r. All parts of this sub-assembly, which consists of 32 parts in total, are shown in Table 5.4.

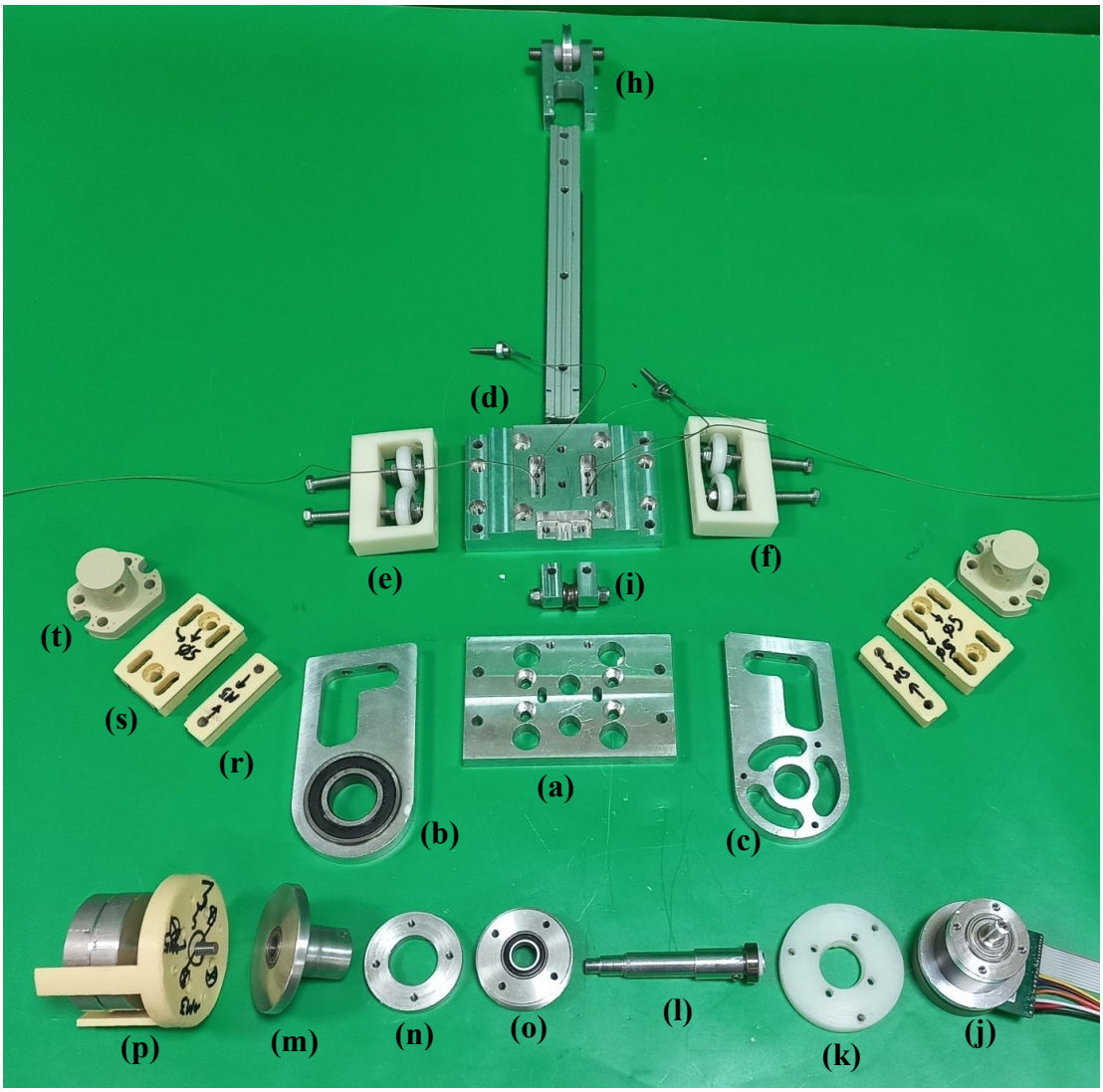

Figure 5.15. Radial carriage assembly parts (a) C1-1 middle holder, (b) C1-2 right holder, (c) C1-3 left holder, (d) C2-1 middle carriage, (e) C2-2 right carriage, (f) C2-3 left carriage, (g) C2-4 linear rail, (h) C2-5 big pulley group, (i) C2-6 small pulley group, (j) C3-1 the third motor, (k) C3-2 third motor connector, (l) C3-3 inner shaft, (m) C3-4 outer shaft I, (n) C3-5 outer shaft II, (o) C3-6 grooved pulley, (p) C3-7 the third spring system, (r) C4-1 squeezing plate, (s) C4-2 housing, (t) C4-3 coupling half

Table 5.4. Material list of radial carriage (sub-assembly C)

Part Code	Part Name	Materials	Number of Parts	Mass (gr)
C1-1	Middle Holder		1	125.5
C1-2	Right Holder		1	74.8
C1-3	Left Holder		1	132.9
C2-1	Middle Carriage		1	234.6
C2-2	Right Carriage		1	51.6
C2-3	Left Carriage		1	51.6
C2-4	Linear Rail			114.1
C2-5	Big Pulley Group			62.5
C2-6	Small Pulley Group			17.5
C3-1	3rd Motor		1	216.2
C3-2	3rd Motor Connector		1	12.8
C3-3	Inner Shaft		1	18.1
C3-4	Outer Shaft a		1	39.6
C3-5	Outer Shaft b		1	17.3
	Bearing 6800		2	51.2 x 2
	Bearing 6004		1	69.4
C3-6	Grooved Pulley		1	34.3
	Bearing 608		2	101.4
C3-7	3rd Spring System		1	128.5
	Coupling		1	6.6
	2nd Encoder		1	
	2nd Encoder Connector	PLA	1	
	Shaft coupling	Aluminum	1	
C4-1	Squeezing Plate	PLA	2	59.3 x 2 (/w screws and nuts)
C4-2	Housing	PLA	2	
C4-3	Coupling Half	PLA	2	
	Hex Jam Nut M8		4	
	Socket Head M4 X 30 mm		1	
	Socket Set Screw M4 X 6 mm		2	
	Socket Head M5 X 16 mm		6	
	Socket Head M4 X 20 mm		2	
	Prevailing Torque Hex Nut M4		2	
	Hex Nut Style M5		8	
	Socket Head M5 X 16 mm		4	
	Socked Head Bolt M3 X 12 mm		4	
	Socked Head Bolt M3 X 16 mm		5	

(cont. on next page)

Table 5.4 (cont.)

	Socked Head Bolt M3 X 20 mm		5	
	Socked Head Bolt M4 X 12 mm		1	
	Socket Set Screw M4 X 4 mm		2	
	Socked Head Bolt M6 X 50 mm		1	

5.3.1. Manufacturing of Radial Carriage

The holder/connector group (C1), which is a group of radial carriage sub-assembly, comprises left, right and middle connectors, as shown in Table 5.4. The manufacturing process of these parts is mentioned respectively.

In the manufacturing process of shaft holders, aluminum plates were used as raw material. Accurate positioning of drilled holes is essential for obtaining straight shafts axis and not allowing them to tighten. Therefore, the part was machined by a side mill to obtain two identical rectangular shapes. Then holes were drilled by referencing this rectangular shape. After that, parts were machined for other details, such as removal patterns, to decrease weight. The manufacturing process of these parts is shown in Figure 5.16

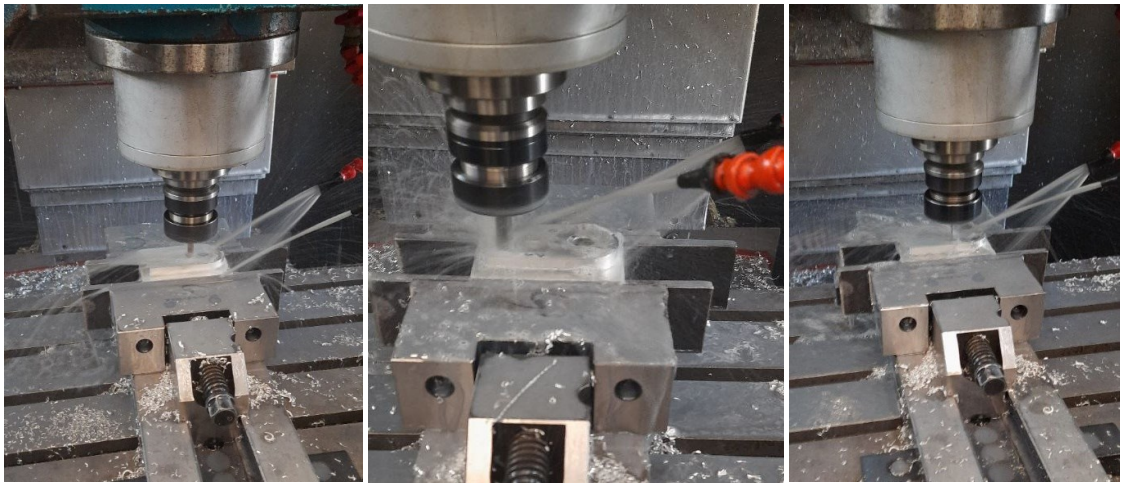

Figure 5.16. Manufacturing process of shaft holders

In Figure 5.17, one face of the part can be seen after machining. Finally, parts are fixed, whereas other faces will be machined. After that, the manufacturing is finished except for thread cutting. Figure 5.18 shows the left shaft holder and right shaft holder.

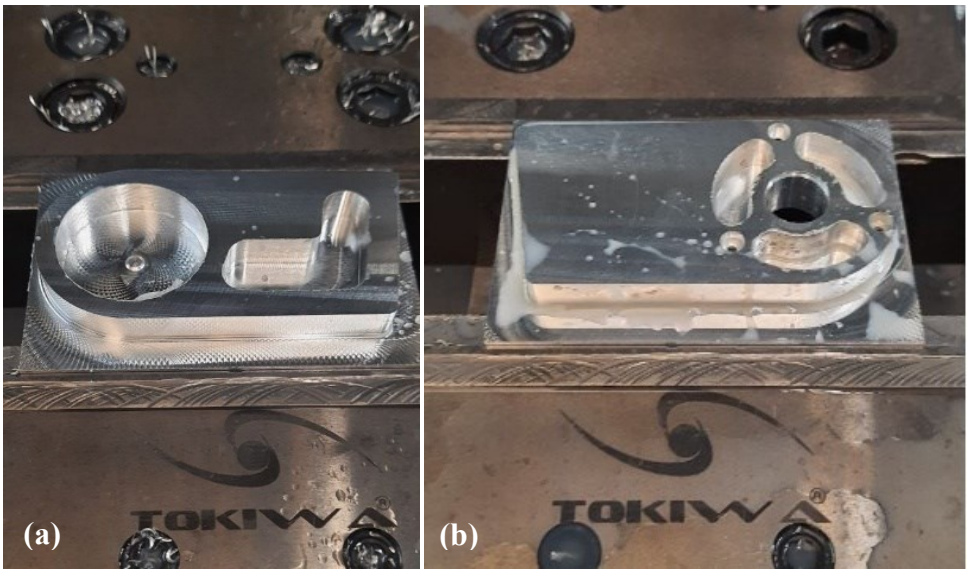

Figure 5.17. Shaft holders after machining is finished for one face (a) left shaft holders, (b) right shaft holders

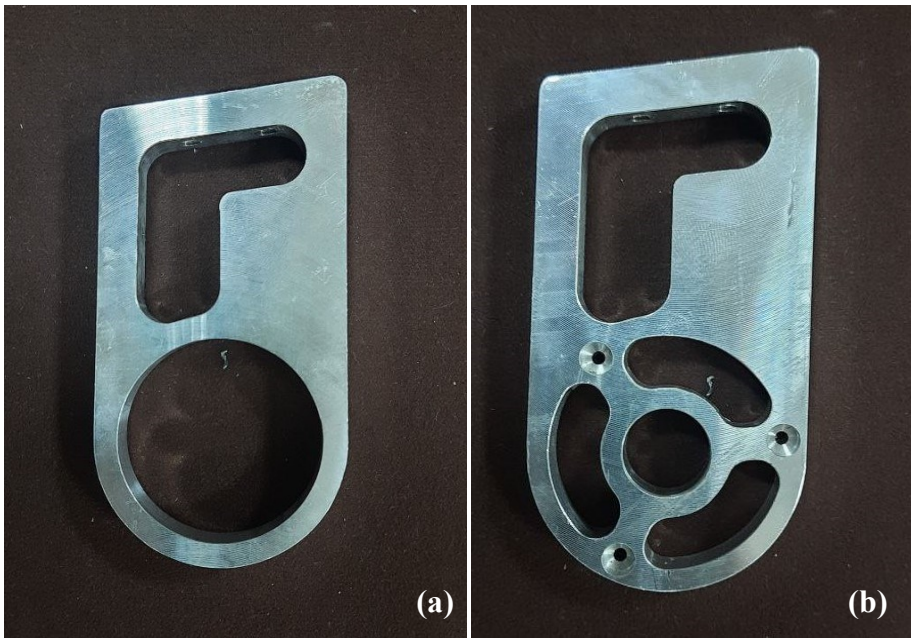

Figure 5.18. Manufactured shaft holders (a) left shaft holder and (b) right shaft holder

The second group of the sub-assembly C is the third actuator group (C2). The production of the outer shaft and grooved pulley parts belonging to this group is as follows. The outer shaft, manufactured from the aluminum cylinder, was machined with a CNC lathe, and then a CNC milling machine was used to drill the holes. The manufactured outer shaft can be seen in Figure 5.19(a).

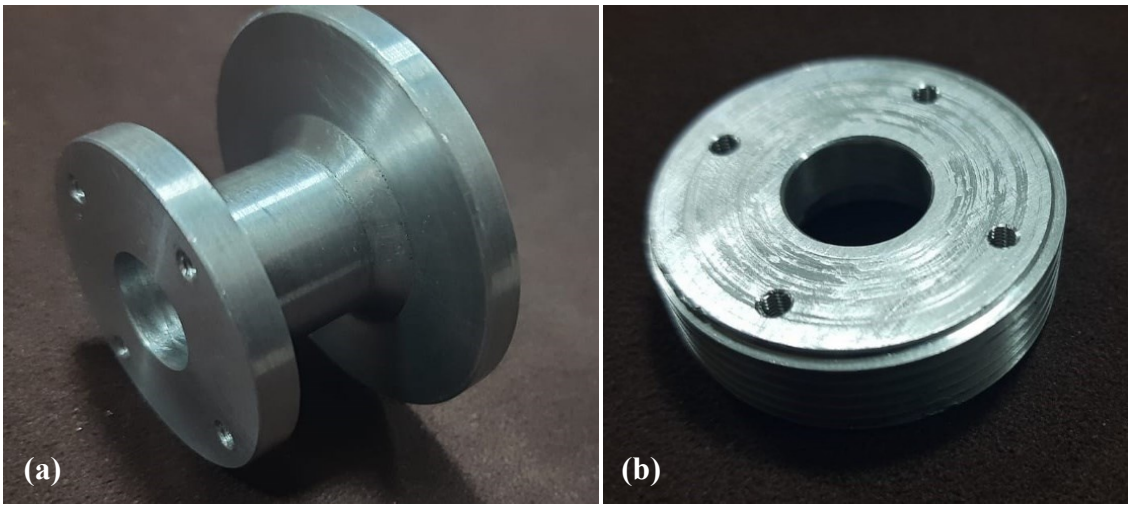

Figure 5.19. Manufactured outer shaft (a) and grooved pulley (b)

The grooved pulley is also machined from an aluminum cylinder. Both lathe and milling machines are used in manufacturing. First, a hole is grooved for the bearing after the desired geometry was obtained. Then the threading operation was performed, and holes were drilled in the CNC milling machine. The manufactured part can be seen in Figure 5.19(b).

One of the most important parts of the radial carriage group (C2) is the middle carriage (C2-1). It is manufactured with a CNC milling machine from an aluminum block. There are details on both faces of the part and some through holes common to both faces. First, the part is machined using a side mill for manufacturing a rectangular prism with the specified dimensions. Then, the through holes reaching both faces were drilled. After drilling holes, the radial car middle is shown in Figure 5.20(a). The next step is to machine other details, such as grooves for linear rail and holes for the bolt heads, as shown in Figure 5.20(b). The machining process of one face after finishing the part is shown in Figure 5.20(c).

After the machining process is completed on one face of the part, the details on the other side begin to be machined as shown in Figure 5.21(a) and (b). These details are screw heads, grooves with different geometries for cable clampers and pulley connectors, etc. During the process, side and face mills are used. The machining process of the other face after finishing can be seen in Figure 5.21(c). Finally, different views of the manufactured radial car middle are shown in Figure 5.22.

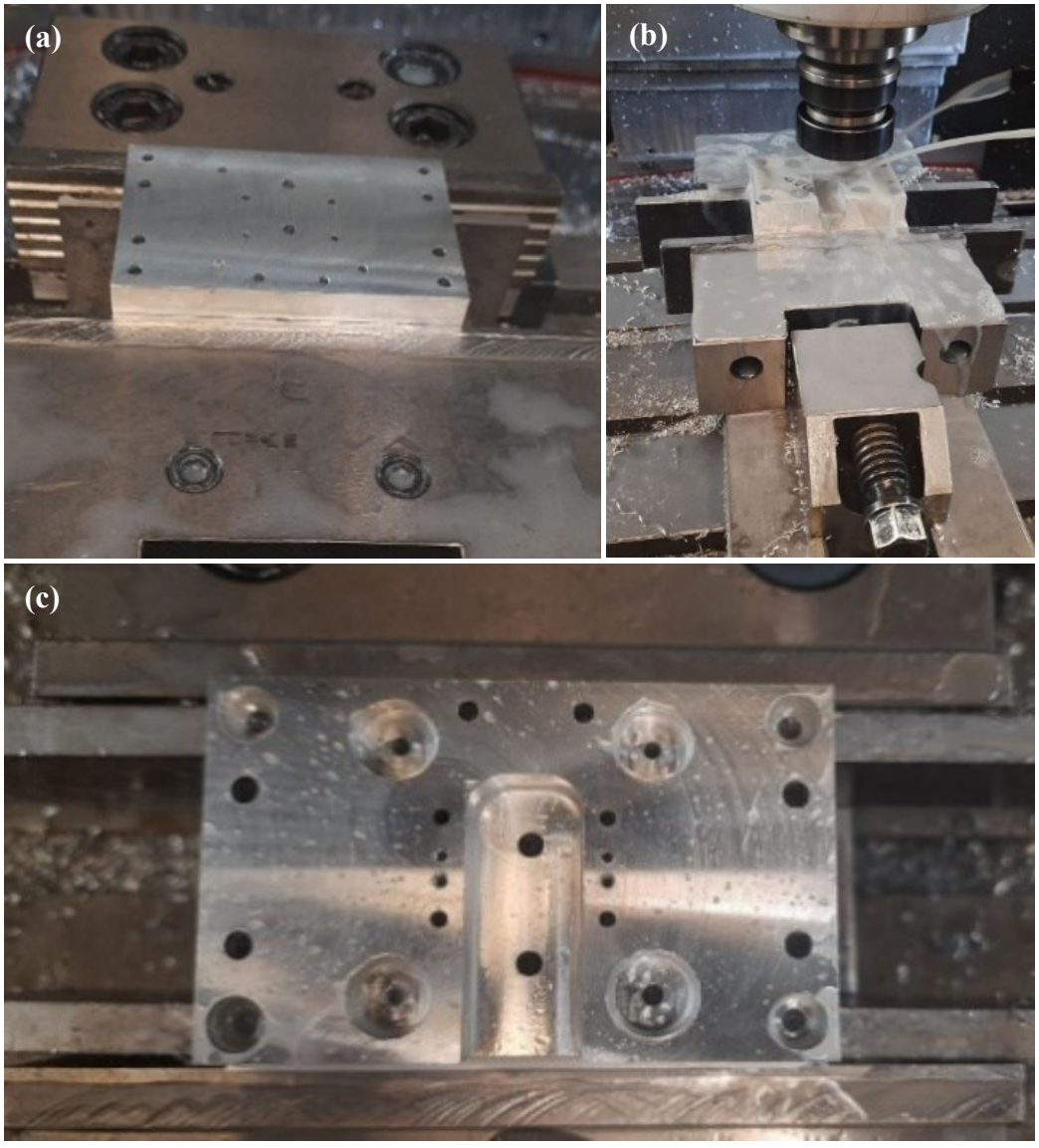

Figure 5.20. First face radial car middle during machining process (Left: fixing part and drilling holes, middle: machining other derails, bottom: end of first face machining)

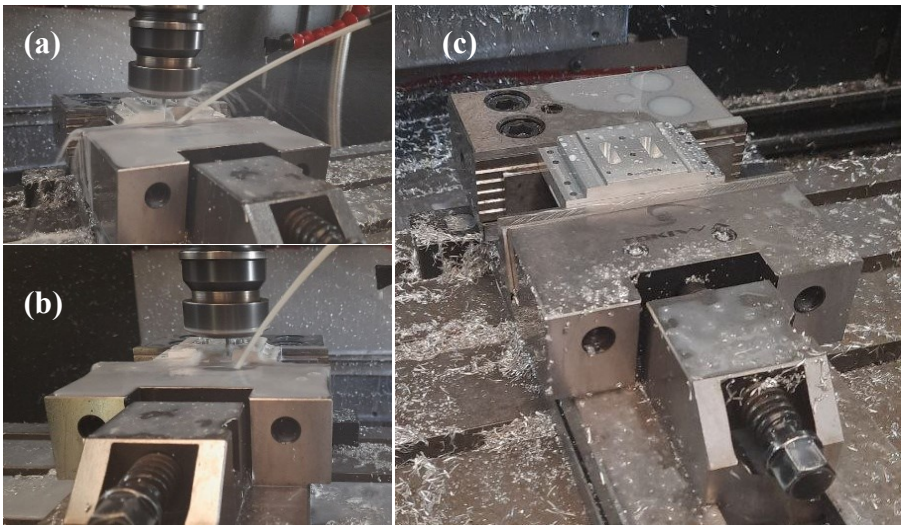

Figure 5.21. Other face radial car middle during machining process: (a) and (b) machining one side of the part and (c) end of machining for one side

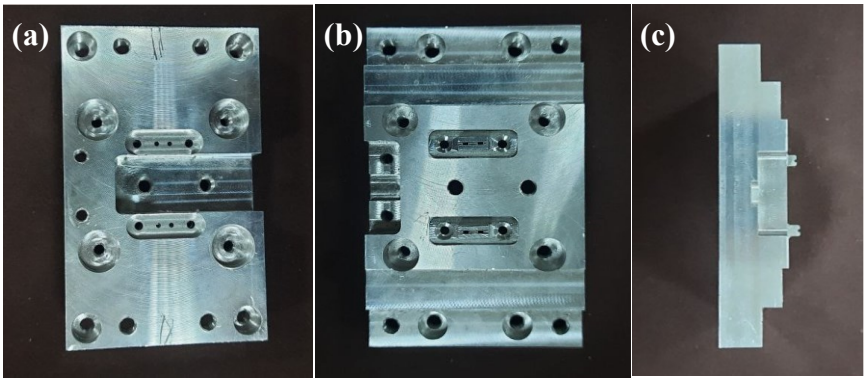

Figure 5.22. Middle radial car: (a) front view, (b) back view and (c) side view

5.3.2. Assembly of the Radial Carriage (C)

The masses of Connector/holder (C1), third actuator (C3) groups are measured as 360.9 and 540.7 gr, respectively. The linear carriage (C3) group was not measured alone, but the total mass of the sub-assembly C is 1390.4 gr (Figure 5.23).

The assembly of the holder/connector group (C1) involves the left (C1-3) and right shaft (C1-2) holders and these parts are fastened to the middle holder (C1-1) by M5 bolts. It is important to follow the correct assembly sequence, as the outer shaft II in the C3 group needs to be installed into the bearing on the left shaft housing in the C1 group before connecting the C3 group to the C1 group.

C2 group consists of middle carriage (C2-1), right carriage (C2-2), left carriage (C2-3), linear rail (C2-5), big pulley group (C2-6), and small pulley group (C2-7). C2-2

and C2-3 parts in this group have been changed many times since they directly affect the radial rail-carriage performance, and the most suitable one has been selected. The assembly of Group C2, begins with fastening the right and left carriages to the middle carriage. The linear rail is then placed on the middle carriage and fastened by M5 bolts. The big pulley group is positioned at the end of the linear rail and attached using M3 bolts.

C3 group consists of 7 parts: the third motor (C3-1), third motor connector (C3-2), inner shaft (C3-3), outer shaft I (C3-4), outer shaft II (C3-5), grooved pulley (C3-6), third spring system (C3-7). In assembly, the outer shaft-II is first fixed on the splined pulley, and then the outer shaft-I is inserted into the outer shaft-II and mounted by a setscrew. The bearing side of the inner shaft is then installed through the bearing inside the grooved pulley. When connecting the C3 group to the C1 group, one of the shaft holders (C1-2 or C1-3) needs to be unassembled. The third spring system is attached to the end of the inner shaft using a coupling, and the motor connector is fastened to the right shaft holder.

Last group to be mentioned is 1st CoM Apparatus (C4 group) that composed of three different parts; squeezing plate (C4-1), housing (C4-2) and coupling half(C4-3). All parts are manufactured from 3D printed and their materials are PLA. The assembly starts with inserting M5 bolt heads into slots of C4-2 then, coupling half is placed on the screw ends, and tightening the nuts. The squeezing plate is then fastened to compress the shaft holders.

5.4. Linear Carriage Assembly (Sub-assembly D)

Linear carriage assembly contains 3 groups: linear carriage group (D1), the second CoM apparatus (D2) and endoscope group (D3) as seen in Table 5.1. All parts of the sub-assembly D is shown in Figure 5.24. These are linear carriage (D1-1), bridge connector (D1-2), left bridge (D1-4), right bridge (D1-3), left apparatus (D1-6), right apparatus (D1-5), endoscope locking mechanism (D3-1), endoscope (D3-2) and the second CoM apparatus (D2-1, D2-2, D2-3). Basic information about these parts can be found in Table 5.5. The remainder of the assembly involves attaching the endoscope locking mechanism to D1-5 and D1-6.

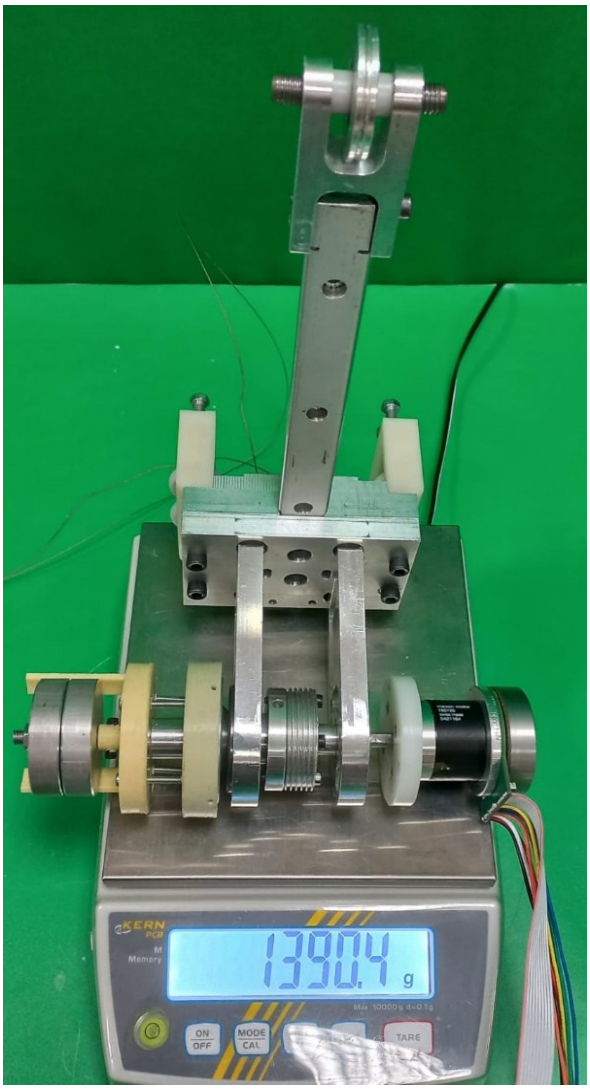

Figure 5.23. Radial carriage assembly

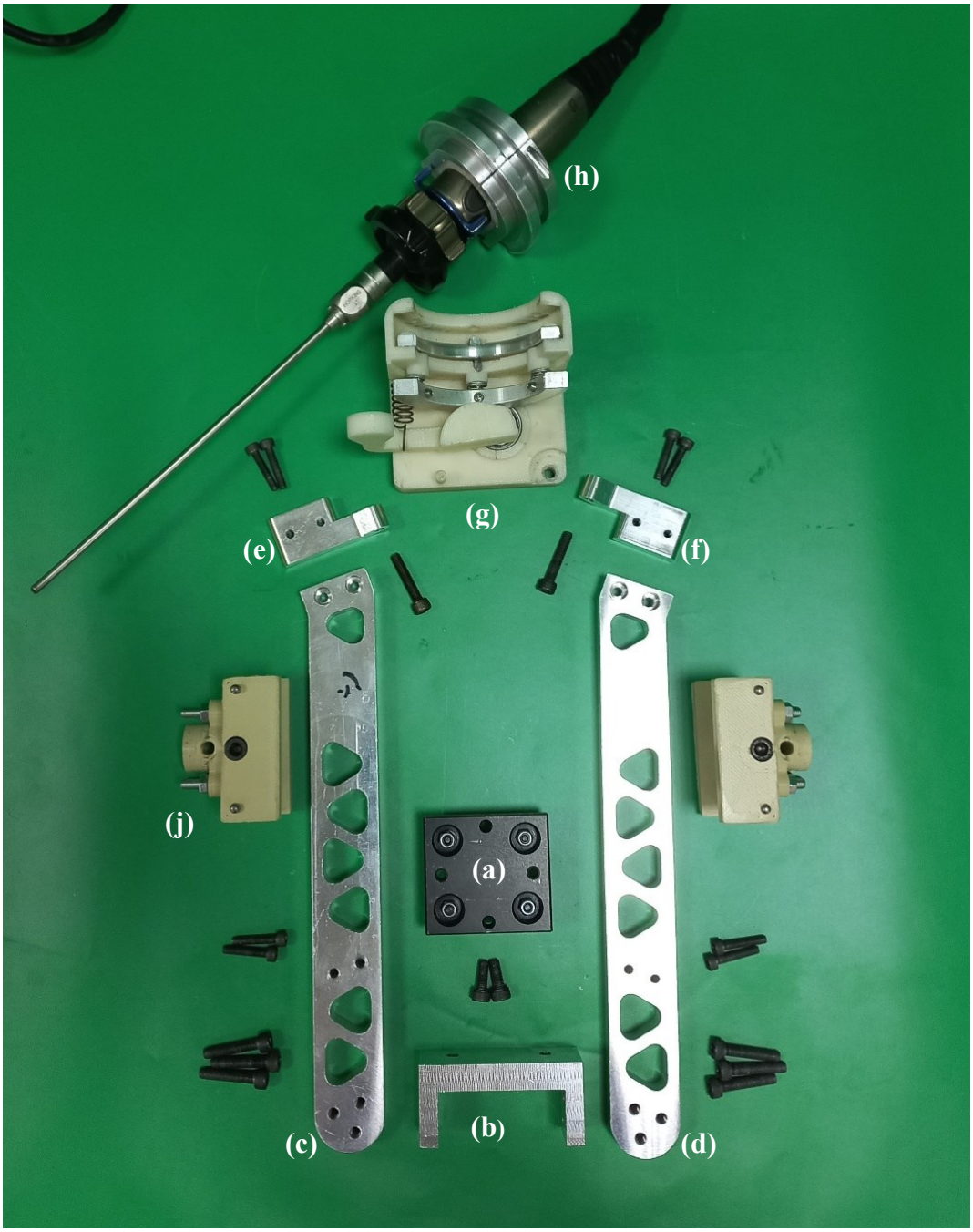

Figure 5.24. Linear carriage parts: linear carriage assembly parts (a) Linear carriage (D1-1), (b) Bridge connector (D1-2), (c) Left bridge(D1-4), (d) Right bridge (D1-3), (e) left Apparatus (D1-6), (f) Right apparattus (D1-5), (g) Endoscope locking mechanism (D3-1), (h) endoscope (D3-2), (j) Second CoM apparatus (D2-1, D2-2, D2-3)

5.4.1. Manufacturing of Linear Carriage (D) parts

The bridges are parts of the linear carriage group (D1). These parts are machined from aluminum blocks with a CNC milling machine. For the manufacturing process, the aluminum blocks are fixed from the long edges, as seen in Figure 5.25(a). Since these parts are mirror symmetry of each other and the holes on them must be co-axial, both parts were machined with a side mill so that hole centers can be referenced from an identical rectangular prism. After that, other details on the face of the part are machined. As seen at the top of Figure 5.25(b), the removal pattern and outer of the part are machined by an end mill and a side mill, respectively. Once one face of the part is machined completely, it is secured again so that the other face can be machined, and finally a face mill is used. The part whose machining operation is completed on one face can be seen in Figure 5.25(c). Finally, manufactured left and right bridges are shown in Figure 5.26.

Table 5.5. Material list of endoscope holder (sub-assembly D)

Part Code	Part Name	Materials	Number of Part	Mass (gr)
D1-1	Linear Carriage	Steel	1	104.4
D1-2	Bridge Connector	Aluminum	1	70.1
D1-3	Right Bridge	Aluminum	1	190.2
D1-4	Left Bridge	Aluminum	1	190.2
D1-5	Right Apparat	Aluminum	1	23.5
D1-6	Left Apparat	Aluminum	1	23.5
D1-7	Clamping Plate Large	Aluminum	1	28.6
D1-8	Clamping Plate Small	Aluminum	1	7.7
D2-1	Lower Housing		2	20.2
D2-2	Upper Housing		2	17.1
D2-3	Coupling Half		2	10.5
D2-4	Steel Pin	Steel	4	3.8
D3-1	Endoscope Locking Mechanism		1	169.3
D3-2	Endoscope		1	351.8
	Socket Head M5 X 20 mm		6	
	Socket Head M5 X 16 mm		2	
	Socked Head M4 X 20 mm		4	
	Socked Head M6 X 35mm		2	
	Hex Screw M5 X 20 mm		4	
	Hex Thin Nut M5		16	

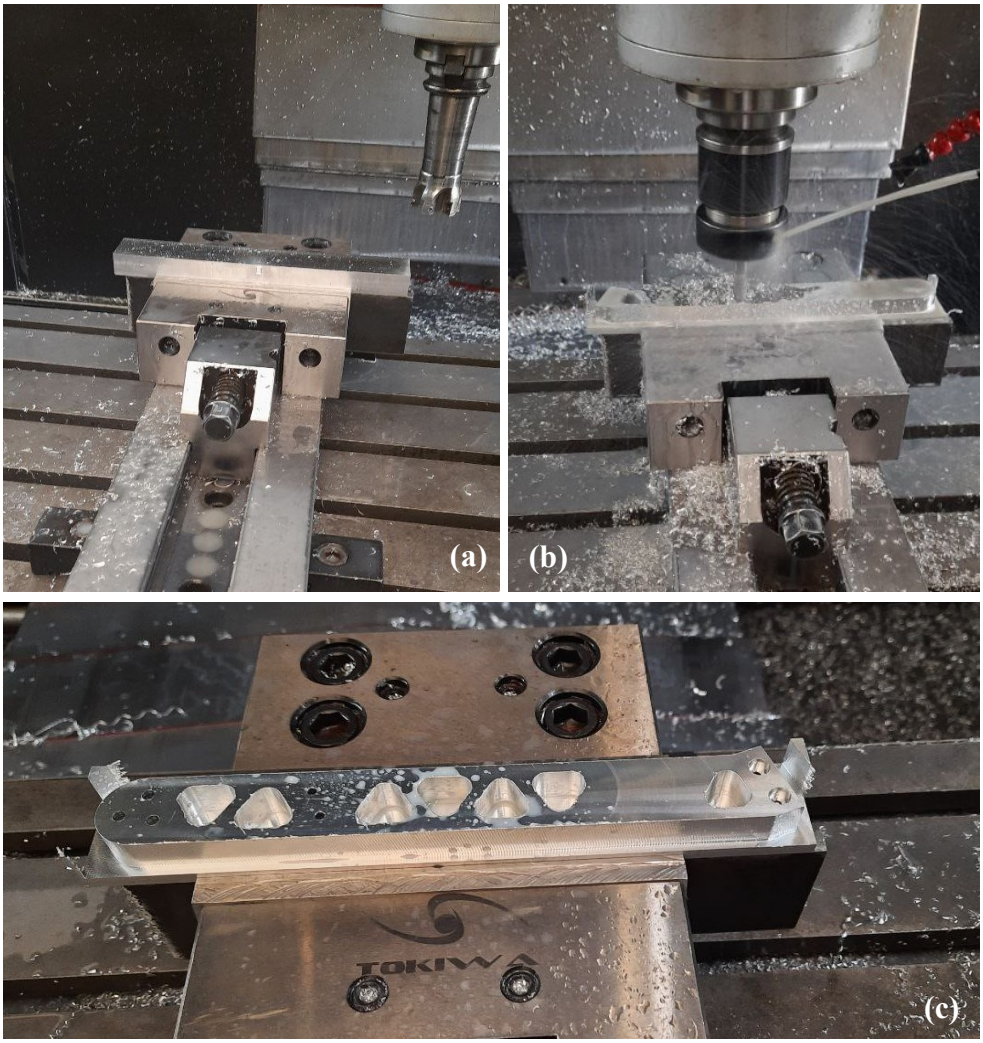

Figure 5.25. Machining process of bridges (a) Fixing raw material on the CNC machine, (b) Machining process of the bridge and (c) After finishing machining on one face

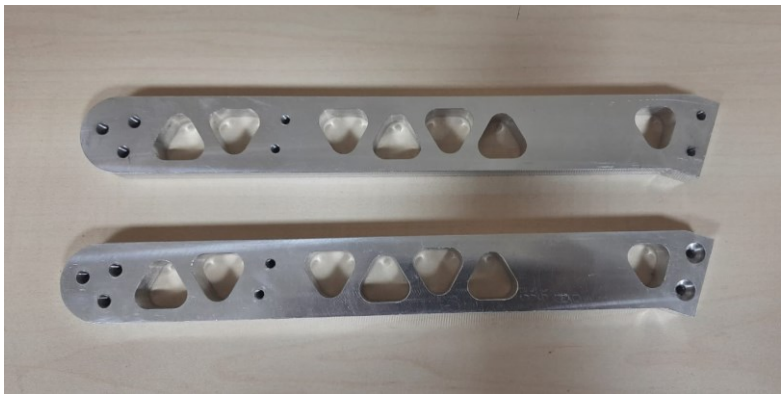

Figure 5.26. Manufactured the bridges

The cable clamper comprises two parts manufactured from aluminum plates, including only hole details. They were machined with a milling machine. Big and small plates can be seen in Figure 5.27(a). These two parts are mounted to each other in such a way as to apply compression to the steel cable between them by using bolts and nuts. The assembly of cable clamping can be seen in Figure 5.27(a) and (b).

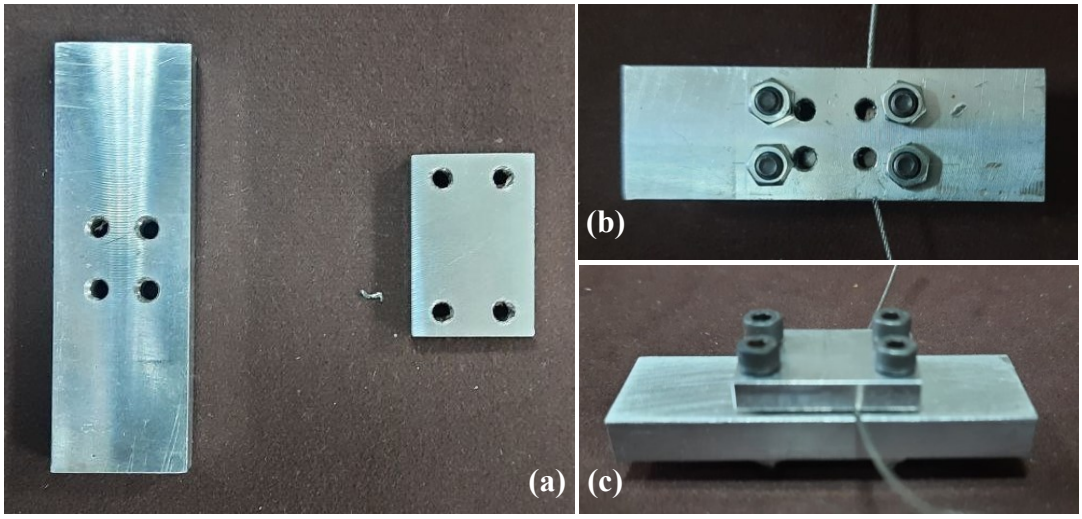

Figure 5.27. Manufactured cable clamper parts

The bridge connector is another part of the linear carriage group, and it is manufactured from an aluminum block. In this part, since the hole details are inside the part, the outer part is machined to form a 'U' shape. After that, the part is fixed to the CNC milling machine from the right and left face to drill smaller holes. Then the more significant holes for bolts and heads are drilled by fixing the part so that the base of the 'U' shape faces down. The manufactured bridge connector can be seen in Figure 5.28(a).

Finally, the endoscope with the locking mechanism and linear carriage are used in the linear carriage sub-assembly. The locking mechanism was already designed, while linear carriage and endoscope are commercial products. These two parts are included directly in the sub-assembly without any changes. They can be seen in Figure 5.28(b)-(c).

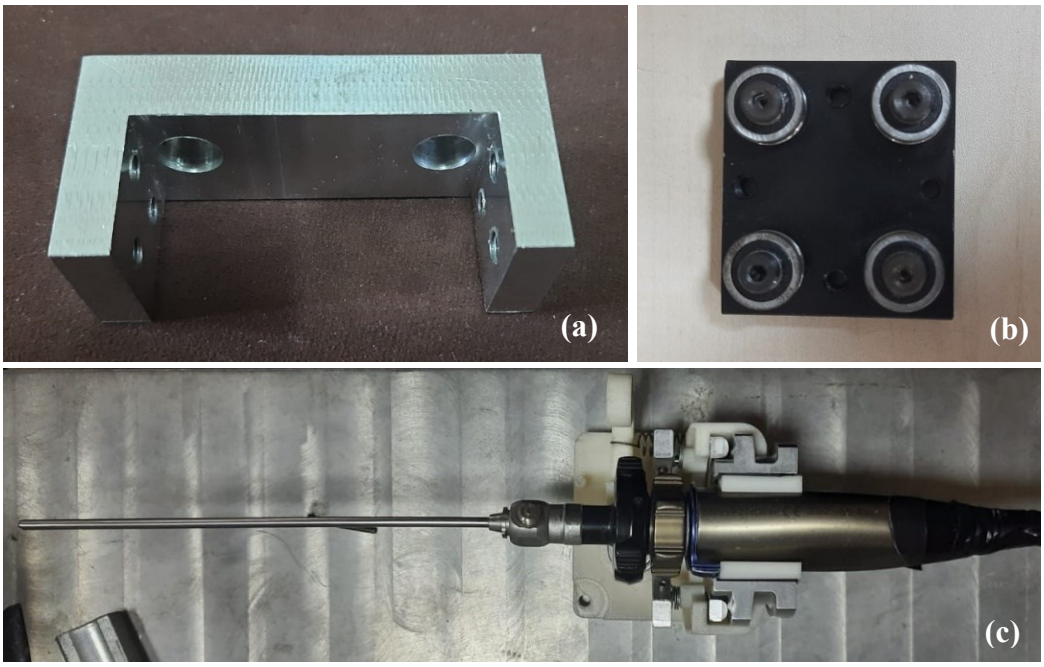

Figure 5.28. Remain parts of the linear carriage (a) bridge connector (b) Linear carriage, (c) Endoscope with the locking mechanism

5.4.2. Assembly of the Linear Carriage (D)

Assembly of the linear carriage (D1) is as follows: linear carriage(D1-1) is fastened to the bridge connector using two M5 bolts, and the right and left bridges are mounted onto the left and right sides of the bridge connector with three M4 screws for each. The large plate is fastened to the right and left bridges, and small clamping plates are mounted to it by M3 bolts.

The second CoM apparatus (D2) serves the same purpose as the first CoM apparatus by linking the CoM of the linear carriage and the end of the pantograph link. It consists of four parts: the lower housing, upper housing, coupling half, and steel pin. The assembly involves inserting the steel pins, placing the upper part, and fastening the coupling half to complete the assembly. Completed assembly can be seen in Figure 5.29.

Figure 5.29. Completed assembly of the linear carriage (sub-assembly of D)

5.5. Balancing Link groups: Parallelogram (E) and Pantograph (F)

Parts of the auxiliary links of the parallelogram are shown in Table 5.6. These parts are main shaft (E-1), PLA Filler (E-2), counter mass link (E-3), radial carriage link (E-4), revolute joint construction (E-5), extender construction (E-6), counter mass construction (E-7) and connection pipe (E-8).

The completed assembly of one side of the parallelogram and all parts used in assembly can be seen in Figure 5.30. The parallelogram assembly is completed by fastening two sub-assemblies manufactured mirror symmetrically to the left and right of the parallelogram shaft, as shown in Figure 5.2. The mass of one side of the parallelogram was also measured as 1646.8 gr, including the counter mass.

Table 5.6. Material list of parallelogram (sub-assembly E)

Part Code	Part Name	Materials	Number of Parts
E-1	Main Shaft	Aluminum	1
E-2	PLA Filler	POM	2
E-3	Counter Mass Link	Aluminum	2
E-4	Radial Carriage Link	Aluminum	2
E-5	Revolute Joint Construction	Brass + Steel + POM	6
E-6	Extender Construction	PLA	2
E-7	Counter Mass Construction	PLA + Steel	2
E-8	Connection Pipe	POM + Aluminum	2

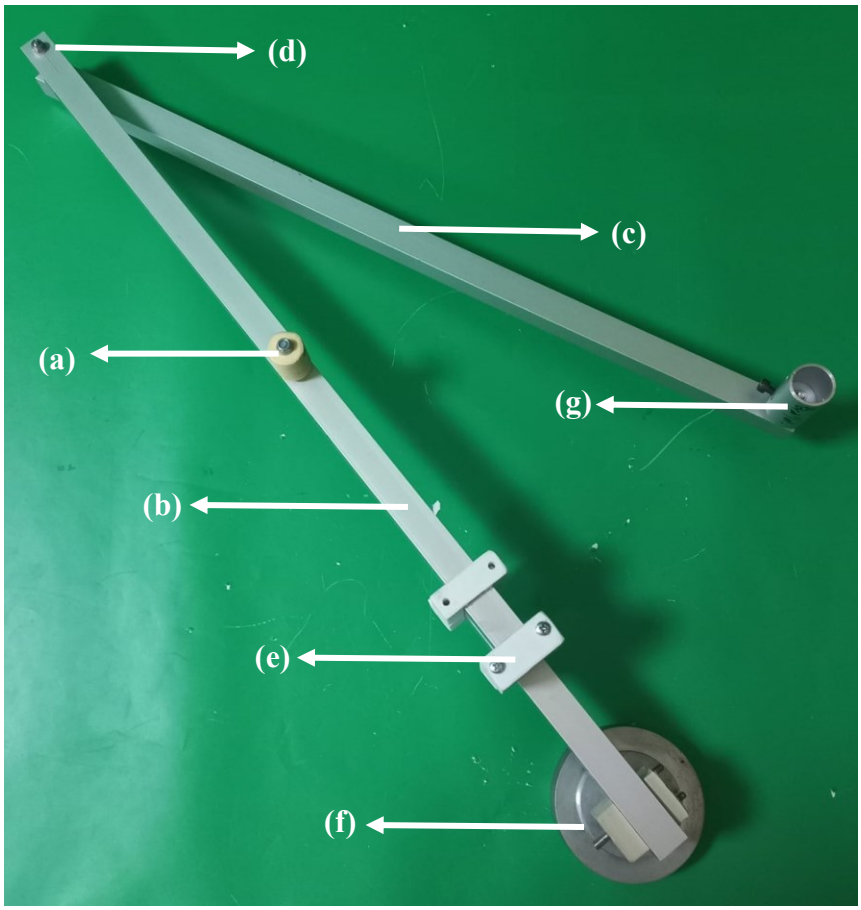

Figure 5.30. Completed assembly of one side of parallelogram and all parts of it (a) PLA filler (E-2), (b) counter mass link (E-3), (c) Radial carriage link (E-4), (d) Revolute joint construction (E-5), (e) Extender construction (E-6), (f) Counter mass construction (E-7), (g) Connection pipe (E-8)

The pantograph (sub-assembly F) consists of 9 different parts or groups of parts. Basic information about these parts can be seen in Table 5.7. These parts are main shaft (F-1), POM filler (F-2), counter mass link (F-3), linear carriage link (F-4), short link (F-5), long link (F-5), revolute joint construction (F-6), counter mass construction (F-7) and connection pipe (F-8). The completed assembly of the pantograph is shown in Figure 5.31. As with the parallelogram assembly, the parts with the number F-7, F-8, and F-9 are a structure consisting of more than one part. One side of the pantograph is measured as 1439.4 gr.

E-3, E-4 parts in the parallelogram and F-3, F-4, F-5 and F-6 parts in the pantograph are hollow aluminum box profiles that are cut to desired sizes and drilled at certain positions. Also, main shafts for both parallelogram (E-1) and pantograph (F-1) are manufactured from aluminum pipes which.

Table 5.7. Material list of pantograph (sub-assembly F)

Part Code	Part Name	Materials	Number of Parts
F-1	Main Shaft	Aluminum	1
F-2	POM Filler	POM	2
F-3	Counter Mass Link	Aluminum	2
F-4	Linear Carriage Link	Aluminum	2
F-5	Short Link	Aluminum	2
F-6	Long Link	Aluminum	2
F-7	Revolute Joint Construction	Brass + Steel + POM	10
F-8	Counter Mass Construction	Aluminum	6
F-9	Connection Pipe	Aluminum + POM	2

E-2 and F-2 parts are manufactured from PLA by 3D printer and POM by lathe machine, respectively. These parts are used in multiple places in the sub-assembly of parallelogram and pantograph. Brass housing is inserted with shrink fit inside these parts, as shown in Figure 5.32. In addition, screw holes are drilled on both these parts to be fastened with aluminum pipes (E-8 and F-9) or main shafts (E1 and F1).

The E-5 and F-7 group of parts are identical and used as revolute joints for both the parallelogram and the pantograph. Assembled E-5 and F-7 are shown in Figure 5.33(a) and (b) respectively. Revolute joint structure consists of two brass housings, one steel rod and one POM washer. These parts with references within assembly, can be seen in Figure 5.33. All parts are manufactured by a lathe machine and manufactured from brass, steel and POM, respectively. Brass housings are installed into the aluminum links in a manner to ensure a shrink fit. Then steel rod is inserted into both housing so that flange parts of the housings is placed between aluminum links, as in the Figure 5.33, so that the POM washer remains between them. The joint assembly is completed by tightening nuts on both sides of the steel rod.

To prevent link collision between the counter mass link of parallelogram (E-3) and 2nd actuator group (B3), an extender construction is designed. It provides an increment in distance with respect to the symmetry plane of the parallelogram by compressing a 6 cm aluminum profile part at the end of the counter mass link. This structure, which is assembled by screws and nuts as seen in Figure 5.34, consists of a total of four parts, two of which are identical, all manufactured from PLA using a 3D printer.

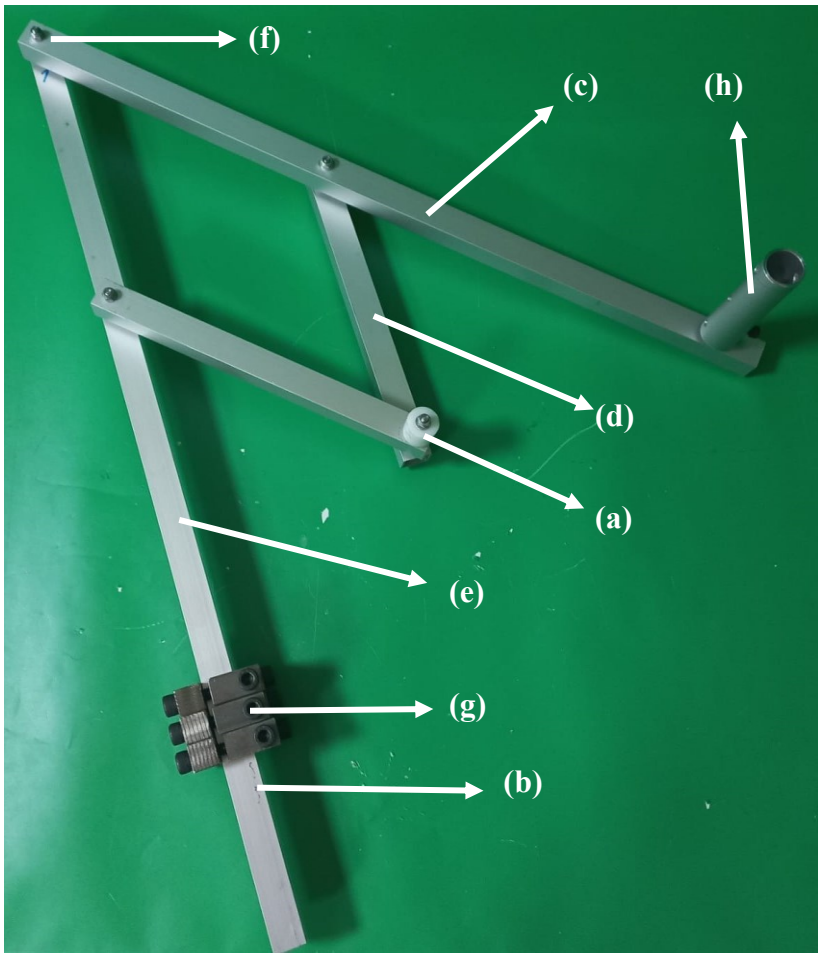

Figure 5.31. Completed assembly of one side of pantograph and all parts of it (a) POM filler (F-2), (b) Counter mass link (F-3), (c) Linear carriage link (F-4), (d) Short link (F-5), (e) Long link (F-6), (f) Revolute joint construction (F-7), (g) Counter mass construction (F-8), (h) Connection pipe (F-9)

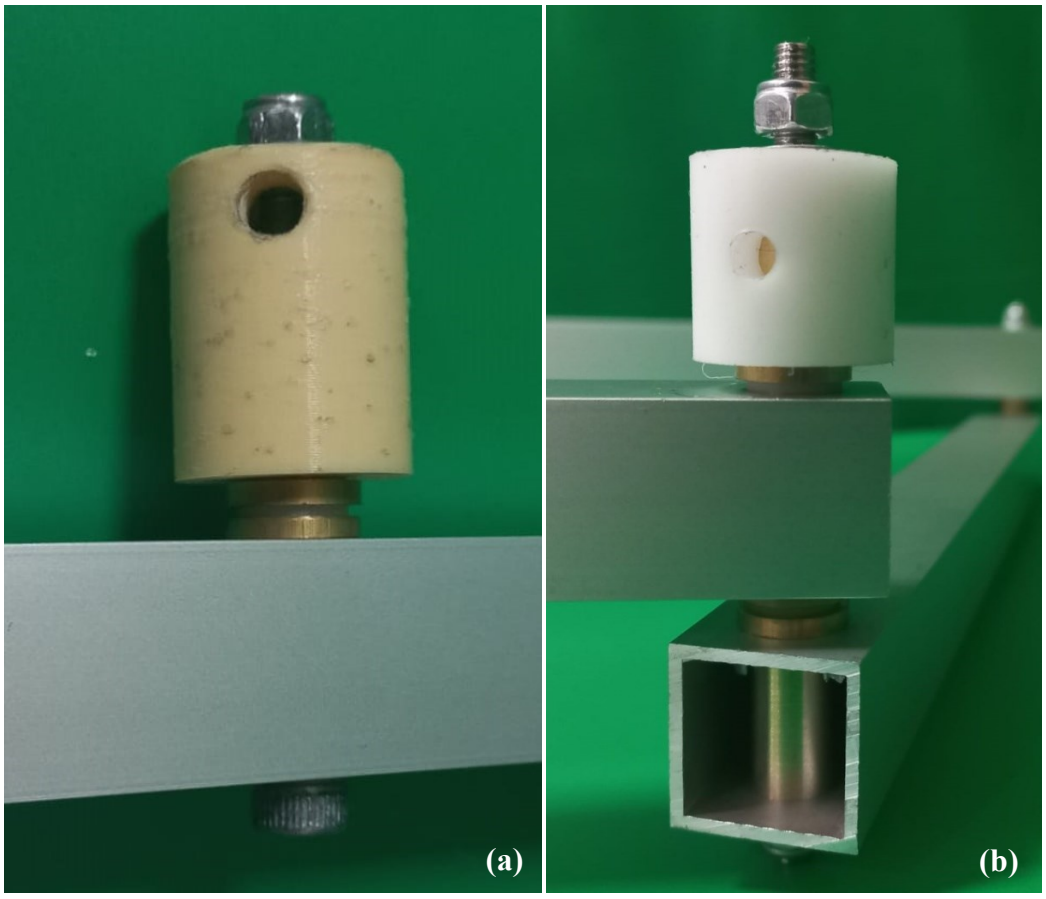

Figure 5.32. Fillers for pantograph and parallelogram (a) PLA Filler (E-2) used on the Parallelogram and (b) POM filler (F-2) used on the Pantograph

The last parts are mentioned in the parallelogram and pantograph are E-7 and F-8 respectively. To avoid the above-mentioned collision occurring in the parallelogram, an additional apparatus shown in Figure 5.35(a) is used. This apparatus except bolts and nuts; It consists of two 3d printed parts and 2 steel rods with 4 mm diameter. By using M6 bolt and nuts, aluminum link is compressed by two plastic parts at appropriate position on the link. Last, cylindrical counter mass is fastened into the large PLA part as shown in Figure 5.35(a).

Since there is no link collision in the pantograph, the counter mass construction is simpler than in the parallelogram. The design consists of 4 identical parts manufactured from flat steel and these parts are fastened to each other with 4 M8 bolts. Completed assembly of the F-8 is shown in Figure 5.35(b).

The final assembly of the system is yet to be constructed. An initial assembly of the system can be seen in Figure 5.2.

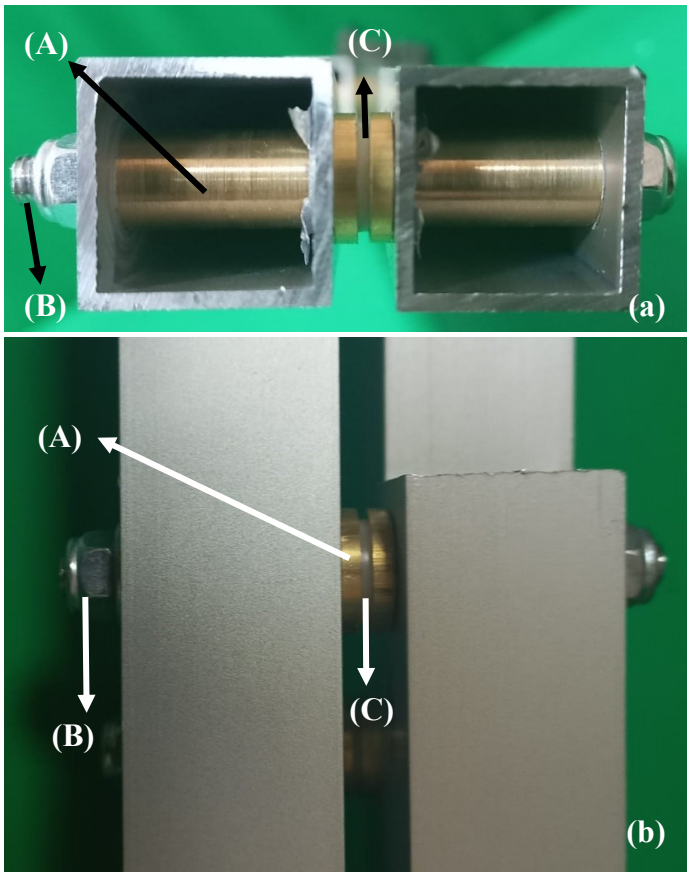

Figure 5.33. Revolute joint constructions for parallelogram and pantograph (a) Revolute joint construction (E-5) in parallelogram (b) Revolute joint construction (F-7) in pantograph (both figures are referred to identical parts: (A) brass housing, (B) steel rod, (C) POM washer)

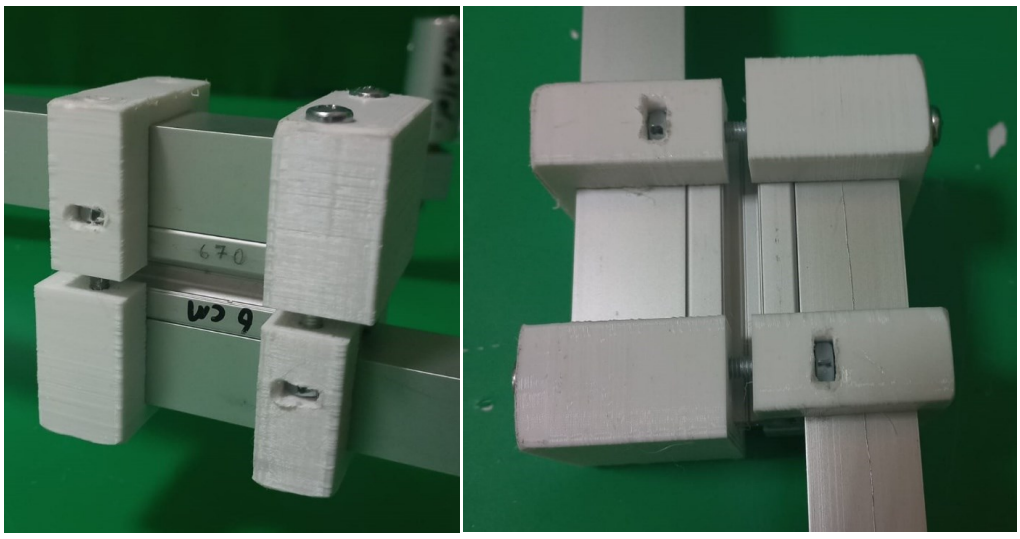

Figure 5.34. Extender construction (E-6) for the parallelogram

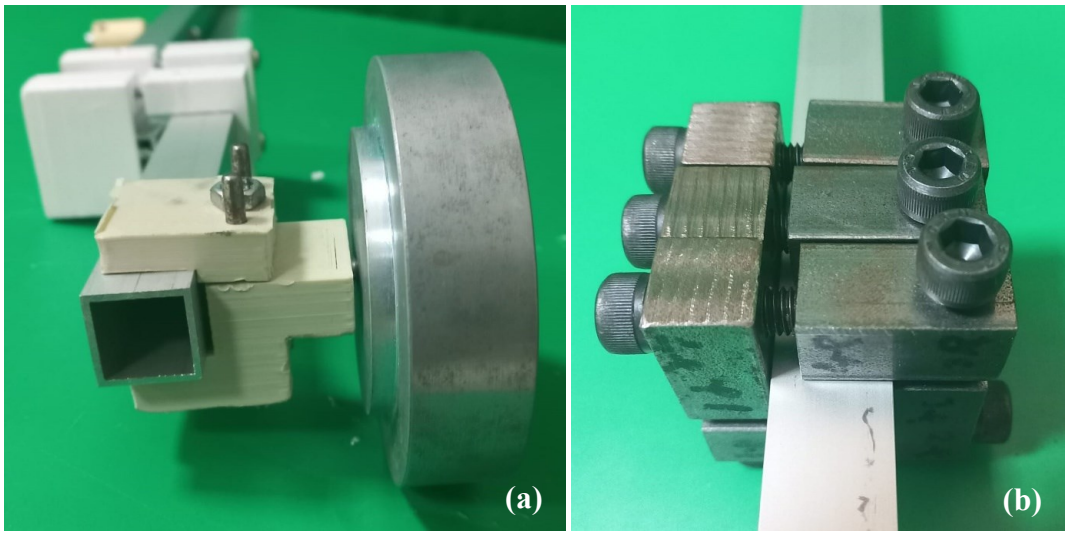

Figure 5.35. Counter mass constructions for parallelogram and pantograph (a) Counter mass construction for parallelogram (E-7), (b) Counter mass construction for pantograph (F-8)

CHAPTER 6

CONCLUSIONS

This study presents the design, manufacturing and assembly of a 3-dof robotic arm with a 2R1T motion pattern for minimally invasive transnasal surgery applications. This robot has a remote center of motion and performs all its movements around the pivot point planned to be located at the tip of the nose.

Various kinematic structures were studied for the conceptual design of this manipulator. The most suitable one was selected according to criteria such as balancing and workspace. A fully serial kinematic structure with an RCM based on the circular tracking arc was selected. Although the circular tracking arc mechanism is a well-documented concept in the literature, the presented manipulator design is a modified version of the circular tracking arc. Furthermore, the literature does not include any references to the gravity compensation of a circular tracking arc mechanism.

After the evaluation of the kinematic structure, a static balancing solution is performed parametrically. Then, CAD models were designed to reveal the constructional details. Finally, the production and assembly were carried out. Tests on the prototype, including precision and repeatability, as well as design revisions, remain pending. These will be addressed in future works.

REFERENCES

Agrawal, Sunil K., and Abbas Fattah. 2004. “Gravity-Balancing of Spatial Robotic Manipulators.” *Mechanism and Machine Theory* 39(12): 1331–1344. https://doi.org/10.1016/j.mechmachtheory.2004.05.019.

Alamdari, Aliakbar, and Venkat Krovi. 2016. “Static Balancing of Highly Reconfigurable Articulated Wheeled Vehicles for Power Consumption Reduction of Actuators.” *International Journal of Mechanisms and Robotic Systems* 3(1): 15-31. https://doi.org/10.1504/ijmrs.2016.077035.

Arakelian, V., Dahan, M., and Smith, M. 2000. “A Historical Review of the Evolution of the Theory on Balancing of Mechanisms.” *International Symposium on History of Machines and Mechanisms Proceedings HMM 2000,* edited by M. Ceccarelli, 291–300, Dordrecht: Springer. https://doi.org/10.1007/978-94-015-9554-4_33.

Arakelian, Vigen, and Michael R. Smith. 2005. “Shaking Force and Shaking Moment Balancing of Mechanisms: A Historical Review with New Examples.” *Journal of Mechanical Design* 127(2): 334–339. https://doi.org/10.1115/1.1829067.

Boyraz, Pinar, et al. 2019. "Robotic Surgery." In *Biomechatronics*, Chapter 15, 1st ed., 431-450. Academic Press, an imprint of Elsevier. https://doi.org/10.1016/b978-0-12-812939-5.00015-x.

Briot, Sébastien, and Vigen Arakelian. 2015. "A New Energy-free Gravity-compensation Adaptive System for Balancing of 4-DOF Robot Manipulators with Variable Payloads." In *Proceedings of the 14th IFToMM World Congress*, 179-187. https://doi.org/10.6567/IFToMM.14TH.WC.OS13.038.

Chen, Ze, et al. 2015. "A Class of 1 DOF Planar RCM Mechanism Based on Motion-Reproduce Method." Paper presented at *the 2015 IEEE International Conference on Robotics and Biomimetics (ROBIO)*, 1433-1438. doi: 10.1109/ROBIO.2015.7418972

Davies, B., et al. 2000. "Neurobot: A Special-Purpose Robot for Neurosurgery." In *Proceedings - IEEE International Conference on Robotics and Automation*, 4:4103-4108. doi:10.1109/ROBOT.2000.845371.

Davies, B. L., et al. 1996. "A Clinically Applied Robot for Prostatectomies." In *Computer-Integrated Surgery: Technology and Clinical Applications*, edited by R. H. Taylor, et al., 593–601. Cambridge, Massachusetts: MIT Press.

Hilpert, H. 1968. "Weight Balancing of Precision Mechanical Instruments." *Journal of Mechanisms* 3(4): 289–302. https://doi.org/10.1016/0022-2569(68)90005-0.

Chin-Hsing Kuo, Jian S. Dai, and Prokar Dasgupta. 2012. "Kinematic Design Considerations for Minimally Invasive Surgical Robots: An Overview," *International Journal of Medical Robotics and Computer Assisted Surgery* 8(2): 127–145, https://doi.org/10.1002/rcs.453.

Chin-Hsing Kuo and Jian Dai. 2009. "Robotics for Minimally Invasive Surgery: A Historical Review from the Perspective of Kinematics," in *Springer EBooks*, 337–54, https://doi.org/10.1007/978-1-4020-9485-9_24.

Lanfranco, A. R., et al. 2004. "Robotic Surgery: A Current Perspective." *Annals of Surgery* 239(1): 14–21. https://doi.org/10.1097/01.sla.0000103020.19595.7d.

Lu, Qi, Carlos Ortega, and Ou Ma. 2011. "Passive Gravity Compensation Mechanisms: Technologies and Applications." *Recent Patents on Engineering* vol.5: 32-44. https://doi.org/10.2174/1872212111105010032.

Mariani, Alessandro Wasum, and Paulo Manuel Pêgo-Fernandes. 2013. "Minimally Invasive Surgery: A Concept Already Incorporated." *Sao Paulo Medical Journal* 131(2): 69–70. https://doi.org/10.1590/s1516-31802013000100015.

Pal, Raj, Sanjeev Kumar, and Amod Kumar. 2011. "The Journey of Robotic Surgery: Past, Present and Future." *5th International Multi-conference on Intelligent Systems, Sustainable, New and Renewable Energy Technology & Nanotechnology*. https://doi.org/10.13140/RG.2.1.1376.8723.

Sackier, J. M., and Y. Wang. 1994. "Robotically Assisted Laparoscopic Surgery: From Concept to Development." *Surgical Endoscopy* 8(1): 63–66. https://doi.org/10.1007/BF02909496.

Sadeghian, H., F. Zokaei, and S. Hadian Jazi. 2019. "Constrained Kinematic Control in Minimally Invasive Robotic Surgery Subject to Remote Center of Motion Constraint." *Journal of Intelligent Robotic Systems* 95: 901–913. https://doi.org/10.1007/s10846-018-0927-0.

Schena, Bruce. 2007. "Center Robotic Arm with Five-Bar Spherical Linkage for Endoscopic Camera." International Patent WO2007114975.

Schreuder, HWR, and R. Verheijen. 2009. "Robotic Surgery." *BJOG: An International Journal of Obstetrics and Gynaecology* 116: 198–213. https://doi.org/10.1111/j.1471-0528.2008.02038.x.

Takács, Árpád, Dénes Nagy, Imre Rudas, and Tamas Haidegger. 2016. "Origins of surgical robotics: From space to the operating room." *Acta Polytechnica Hungarica* 13(1): 13-30.

van der Wijk, V. 2014. "Methodology for analysis and synthesis of inherently force and moment-balanced mechanisms." Ph.D. diss., University of Twente. https://doi.org/10.3990/1.9789036536301.

van der Wijk, V., and J.L. Herder. 2012. "The Work of Otto Fischer and the Historical Development of His Method of Principal Vectors for Mechanism and Machine Science." *History of Machines and Mechanisms*, edited by T. Koetsier and M. Ceccarelli, vol. 15, 521-534. https://doi.org/10.1007/978-94-007-4132-4_36.

van der Wijk, V., and J.L. Herder. 2009. "Dynamic Balancing of Clavel's Delta Robot." In *Computational Kinematics: Proceedings of the 5th International Workshop on Computational Kinematics, edited by A. Kecskemethy and A. Müller*, 315-322. Springer. https://doi.org/10.1007/978-3-642-01947-0_39.

van der Wijk, V., J.L. Herder, and B. Demeulenaere. 2009. "Comparison of Various Dynamic Balancing Principles Regarding Additional Mass and Additional Inertia." *Journal of Mechanisms and Robotics* 1(4): 041006. https://doi.org/10.1115/1.3211022.

van der Wijk, Volkert, and Just Herder. 2010. "On the Development of Low Mass Shaking Force Balanced Manipulators." *Advances in Robot Kinematics*: Motion in Man and Machine, 411-420. doi: 10.1007/978-90-481-9262-5_44.

Van Hee, Robrecht. 2014. "History of Surgery: a Global View." *Acta chirurgica Belgica* 113(6): 471-482. https://doi.org/10.1080/00015458.2013.11680968.

Veer, Sushant, and Sujatha Srinivasan. 2015. "Approximate spring balancing of linkages to reduce actuator requirements." *Mechanism and Machine Theory* 86. https://doi.org/10.1016/j.mechmachtheory.2014.11.014.

Xu, Pei, Jingjun Yu, and Zong Guanghua. 2007. "Enumeration and Type Synthesis of One-DOF Remote-Center-of-Motion Mechanisms." *Mechanism and Machine Theory* 43: 1585–1595.

Kwoh, Y. S., J. Hou, E. A. Jonckheere, and S. Hayati. 1988. "A robot with improved absolute positioning accuracy for CT guided stereotactic brain surgery." *IEEE Transactions on Biomedical Engineering* 35(2): 153-160. https://doi.org/10.1109/10.1354.

Yaşır, Abdullah, and Gökhan Kiper. 2018. "Structural Synthesis of 2R1T Type Mechanisms for Minimally Invasive Surgery Applications." In *Mechanisms, Transmissions and Applications,* edited by Mehmet Ismet Can Dede, Mehmet İtik, Erwin-Christian Lovasz, and Gökhan Kiper, 31-38. Cham: Springer International Publishing. https://doi.org/10.1007/978-3-319-60702-3_4.

Yaşır, A., Kiper, G., Can Dede, M.İ., & van der Wijk, V. (2019). "Static Force Balancing of a 2R1T Parallel Manipulator with Remote Center of Motion." In *Advances in Mechanism and Machine Science*, edited by T. Uhl, vol. 73, 3219-3226. Cham: Springer. https://doi.org/10.1007/978-3-030-20131-9_317.

Yaşır, Abdullah. 2018. "Design of a 2R1T Mechanism with Remote Center of Motion for Minimally Invasive Transnasal Surgery Applications." Master's thesis, Izmir Institute of Technology.

Yun-ping, Z., and Fan, Z. 2015. "A Novel Remote Center-of Motion Parallel manipulator for Minimally Invasive Celiac Surgery."

Zong, G., X. Pei, J. Yu, and S. Bi. 2008. "Classification and type synthesis of 1-DOF remote center of motion mechanisms." *Mechanism and Machine Theory* 43(12): 1585-1595. https://doi.org/10.1016/j.mechmachtheory.2007.12.008.